TECHNISCHE UNIVERSITÄT MÜNCHEN

Lehrstuhl für Technische Chemie II

Stability of silica supported Pd/Au catalysts in gas phase vinyl acetate monomer synthesis

Stefanie Simson

Vollständiger Abdruck der von der Fakultät für Chemie der Technischen Universität
München zur Erlangung des akademischen Grades eines
Doktor-Ingenieurs (**Dr.-Ing.**)

genehmigten Dissertation.

Vorsitzender: Univ.-Prof. Dr. Dr. h.c. B. Rieger

Prüfer der Dissertation:

1.   Univ.-Prof. Dr. J. A. Lercher

2.   Univ.-Prof. Dr. H. Klein

3.   Univ.-Prof. Dr. M. Tromp

Die Dissertation wurde am 17.06.2013 bei der Technischen Universität München
eingereicht und durch die Fakultät für Chemie am 11.10.2013 angenommen.

"Ernst zu nehmende Forschung erkennt man daran, dass plötzlich zwei Probleme existieren, wo es vorher nur eines gegeben hat."

Thorstein Bunde Veblen (1857-1929)

Acknowledgements

First of all I want to thank Professor Johannes A. Lercher for giving me the opportunity to do my PhD thesis in his group and providing me with an interesting and challenging research topic. While allowing me to follow my own ideas and interests, our discussions always offered fresh ideas, insights and new points of view!

My special thanks go to (apl.) Professor Andy Jentys, who was always open for questions and discussions. Thank you for the funny moments and all your time while introducing me into vacuum systems and the right way to tight a copper ring ;)

Special thanks go to Xaver Hecht, for helping me to set up and repair my setups again and again and again, Andreas Marx for making my computer run and Martin Neukamm for elemental analysis. Stefanie Maier, Bettina Federmann and Karen Schulz must not be forgotten, because without them doing all organizations, nothing here could go about its course at all!

I am grateful to the Wacker Chemie AG for the financial support and Dr. Jürgen Eberle as well as Dr. Anja Roscher for the helpful discussions and their continual interest in new findings and ideas.

Moreover I want to thank all participants of the Workshops of the Wacker-Institut für Siliciumchemie for fruitful discussions.

Many students did a great job and contributed to the present work. I would like thank Elisabeth Hanrieder, Jan Hammes, Patrick Schuh, Andreas Schiff, Niko Kromer, Volker Mertl, Christian Haidn, Andreas Ehrmeier, Theresa Ludwig, Ines Freudensprung and Meltem Karaismailoglu. Particularly I want to thank Elisabeth, who joined the project for her Phd thesis, for numerous helpful discussions and all the chatting in-between.

Special thanks to all dear colleagues, who were working alongside me, for all the discussions, all the help and of course for the countless funny moments! While it would be impossible to mention everybody I want to stress out several special people. Without Jennifer Hein, Monica Pop, Stefan Schallmoser, Robin Kolvenbach and John Ahn to break the everyday routine in office 46303, three years of PhD would have definitely been less fun. Not to forget Conny Ablasser, Eva Schachtl, Franz Haseidl, Florian

Abbreviations

Å	Angström
AAS	atom absorption spectroscopy
AcOH	acetic acid
Au	gold
a.u.	arbitrary units
at.-%	atomic percent
BET	Brunauer-Emmet-Teller
°C	degree Celsius
cm	centimeter
DFT	density functional theory
DRIFT	diffuse reflectance infrared Fourier transform
(G)eV	(giga)electronvolt
EXAFS	extended X-ray absorption fine structure
FT	Fourier transformation
FTIR	Fourier transform infrared spectrometer
GC	gas chromatography
h	hour
HR-TEM	high resolution transmission electron microscopy
IR	infrared
(FT)IR	(Fourier transformed) infrared spectrometry
(k)J	(kilo)joule
K	Kelvin
K	potassium
KOAc	potassium acetate
kV	kilovolt
L	liter
mA	milliamp
mol	mol
mol-%	mol percent

min	minute
mL	milliliter
mm	millimeter
nm	nanometer
Pa	pascal
Pd	palladium
Pd-ac	palladium acetate
$Pd(OAc)_2$	palladium acetate
PVOH	polyvinyl alcohol
rds	rate determining step
s	second
SiC	silicon carbide
STEM-XDS	scanning transmission electron microscopy-X-ray dispersion spectroscopy
T_c	order-disorder temperature
TCD	thermal conductivity detector
TOF	turn over frequency
TOS	time on stream
TUM	Technische Universität München
VAM	vinyl acetate monomer
wt.- %	weight percent
XAS	X-ray absorption spectroscopy
XANES	X-ray absorption near edge structure
XPS	X-ray photoelectron spectroscopy
XRD	X-ray diffraction

Table of contents

Chapter 1

General Introduction

The heterogeneously catalyzed synthesis of vinyl acetate is an important industrial process involving the acetoxylation of ethylene. Initially, vinyl acetate was produced as byproduct in the liquid phase synthesis of ethylidene diacetate, whereas nowadays the global production is above 4.7 million metric tons, with an increase of approximately 8 % from 2009.[1] Vinyl acetate has a wide range of applications, referable to its outstanding adhesive, optical, electrical and fiber-forming properties. Nowadays polyvinyl acetate accounts for approximately 50 % of the global vinyl acetate consumption, followed by polyvinyl alcohol PVOH as the second largest end-use category.[2] Due to the high market potentials of vinyl acetate, both reaction conditions and the Pd based catalyst system are subject to intensive research.[3,4] Especially the structural properties of silica supported bimetallic Pd/Au catalysts have been widely investigated. However catalyst deactivation by restructuring and sintering are important problems that trouble long term usability and performance of the catalysts. The reasons for sintering and restructuring are still controversially discussed. Sintering is currently assumed to occur as combination of Ostwald ripening (through atom migration on the support) as well as particle migration and coalescence. Thus understanding of the restructuring processes and identification of possible reasons for long time deactivation is essential to improve the existing bimetallic Pd/Au catalyst system.

1.1. Vinyl acetate synthesis – industrial application

The first reported industrial process for the synthesis of vinyl acetate was performed over a carbon supported zinc acetate catalyst as a gas-phase acetoxylation of acetylene. The process was based on the synthesis invented by the chemist Fritz Klatte, patented in 1913[5] and exhibited high activity and selectivity levels, reaching yields with respect to acetylene ranging from 92 to 98 %. The application of polymerized vinyl acetate as replacement for e.g celluloid was patented in the same year.[6] Scheme 1-1 illustrates the gas-phase acetoxylation of acetylene. The process exhibits a reaction enthalpy of -118 kJ/mol and was operated at temperatures between 170 °C and 250 °C.[7]
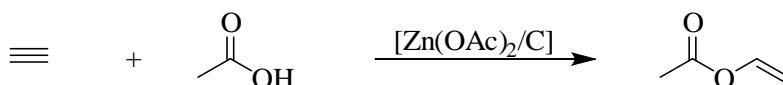
Scheme 1-1: Gas-phase acetoxylation of acetylene.

Despite the high selectivity and activity levels, the cost and explosiveness of acetylene led to a replacement of the acetoxylation of acetylene by the acetoxylation of ethylene.[8] Moiseev[9] and Smidt[10] were the first to report a homogeneous, liquid phase process based on $Pd(OAc)_2$ and a co-catalyst such as $CuCl_2$. In this homogeneous process vinyl acetate is formed via reaction of ethylene with palladium acetate, leading to reduction of Pd^{2+} species to Pd^0.[11] Pd^0 then is re-oxidized by the co-catalyst, which itself is re-oxidized by O_2. Typical reaction conditions are 100 – 130 °C and 30 to 40 atm total pressure. Scheme 1-2 illustrates the liquid-phase acetoxylation of ethylene.
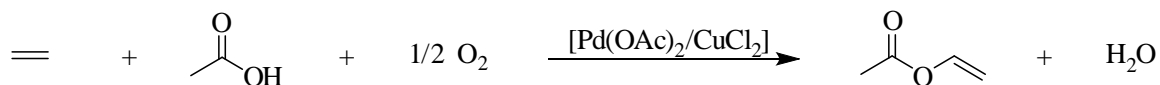
Scheme 1-2: Liquid-phase acetoxylation of ethylene.

The process used for the liquid-phase acetoxylation of ethylene is similar to the reaction steps in the homogeneous formation of acetaldehyde via the Wacker process.[12,13]

The liquid-phase acetoxylation of ethylene was transformed into a heterogeneous gas-phase process in the late 1960s, which was developed by Hoechst[14] and Bayer[15].

Catalysts used in the gas phase process were based on supported palladium particles, whereby the catalyst was additionally impregnated with a Mg^{2+} salt (Hoechst) or an alkaline earth metal acetate (Bayer).

Nowadays vinyl acetate is produced on a large scale via a gas-phase acetoxylation process.[16,17,18] Scheme 1-3 illustrates the three component reaction. For this heterogeneous, ethylene based process the reaction enthalpy reaches a value of -176 kJ/mol.
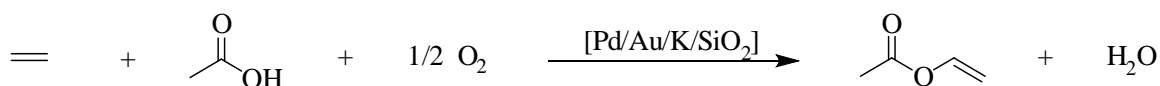
Scheme 1-3: Heterogeneous gas-phase acetoxylation of ethylene.

Industrially applied reaction conditions are within a temperature range of 150 °C to 190 °C and a pressure range of 5 to 10 atm.[19] The mainly used catalyst system is based on SiO_2 supported bimetallic Pd/Au catalysts promoted with potassium acetate.[18,20] With these catalysts high activity levels, combined with high selectivity and stability levels are achieved.

The main side reaction observed over bimetallic Pd/Au catalysts is the total oxidation of ethylene. Moreover combustion of acetic acid was found to be promoted by palladium.[21] Scheme 1-4 illustrates both combustion reactions, together with the respective reaction enthalpy.
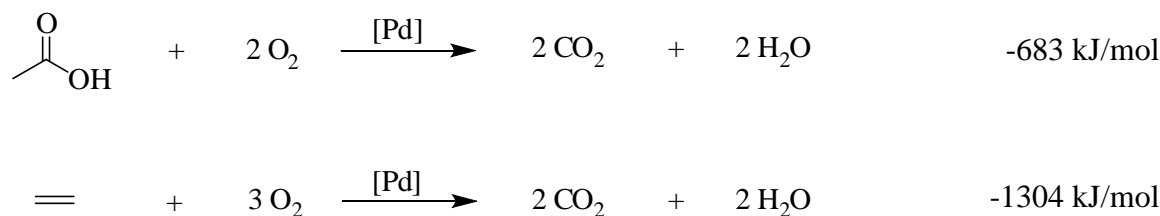
Scheme 1-4: Main side reactions in vinyl acetate synthesis.

1.2. Pd based catalyst system

1.2.1. Vinyl acetate synthesis over monometallic Pd catalysts

With the replacement of acetylene by ethylene as reactant for vinyl acetate synthesis, palladium based catalyst systems were used. For the initially performed homogeneous process, Pd^{2+} salts (e.g. $PdCl_2$) dissolved in acetic acid together with $CuCl_2$ were applied.[22,11,9] However yields to vinyl acetate were low and with increasing amount of water the formation of acetaldehyde (similar to the Wacker process) was promoted. With the introduction of an alkaline earth metal salt, the yield to vinyl acetate was significantly improved.[23]

For the heterogeneous gas-phase process, supported palladium catalysts with an excess of alkaline earth metal acetate, such as sodium acetate or potassium acetate, were used. Samanos et al.[24] investigated the size dependence for the supported monometallic palladium particles and found that the vinyl acetate formation first increases with increasing dispersion, reaches a maximum at particle sizes of ~ 2-3 nm and decreases to very low values for high dispersion levels. This trend was explained with a liquid surface layer present under reaction conditions consisting of water, acetic acid and vinyl acetate, which covers small palladium particles and thus inhibits the reaction on the metallic surface. This assumption was supported by a variation of the support. For alumina supported palladium catalysts with high dispersion, suitable activity towards vinyl acetate formation was found. This discrepancy between silica and alumina based catalysts was attributed to different adsorption properties of acetic acid and water. On alumina, the liquid surface layer is not as pronounced as on silica and thus less particles are covered with liquid and hence less particles are inaccessible for gaseous reactants. Han et al.[25] also studied particle size effects for vinyl acetate synthesis over Pd/SiO_2. With particle sizes ranging from 2.8 – 3.8 nm before reaction and 3.7 to 4.2 nm after reaction, an increase in vinyl acetate formation with increasing dispersion was observed.

Regarding deactivation over monometallic palladium catalysts, palladium carbide formation[25] was reported to be the reason for deactivation, besides particle sintering. Moreover it was found that palladium carbide formation is less pronounced for smaller particles.[26] Activation energies found over monometallic palladium catalysts vary with

size, with higher values for smaller particles. For example, an activation energy of approximately 39 kJ/mol was found for 1.0 wt.-% Pd/SiO_2 (dispersion 40 %), whereas only 17 kJ/mol were found for 5.0 wt.-% Pd/SiO_2 (dispersion 30 %). Samanos et al.[24] found 30.5 kJ/mol for 2.0 wt.-% Pd/SiO_2, which is in line with increasing activation energies for decreasing particle sizes. Augustine and Blitz[27] determined activation energies in dependency of acetic acid partial pressure. They observed decreasing activation energies with increasing partial pressure, ranging from 29.3 to 10.8 kJ/mol. The influence of the reactant concentrations was found to be different for C_2H_4 and O_2. Samanos et al.[24] and Nakamura et al.[28] found positive reaction orders with respect to C_2H_4, with a positive influence on selectivity. The positive influence of high ethylene partial pressures on the selectivity was supported by Gao et al.[29], who found that ethylidyne species, present on the metallic surface are not involved in the reaction pathway, but inhibit vinyl acetate decomposition. However Han et al.[25] found negative effects of increasing C_2H_4 partial pressure for both vinyl acetate reaction rate and selectivity. A possible explanation for the findings of Han et al. is the relatively low O_2 concentration used in this study and the resulting low surface coverage of O_2. With originally low coverage of O_2, an increasing coverage of C_2H_4 results in an insufficient O_2 surface concentration via additional blockage of the dissociative adsorption of O_2. Zero-order dependence for acetic acid over monometallic palladium catalysts was demonstrated by several authors[27,25,24], however a minimum acetic acid partial pressure of approximately 8 vol.-% is necessary to reach the necessary AcOH coverage.

1.2.2. Vinyl acetate synthesis over bimetallic Pd/Au catalysts

The introduction of Au to the Pd based catalyst system for vinyl acetate synthesis led to higher activity and especially stability[30] via ligand and structural effects.[31] Due to the outstanding properties of the bimetallic catalysts, nowadays research focuses on the properties of bimetallic PdAu particles and possible reasons for the observed improvements in vinyl acetate synthesis.

1.2.2.1. Properties of the Pd-Au system

In general, the physicochemical properties of Pd and Au exhibit pronounced similarities. Pd and Au have similar electronegativities, metal radii and number of valence electrons.[32] Moreover the mixing enthalpies for Pd and Au are positive and of equal order and thus a pronounced phase separation is not expected.[33,34] The lattice parameter for pure Pd is 0.389 nm and for pure Au 0.408 nm. The lattice parameter for the alloys vary according to Vegard's law[35], with a small deviation of 0.0004 nm at about 30 at.-% Pd.[36] Okamoto and Massalski[37] studied the alloy stability of the Pd-Au system and reported an ordering in the solid solution phase for Au_3Pd, $AuPd_3$ and, at lower temperatures, also for Au_1Pd_1. Au_3Pd and $AuPd_3$ show an ordered $L1_2$ structure, whereas the structure for the Au_1Pd_1 phase was considered to be the $L1_0$ phase.[38] The proposed phase diagram is shown in Figure 1-1.
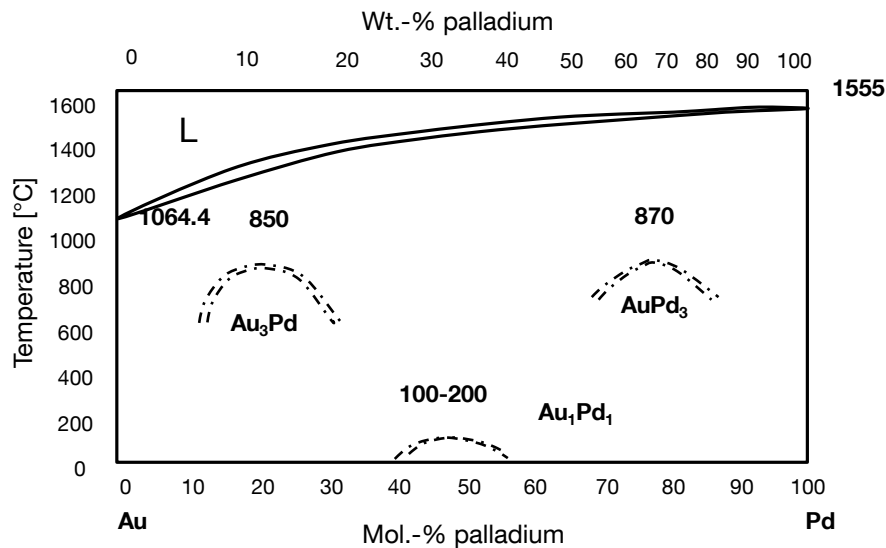
Figure 1-1: PdAu phase diagram proposed by Okamoto and Massalski.

Sluiter et al.[39] proposed based on ab initio studies that Au-Pd alloys show mainly the <1 1/2 0> type ordering with a possibility for the existence of long-period superlattices. Moreover they reported lower order-disorder temperatures T_c's for Au_3Pd and $AuPd_3$ than Okamoto and Massalski and an order-disorder temperature for the equimolar Pd_1Au_1 alloys of lower than 200 °C. The proposed stable phases with long rang order were recently supported by Zhu and Hou[40], who investigated the role of mechanical stress, induced by an inhomogeneous stress field displayed at equilibrium, on the chemical

ordering of Pd-Au nanoalloys for 309 and 561 atom clusters. Three stable phases in good agreement to the Pd-Au phase diagram were identified, which correspond to well defined plateaus in the chemical potential as a function of the Pd fraction present. Similar ordered phases were found by Atanasov and Hou[41] for 923 atom clusters. For cuboctahedral clusters the formation of ordered phases was found to be driven by the negative mixing enthalpy. The stress field which would provoke a disordering does not overcome the ordering. Another theoretical study addressed effective pair interactions between palladium and gold and showed a maximum for a composition of $Au_{0.6}Pd_{0.4}$.[33] The preference for a $Au_{0.6}Pd_{0.4}$ alloy composition is confirmed by calculations of heat of mixing minima by Weinberger et al.[34] Moreover Mohri et al.[38] simulated heats of alloy formations, taking thermal vibrational effects into account, and also obtained a preferred formation for $Au_{0.6}Pd_{0.4}$ composition.

Besides bulk properties as described above, several studies focused on the surface compositions and possible enrichments of one metal over the other. Christensen et al.[42] presented a Pd-Au phase diagram for surface alloys, which was constructed from surface energies as a function of the corresponding composition. The calculated segregation energy for Pd on Au was found to be positive, whereas it is negative for Au on Pd. Thus Pd preferentially diffuses into the bulk, whereas Au remains in the surface layer. For evaluation of the mixing degree in the surface layer, the curvature of the equation for the surface energy per surface atom was used. It was calculated to be positive for both Pd on Au and Au on Pd, whereby it is higher for Pd on Au. Thus, in the case of low bulk diffusion, surface mixing of the two metals is preferred. Soto-Verdugo and Metiu[43] additionally calculated the relative energies for palladium atoms in the surface layer and in the bulk, using density functional theory. The results are in good agreement to the experimental data by Goodman[44], who assigned high activity levels for vinyl acetate formation over bimetallic PdAu catalysts to the existence of closely neighboring Pd atoms (palladium monomer pairs). Soto-Verdugo and Metiu did not find any interaction between Pd atoms and concluded that the formation of large Pd ensembles is not favored. Via characterization of different sizes of PdAu bimetallic particles, Ferrer et al.[45] found that the degree of alloying is dependent on the particle size. For particles smaller than 5 nm, an alloyed core and a weakly palladium rich outer shell was detected by STEM-

XDS line scanning, whereas larger particles showed clear segregation in form of a three layer structure, with high palladium concentrations in the inner core and the outer shell. The intermediate layer, in contrast, was found to be highly gold rich. A recent study by Bulushev et al.[46] describes the formation of PdAu alloys dependent on the applied Pd_xAu_y composition during synthesis. For low concentrations of Au a surface enrichment in Au was detected. At a composition of Pd_2Au_1, surface and bulk compositions were found to be identical. With a further increase in Au concentration, the surface maintains a composition of Pd_2Au_1 and consequently an increased Au content in the particle core is observed. However it was stated that this core-shell structure is not equilibrated, since atomic diffusion processes are slow at low temperatures (maximum temperature during synthesis 137 °C).

1.2.2.2. Reaction properties of bimetallic PdAu catalysts

The addition of Au to the monometallic palladium catalyst system led to several important improvements in the reaction performance, including a boost in production rate[47] and an improvement in intrinsic selectivity towards vinyl acetate[48]. Provine et al.[49] systematically studied the role of Au in the catalysis of vinyl acetate by comparing monometallic Pd and bimetallic PdAu catalysts with and without additional impregnation of KOAc and found an improved reactivity of a factor of 5-7. Besides activity and selectivity levels, especially the catalyst stability is enhanced for bimetallic PdAu catalysts. As mentioned above, deactivation over monometallic palladium catalysts was partially attributed to the formation of PdC_x[50] and a related alteration of bulk and surface properties[51]. Han et al.[50] addressed the formation of PdC_x species in bimetallic PdAu catalysts and compared Pd/SiO_2 and $PdAu/SiO_2$ samples after reaction via XPS and XRD studies. The interaction of carbon with the bimetallic catalyst was found to be significantly weaker than it was observed for the monometallic samples. Pd carbide formation was not detected for alloyed PdAu particles. Moreover it was shown that bimetallic catalysts exhibit different dependencies on reactant concentrations and temperature. Han et al.[20] determined a negative influence of C_2H_4 partial pressure for monometallic palladium catalysts and a positive reaction order with respect to C_2H_4 of 0.35 for a Pd/Au bimetallic sample with a molar ratio of 4.0. Moreover an increase in

selectivity was observed with increasing partial pressure of C_2H_4. This effect was attributed to a coverage of C_2H_4 over bimetallic samples which is far from saturation. With increasing coverage of C_2H_4 and simultaneously decreasing coverage of O_2, less total oxidation of C_2H_4 takes place, which favors the formation of vinyl acetate monomer. The reaction order with respect to O_2 was found to be more positive for bimetallic samples than observed over monometallic ones[20] and a decrease in selectivity with increasing O_2 concentration was observed over the bimetallic sample. For comparable reaction conditions and O_2 concentration the vinyl acetate selectivity decreased from approximately 92 to 77 % for monometallic Pd samples[52], whereas a significantly less severe decrease from 93 to 86 % was found over a bimetallic PdAu sample with a PdAu molar ratio of 4.0[20]. Similar to findings over monometallic catalysts, the influence of acetic acid was found to be of zero order.[20] Kinetic studies over PdAu catalysts with a Pd/Au molar ratio of 4.0 by Motahari et al.[53] show similar trends for the dependency on reactant concentrations.

The temperature dependence over bimetallic samples exhibits a different behavior compared to monometallic ones. Over bimetallic samples a severe change in the selectivity regime was observed for elevated temperatures[20]. At higher temperatures the formation of CO_2 is favored over the formation of vinyl acetate monomer. Gerberich et al.[54] studied the influence of PdAu alloy compositions on the oxidation of ethylene and found in a composition range of 16 - 75 at.-% Pd, that the initial rate was independent of the alloy composition, however CO_2 formation rates were two orders of magnitude lower than found over monometallic palladium.

The variations in the dependencies on reactant concentrations originate to a great extent from differences in adsorption properties. Li et al.[55] studied the adsorption of acetic acid on Au/Pd(111) surfaces and found that the adsorbed structures depend on the gold concentration. For Au concentrations above the equimolar composition, acetic acid does not form acetate spices but adsorbs and desorbs as intact molecule. For lower concentrations acetate species are formed. For catalysts with $0.5 - 0.17$ at.-% of Au η^1 acetate species were formed, and for even lower Au concentrations η^2 acetate species. Thus the electronic influence of Au on Pd leads to a decreased interaction between Pd and acetic acid. Figure 1-2 shows η^1 and η^2 acetate species.
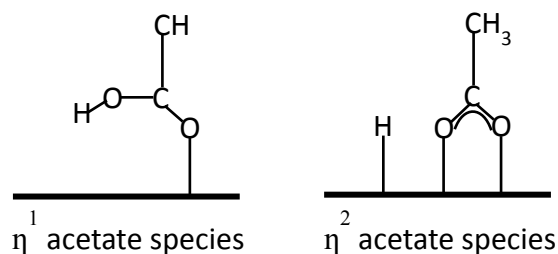
Figure 1-2: η^1 acetate and η^2 acetate species.

Calaza et al.[56] investigated the adsorption of C_2H_4 on a set of PdAu alloys. Similar to the adsorption of acetic acid, the Au concentration has an effect on the adsorption of C_2H_4. For high Au coverages (> 0.7) π-bonded ethylene on Au was observed. With decreasing Au concentration ethylene adsorbs π-bonded on the alloy surface, whereas the σ-π parameter is increasing. The σ-π parameter is defined to be zero for solely π-bonded C_2H_4 and 1 for solely σ-bonded C_2H_4.[57] Figure 1-3 shows the structure of σ-bonded and π-bonded ethylene.
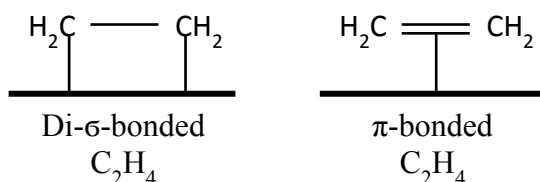
Figure 1-3: σ-bonded and π-bonded ethylene.

Even for very low Au concentration, π-bonded C_2H_4 is observed, while in contrast, only σ-bonded C_2H_4 was found by Stacchiloa et al.[58] on monometallic Pd(111), implying a pronounced impact of Au on the adsorption strength of C_2H_4 on Pd.

The influence of oxygen was studied via pre-adsorption of O_2 and sequential adsorption of acetic acid.[59] With pre-adsorbed oxygen, only η^2 acetate species were detected both over Pd(100) and Au/Pd(100), implying that the presence of oxygen facilitates acetate dehydrogenation. Moreover adsorbed oxygen stabilizes the adsorbed acetate.

Besides the reactants, the adsorption-desorption properties of the product are influenced by the surface composition of the bimetal. Li et al.[60] found that for high Au coverages, equivalent to the presence of palladium monomers (palladium atoms surrounded by gold

atoms), vinyl acetate adsorbs in a flat-laying geometry. Desorption form such palladium monomers includes only little decomposition. Pd-rich surfaces which exhibit large palladium ensembles, however favor decomposition of vinyl acetate. Adsorption on neighbored palladium takes place via a re-hybridization of the vinyl group and thus initial decomposition towards an acetate species and an adsorbed vinyl species is likely.

1.3. Active sites and reaction mechanism for vinyl acetate synthesis

1.3.1. Homogeneous pathway

The homogenous pathway to form vinyl acetate was invented in 1913 and firstly studied by Moiseev et al.[9] in 1960 who determined the active species to be Pd^{2+}. Kitching et al.[61] supported Pd^{2+} as active species in 1966 by performing various allyl acetoxylations and comparing the product distributions.

Industrially, a Pd^{2+} salt (e.g. $PdCl_2$ or $Pd(OAc)_2$) was dissolved in acetic acid and a copper salt was added as co-catalyst. In order to improve the yield towards vinyl acetate, additionally an alkaline promoter was added to the system.[23]

Grennberg et al.[62,63] studied palladium-catalyzed allylic acetoxylations and discovered the following reaction steps. After the coordination of the alkene to Pd^{2+}, a C-O bond is formed via a nucleophilic addition (acetoxypalladium complex). Afterwards the C-H bond is cleaved (β-H elimination) and a C-C double bond is formed. The now reduced palladium is regenerated by the co-catalyst, which itself is re-oxidized by O_2. Typical co-catalysts are copper chloride or the benzoquinone/hydroquinone redox-system.[64] Figure 1-4 illustrates the reaction scheme for the homogeneous pathway.
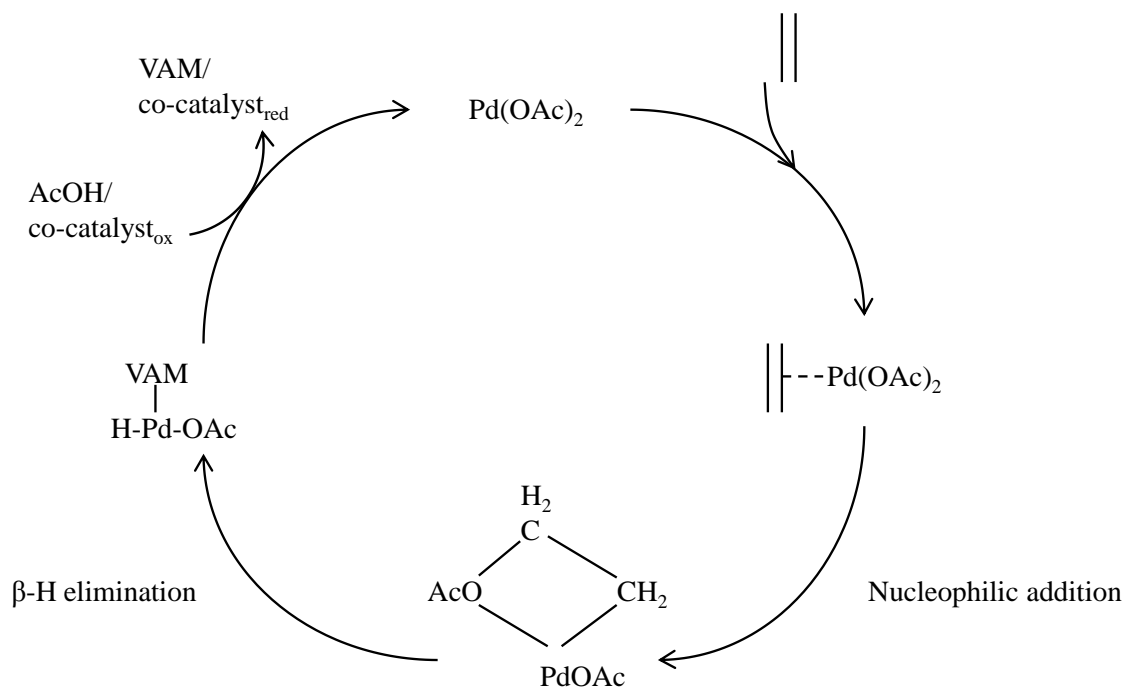
Figure 1-4: Reaction scheme of the homogenous pathway for vinyl acetate synthesis.

1.3.2. Heterogeneous pathway

1.3.2.1. Active species

Whereas the question concerning the active species in the homogeneous vinyl acetate synthesis is convincingly answered with a Pd^{2+} species, the active species is controversially discussed for the heterogeneously operated synthesis and has focused on Pd^0 and Pd^{x+} species. Vargaftik et al.[65] found an increase in selectivity towards vinyl acetate for Pd^0 species, originating from a drastic decrease in acetaldehyde formation. Because of the exclusive formation of vinyl acetate over Pd^0 they draw the conclusion that Pd^0 has to be the active species for vinyl acetate formation. However several other groups state that palladium acetate species are active for vinyl acetate synthesis. Augustine and Blitz[27] showed in DRIFT studies that $Pd(OAc)_2$ forms on Pd/Al_2O_3 catalysts under reaction conditions. However they observed significantly lower rates for pure $Pd(OAc)_2$, which was attributed to an interaction of metallic, respectively metal-oxide phases with islands of $Pd(OAc)_2$. This is supported by findings of Li et al.[60], who

stated that adsorbed oxygen promotes the dissociative adsorption of acetic acid. Besides Pd^{2+} species, Pd^+ species are discussed in literature. Nakamura et al.[28,66] state that Pd^+-OAc species form during reaction, presumably through the activation of associatively adsorbed acetic acid through the abstraction of hydrogen on palladium in the presence of oxygen.

With the introduction of Au to the palladium based catalyst system, additional geometric and electronic effects were introduced, which led to a more specific picture of the nature of active sites for vinyl acetate synthesis. The under 1.2.2.1 presented electronic alteration of Pd by Au can change the strength of Pd-adsorbate bonds.[67] However, so far experiments have not provided conclusive evidence of ligand effects in the synthesis of vinyl acetate.[68] In contrast, geometric effects emerging with the introduction of Au were shown to have crucial impact on vinyl acetate formation. Dilution of surface Pd atoms by catalytically inert Au atoms lead to modifications of the active ensembles required for vinyl acetate synthesis.[67,69] Via sterically preferred chemisorptions of the reactants,[70] overall catalytic activity, selectivity and stability are enhanced.[71] Single crystal studies be Goodman et al.[30] revealed the active PdAu ensemble. Various Pd amounts were deposited on Au(111) and Au(100) and a maximum TOF was found at a Pd coverage of approximately 0.07 monolayer (0.07 Pd atoms per substrate Au atom). However further increase in Pd coverage lead to a decrease in vinyl acetate production.

a)   b)
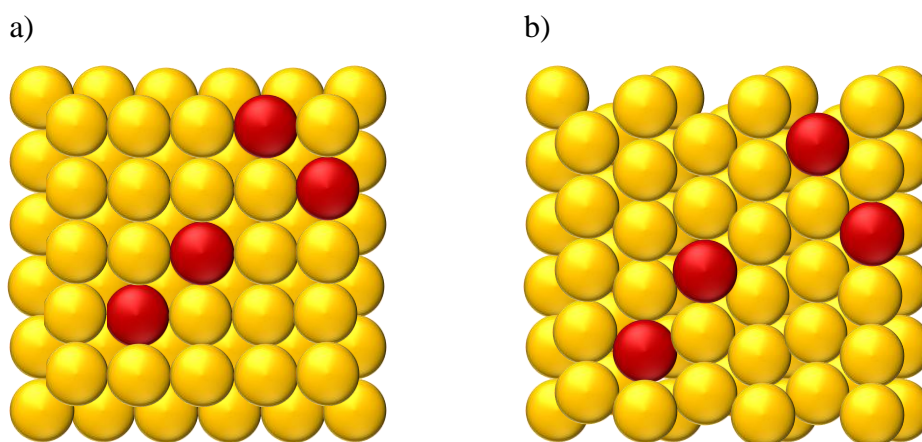
Figure 1-5: Palladium monomer pairs on a) Au(100) and b) Au(111). Yellow represents Au, red Pd.

By additionally comparing the activity levels over Pd/Au(111) and Pd/Au(100), the (100) facet was found to exhibit optimal distance for active ensembles in vinyl acetate synthesis. As a conclusion of these reactivity tests, the active ensemble for vinyl acetate synthesis consists of two noncontiguous, suitable spaced Pd surface monomers. Figure 1-5 illustrates palladium monomers on Au(100) and Au(111). On (100) facets the distance between to palladium monomers is 4.08 Å, whereas on a (111) surface plane two palladium monomers are separated by 4.99 Å. Since the theoretical optimized distance for the formation of vinyl acetate was determined to be 3.3 Å, the higher activity levels found over the (100) surface originate from a less sterically hindered reaction. Figure 1-6 illustrates the distance situation on the respective surface planes.
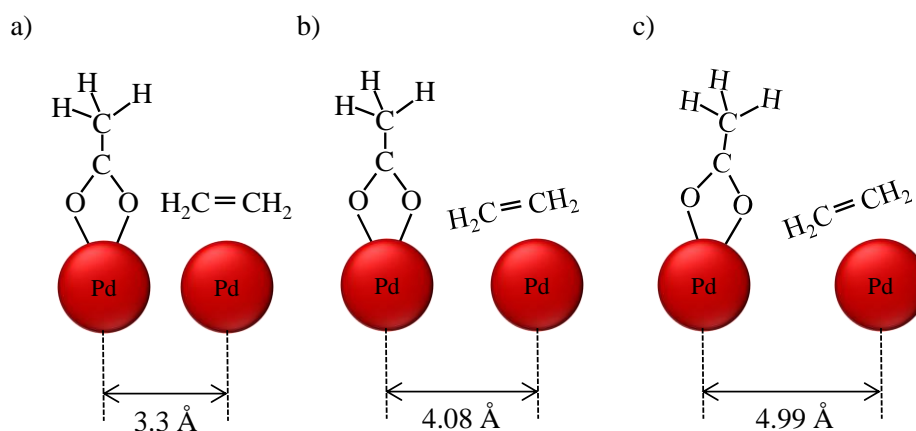
Figure 1-6: Palladium monomer pairs with a) ideal distance for vinyl acetate formation, b) distance on (111) surface plane and c) on (100) surface plane.

The proposed active surface ensemble was supported by CO-IRAS, STM and LEISS studies by Luo et al.[72]. Larger Pd ensembles, predominantly formed with increasing Pd coverage, which contain contiguous Pd atoms are less efficient than a pair of Pd monomers with a spacing of 4.08 Å. Thus the role of Au was stated to be mainly of geometric nature forming isolated Pd monomer sites that facilitate the coupling of critical surface species to form vinyl acetate. Since product formation is favored on Pd monomers in suitable distance, undesirable pathways to CO_2 and surface carbon are suppressed.[30,8] Besides the strong geometric effect, a minor ligand effect originating from the electronic alteration of palladium by gold was discussed to inhibit the decomposition of vinyl acetate and favor its desorption.[49, 73]

1.3.2.2. Reaction mechanism

Reaction pathways

In literature mainly two reaction pathways for the heterogeneously operated vinyl acetate synthesis have been discussed. As discussed in section 1.3.2.1, authors convincingly proposed that metallic palladium is oxidized either to form Pd^{2+}- or Pd^{+}-acetate species.[27,28,66] In the following the two reaction mechanism will be compared.

a) Reaction mechanism according to Nakamura.[28]

   Nakamura and Yasui proposed that in the gas phase vinyl acetate synthesis, the product is formed via the reaction of dissociatively adsorbed ethylene and dissociatively adsorbed acetic acid. They suggested that vinyl acetate is formed via the following steps:

   - Dissociative adsorption of ethylene (abstraction of one hydrogen, mono-adsorbed)
   - Dissociative adsorption of oxygen
   - Associative adsorption of acetic acid, while in the presence of oxygen, hydrogen is abstracted from acetic acid
   - Vinyl acetate formation via the combination of dissociatively adsorbed acetic acid and dissociatively adsorbed ethylene
   - Water is formed via combination of abstracted hydrogen and dissociatively adsorbed oxygen
   - The main byproduct CO_2 is formed via oxidation of dissociatively adsorbed acetic acid and dissociatively adsorbed ethylene by dissociatively adsorbed oxygen

These reaction steps were proposed on the basis of experiments concerning the adsorption of C_2H_4 on palladium in the absence of O_2 and adsorption of acetic acid with and without oxygen present. Figure 1-7 illustrates the reaction mechanism described by Nakamura and Yasui.
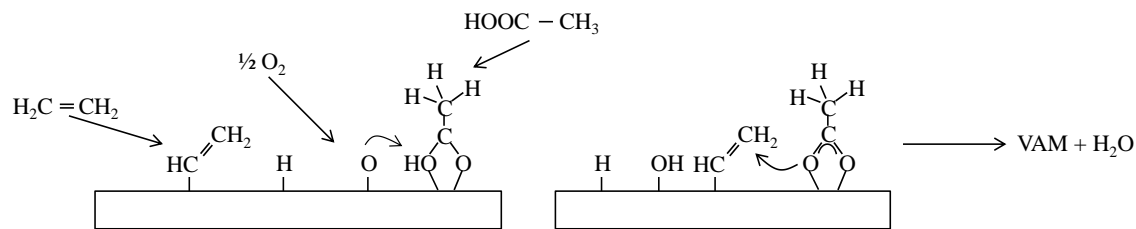
Figure 1-7: Illustration of the Nakamura pathway for vinyl acetate synthesis.

b) Reaction mechanism according to Samanos et al.[24]

Samanos et al. proposed a reaction mechanism which is similar to the one assumed for the homogenous reaction. Under typical industrial operating conditions, the adsorption of acetic acid and water on the support is substantial.[24] A liquid film of at least three monolayers was evident in isotopic transient kinetics and TPD studies.[74] According to Samanos et al. the formation of vinyl acetate proceeds according to the following steps:

- Oxidation of metallic palladium to form palladium acetate $Pd(OAc)_2$ (quadratic planar)
- Addition of a third acetate species to form $[Pd(OAc)_3]^-$ (octahedral coordination of three bidentate acetates)
- π-bonded or gas phase ethylene reacts with an adsorbed acetate nucleophile (ethyl acetate-like intermediate)
- Vinyl acetate monomer is formed via β-H elimination. Simultaneously Pd^0 is formed

Figure 1-8 illustrates the reaction steps included in the Samanos pathway.
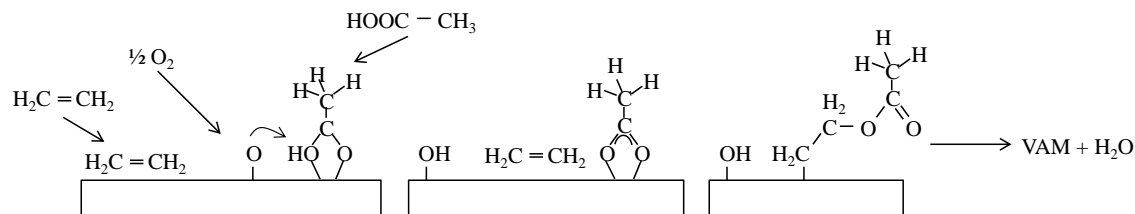
Figure 1-8: Illustration of the Samanos pathway for vinyl acetate synthesis.

Support for the direct insertion of ethylene into an adsorbed acetate species was found by Stacchiola et al.[75], who followed the formation of vinyl acetate from the reaction of ethylene with acetate species on an oxygen-covered Pd surface via RAIRS. Moreover experiments including D_2H_4, CHDCHD and CH_2CD_2 clearly support the Samanos pathway, since product distributions could only by rationalized via this mechanism.[76] Gao et al.[29] combined IR spectroscopy and isotope labeling experiments to proof reaction of gas phase ethylene with acetate species. Among other evidence, an IR feature at approximately 1718 cm^{-1} could not be rationalized via the surface species present in the reaction pathway proposed by Nakamura. However the intermediate acetoxyethyl-palladium species present in the Samanos pathway would induce such a feature. Moreover it was found, that the presence of ethylidyne species inhibits the decompositions of vinyl acetate.[29]

Rate determining step (rds)

Concerning the rate determining step, both Nakamura and Samanos describe the coupling of an ethylenic species with the acetate species to be the rate-determining step of the reaction. This is supported by quantum chemical Monte Carlo simulations from Neurock.[77] Gao et al.[29] confirmed via modeling of isotope labeled reactant concentration profiles that hydrogen has to be involved in the rds. Since the dissociative adsorption of ethylene was excluded before, the rate determining step in the formation of vinyl acetate has to be the β-H elimination. Calaza et al.[78] investigated coverage effects and the electronic origins of these coverage effects were explored using the evolution of frontier molecular orbitals from the reactant to the transition state on the basis of the Samanos pathway. The activation energies were calculated assuming the β-H elimination as rate

determining step and good agreement was obtained for measured and calculated values (measured: 55 ± 4 kJ/mol; calculated: 53 kJ/mol). Although the reaction order with respect to oxygen was found to be positive[20,25], a rate determining dissociative adsorption of oxygen is not likely.

1.4. Alkaline promoter

As already mentioned in chapter 1.1, alkaline promoters are necessary to reach high conversion and selectivity levels. In industry primarily potassium acetate is used in excess and has to be co-fed during the process, since it is removed from the catalyst with time on stream. In general alkali acetates are assumed to promote vinyl acetate formation by stabilizing reaction intermediates and activating palladium as the reactive site for vinyl acetate synthesis.

In the homogeneous reaction pathway palladium acetate is dissolved in acetic acid, whereby the Pd acetate can be present in three different conformations, depending on an equilibrium that is among other factors, controlled through the addition of alkali metal acetates.[79,80,81] Palladium trimers, which exhibit a structure similar to the one found for crystallites[11,82,83], are completely converted to dimers by a bimolecular nucleophilic substitution of acetate ions, respectively via acetate bridges of acetic acid molecules.[11] With increasing alkali metal concentration, trimers decompose completely to dimers, but do not decompose further to form monomers, since the dimer-monomer equilibrium is on the side of the dimer. By changing the concentration of the alkaline metal acetate, the equilibrium is affected, which simultaneously affects the selectivity and activity level. In general an increase in alkaline metal concentrations favors VAM formation, since with high alkaline acetate concentrations; the solution contains mainly catalytically active dimers. However, due to blocking of vacancies by acetate, a optimum concentration of MOAc exists.[79] Besides the concentration of alkaline metal acetate, the kind of alkaline metal determines the equilibrium. The concentration needed to completely convert all Pd acetate trimers to dimers is proportional to the solvation energy of the alkali metal cation. The higher this energy, the more the equilibrium is shifted in the direction of decomposed Pd acetate.[11] Scheme 1-5 illustrates the equilibria of the three palladium acetate species.

$$2\,Pd_3(OAc)_6 \;+\; 6\,MOAc \;\rightleftharpoons\; 3\,M_2 \;+\; 3\,[Pd_2(OAc)_6]^{2-}$$

$$M_2 \;+\; [Pd_2(OAc)_6]^{2-} \;+\; 2\,MOAc \;\rightleftharpoons\; 2\,M_2 \;+\; 2\,[Pd(OAc)_4]^{2-}$$
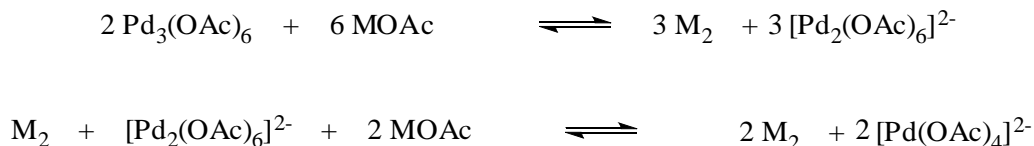
Scheme 1-5: Equilibria for palladium acetate monomer, dimer and trimer species influenced by MOAc.

For solutions containing KOAc and Pd acetate a monodentate ester-like configuration was observed via RAMAN spectroscopy.[84] Augustine and Blitz proposed this species to be a key intermediate in heterogeneous vinyl acetate synthesis.[27] Since the active species palladium is soluble in glacial acetic acid films present on the support under reaction conditions, whereby the formation of palladium acetate is favored under oxidizing conditions[11], the presence of acetate species which are similar to the homogeneous route is likely.

However, the role of MOAc was further discussed to be the retention of acetic acid within the liquid surface layer.[84,74,85] Immobilizing the acetic acid limits the direct combustion of ethylene and thus increases the reaction rate and selectivity towards VAM.[26]

On the surface of the catalyst electropositive promoters such as alkaline earth metals are present in an ionic state.[86,87] Thus the promoting effect of alkali metals is often interpreted to be of electronic nature. This is supported by findings of Gravelle-Rumeau-Maillot et al., who found that alkali addition to Pd/SiO$_2$, leads to very small variations of the initial heats of carbon monoxide and hydrogen adsorptions whereas infrared spectroscopy showed strongly modified adsorption modes, which was attributed to alterations in the palladium-adsorbate bond-strength.[88]

Pellegrini et al. reported that alkali metal promoters can affect the accessibility of the surface of the metal particles and the mobility of metal particles on the support. Via varying the dopant loading (KOAc), activation atmosphere and activation temperature it was shown that Pd^{2+} and KOAc show strong interaction leading to the presence of a mixed KPdO phase. Moreover promoters can facilitate or limit sintering during thermal treatments. The contact between the doping species and the support can cause covering of the metal particle by the support, affecting the availability of Pd.[89]

Summing up, for the homogeneous reaction pathway KOAc controls the equilibrium of unsaturated palladium trimers/dimers. For the heterogeneous pathway the formation of the ester-like, monodentate palladium dimer key intermediates is favored in the presence of KOAc.

1.5. Scope of this thesis

As described above, the synthesis of vinyl acetate monomer is an important industrial process, which has been widely studied. However catalyst deactivation by restructuring and sintering are important problems that limit long term usability and performance of the catalysts and are still not fully understood. In order to investigate the reconstruction processes and to improve catalyst stability, the work in this PhD thesis was divided in the following main topics.

- *Catalyst synthesis and catalytic evaluation*

  It is important to understand how different catalysts, especially in terms of varying Pd/Au molar ratios, affect the reaction in selectivity, activity and stability. Thus a catalyst series was prepared according to patented synthesis routes, ranging from Au-rich to highly Pd-rich catalysts, as they are mainly used in industry. Via normalization of the activity to the active sites, activity levels for alloyed and monometallic palladium will be compared. Ideally a first picture of active ensembles responsible for high selectivity, activity or stability can be drawn. Comparing the restructuring and deactivation behavior of Au-rich and Pd-rich catalysts in long-time studies will provide first information on possible reconstruction mechanisms.

- *Physicochemical characterization of as synthesized and reacted catalysts*

  Based on the findings in activity, selectivity and deactivation, a detailed physicochemical characterization can provide the parameters that distinguish a catalyst with high activity and high long-time stability. The as synthesized and reactively aged samples will be physicochemically characterized combining surface and bulk sensitive methods. CO adsorption at liquid nitrogen temperature will allow determining the degree of surface intermixing, whereas X-ray diffraction and X-ray absorption spectroscopy will be used to evaluate the bulk structure.

  By comparing catalyst properties before and after vinyl acetate synthesis, we will obtain a detailed picture of the restructuring processes, both during the first 20-30 hours time on stream and during long time experiments.

- *Temperature dependent in-situ characterization*

  As mentioned before, the PdAu system is believed to be highly temperature dependent. Especially the ordered phase Pd_1Au_1 is not stable at elevated temperatures. Via temperature dependent in-situ X-ray diffraction and X-ray absorption spectroscopy, the changes in the bimetallic bulk structure with temperature will be evaluated. Ideally this data further supports the established reconstruction mechanism. Since vinyl acetate synthesis is known to be highly structure sensitive, the obtained temperature stability data will be applied to further evaluate the activity, selectivity and stability of the catalyst and to identify active PdAu ensembles. Moreover the temperature-dependent characterization will be compared with temperature dependent deactivation, ideally leading to a full picture of reconstruction under reaction atmosphere.

- *Determination of kinetic parameters*

  Based on the physicochemical characterization and the established reconstruction mechanism, kinetic experiments to further understand the catalyst system will be designed. Kinetic measurements will include e.g. activation energies. Results will be interpreted based on the detailed characterization of the catalyst series. Kinetic data sets for Au-rich and Pd-rich catalysts will be compared to monometallic reference catalysts, which will be designed according to the established reconstruction mechanism. Via comparing kinetic parameters for Au-rich and Pd-rich bimetallic catalysts with monometallic references, the respective role of bimetallic ensembles and monometallic phases in the formation of vinyl acetate will be assigned. Once ensembles providing high stability, activity and selectivity are identified, an improved catalyst can be designed.

1.6. References

1.   http://wwwatsdr.cdc.gov/ToxProfiles/tp59-c4.pdf.

2.   http://www.sriconsulting.com/WP/Public/Reports/vam/.

3.   S. A. Miller, *Ethylene and its industrial derivatives,* Benn, London, **1969**.

4.   B. Elvers, S. Hawkins, *Ullman's Encyclopedia of Industrial Chemistry, Vol. A27*, VCH Verlagsgesellschaft GmbH, Weinheim, **1996**.

5.   F. Klatte (Griesheim-Elektron), *AT 69321B*, **1913**.

6.   F. Klatte (Griesheim-Elektron), *DE 281687A*, **1913**.

7.   H.-J. Arpe, *Industrielle organische Chemie, Vol. 6*, Wiley-VCH, Weinheim, **2007**.

8.   D. Kumar, M. S. Chen, D. W. Goodman, *Catalysis Today* **2007**, *123*, 77.

9.   I. I. Moiseev;, M. N. Vargaftic;, Y. K. Syrkin, *Doklady Akademii Nauk SSSR* **1960**, *133*, 377.

10.   J. Smidt, W. Hafner, R. Jira, R. Sieber, J. Sedlmeier, A. Sabel, *Angewandte Chemie International Edition in English* **1962**, *1*, 80-88.

11.   D. D. Kragten, R. A. van Santen, M. K. Crawford, W. D. Provine, J. J. Lerou, *Inorganic Chemistry* **1999**, *38*, 331-339.

12.   J. Smidt, W. Hafner, J. Sedlmeier, R. Jira, R. Rüttinger (Consortium für elektrochemische Industrie G.m.b.H.), *DE 1049845 B*, **1959**.

13.   J. Smidt, W. Hafner, R. Jira, J. Sedlmeier, R. Sieber, R. Rüttinger, H. Kojer, *Angewandte Chemie* **1959**, *71*, 176-182.

14.   H. Fernholz, L. Hornig, T. Quadflieg, H.-J. Schmidt, F. Wundern (Farbwerke Hoechst A.G.), *US 3658888 A*, **1968**.

15.   W. Krönig, B. Frenz (Farbenfabrik Bayer A.G.), *GB 1117595 A*, **1965**.

16.   T. C. Bissot (E. I. Du Pont de Nemours and Company), *US 4048096*, **1977**.

17.   W. Dafinger, P. Holl, J. Guba (Wacker-Chemie GmbH), *DE 10064084 B4*, **2005**.

18.   H.-J. Eberle, R. Heidenreich, J. Weis (Wacker-Chemie GmbH), *DE 10200605800 A1* Germany, **2008**.

19.   D. Kumar, Y. F. Han, M. S. Chen, D. W. Goodman, *Catalysis Letters* **2006**, *106*, 1-5.

20.   Y. F. Han, J. H. Wang, D. Kumar, Z. Yan, D. W. Goodman, *Journal of Catalysis* **2005**, *232*, 467.

21.   M. Chen, D. W. Goodman, *Chinese Journal of Catalysis* **2008**, *29*, 1178-1186.

22.   C. R. Reilly, J. J. Lerou, *Catalysis Today* **1998**, *41*, 433-441.

23.   P. Henry, *Palladium Catalyzed Oxidation of Hydrocarbons*, D. Reidel, Boston, **1980**.

24.   B. Samanos, P. Boutry, R. Montarnal, *Journal of Catalysis* **1971**, *23*, 19-30.

25.   Y. F. Han, D. Kumar, D. W. Goodman, *Journal of Catalysis* **2005**, *230*, 353.

26.   D. Kumar, M. S. Chen, D. W. Goodman, *Catalysis Today* **2007**, *123*, 77-85.

27.   S. M. Augustine, J. P. Blitz, *Journal of Catalysis* **1993**, *142*, 312-324.

28.   S. Nakamura, T. Yasui, *Journal of Catalysis* **1970**, *17*, 366.

29.   F. Gao, Y. Wang, F. Calaza, D. Stacchiola, W. T. Tysoe, *Journal of Molecular Catalysis A: Chemical* **2008**, *281*, 14-23.

30.   M. Chen, D. Kumar, C.-W. Yi, D. W. Goodman, *Science* **2005**, *310*, 291-293.

31.   G. A. Somorjai, Y. Li, *Introduction to Surface Chemistry and Catalysis*, *2 ed.*, John Wiley and Sons, New York **1994**.

32.   H. P. Myers, L. Walldèn, Ã. Karlsson, *Philosophical Magazine* **1968**, *18*, 725 -744.

33.   P. Weinberger, C. Blaas, B. I. Bennett, A. M. Boring, *Physical Review B* **1993**, *47*, 10158-10163.

34.   P. Weinberger, J. Kudrnovsky, J. Redinger, B. I. Bennett, A. M. Boring, *Physical Review B* **1993**, *48*, 7866-7871.

35.   L. Vegard, *Zeitschrift für Physik* **1921**, *5*, 17-26.

36.   A. Maeland, T. B. Flanagan, *Canadian Journal of Physics* **1964**, *42*, 2364.

37.   H. Okamoto, T. Massalski, *Journal of Phase Equilibria* **1985**, *6*, 229-235.

38.   T. Mohri, S. Takizawa, K. Terakura, *Journal of Physics: Condensed Matter* **1993**, *5*, 1473.

39.   M. H. F. Sluiter, C. Colinet, A. Pasturel, *Physical Review B* **2006**, *73*, 174204.

40.   B. Zhu, M. Hou, *The European Physical Journal D* **2012**, *66*, 63.

41.   I. S. Atanasov, M. Hou, *The European Physical Journal D* **2009**, *52*, 51-54.

42.   A. Christensen, A. V. Ruban, P. Stoltze, K. W. Jacobsen, H. L. Skriver, J. K. Nørskov, F. Besenbacher, *Physical Review B* **1997**, *56*, 5822-5834.

43.   V. Soto-Verdugo, H. Metiu, *Surface Science* **2007**, *601*, 5332-5339.

44. M. S. Chen, D. W. Goodman, *Catalysis Today* **2006**, *111*, 22-33.

45. D. Ferrer, A. Torres-Castro, X. Gao, S. Sepúlveda-Guzmán, U. Ortiz-Méndez, M. José-Yacamán, *Nano Letters* **2007**, *7*, 1701-1705.

46. D. A. Bulushev, S. Beloshapkin, P. E. Plyusnin, Y. V. Shubin, V. I. Bukhtiyarov, S. V. Korenev, J. R. H. Ross, *Journal of Catalysis* **2013**, *299*, 171-180.

47. H. Erpenbach, H. Glaser, K. Sennewald, W. Vogt (Knapsack A.G.), *3631079 A*, **1986**.

48. W. J. Bartley, G. G. Harkreader, S. Jobson, M. Kitson, M. Lemanski (BP Chemicals Limited), *US 5274181 A*, **1992**.

49. W. D. Provine, P. L. Mills, J. J. Lerou, *Studies in Surface Science and Catalysis,* **1996**, *101*, 191-200.

50. Y. F. Han, D. Kumar, C. Sivadinarayana, A. Clearfield, D. W. Goodman, *Catalysis Letters* **2004**, *94*, 131.

51. A. Sarkany, *Applied Catalysis A: General* **1998**, *175*, 245-253.

52. Y. F. Han, D. Kumar, C. Sivadinarayana, D. W. Goodman, *Journal of Catalysis* **2004**, *224*, 60.

53. K. Motahari, H. Atashi, F. Fazlollahi, F. F. Tabrizi, M. Sarkari, *Journal of Industrial and Engineering Chemistry* **2012**, *18*, 266-271.

54. H. R. Gerberich, N. W. Cant, W. K. Hall, *Journal of Catalysis* **1970**, *16*, 204-219.

55. Z. Li, F. Calaza, F. Gao, W. T. Tysoe, *Surface Science* **2007**, *601*, 1351-1357.

56. F. Calaza, F. Gao, Z. Li, W. T. Tysoe, *Surface Science* **2007**, *601*, 714-722.

57. E. M. Stuve, R. J. Madix, *The Journal of Physical Chemistry* **1985**, *89*, 3183-3185.

58. D. Stacchiola, L. Burkholder, W. T. Tysoe, *Surface Science* **2002**, *511*, 215-228.

59. Z. Li, W. T. Tysoe, *Surface Science* **2012**, *606*, 1934-1941.

60. Z. Li, F. Calaza, W. T. Tysoe, *Surface Science* **2012**, *606*, 1113-1119.

61. W. Kitching, Z. Rappoport, S. Winstein, W. G. Young, *Journal of the American Chemical Society* **1966**, *88*, 2054-2055.

62. H. Grennberg, J.-E. Bäckvall, *Chemistry – A European Journal* **1998**, *4*, 1083-1089.

63.	H. Grennberg, V. Simon, J.-E. Backvall, *Journal of the Chemical Society, Chemical Communications* **1994**, 265-266.

64.	J. J. Plata, M. n. García-Mota, A. A. C. Braga, N. r. López, F. Maseras, *The Journal of Physical Chemistry A* **2009**, *113*, 11758-11762.

65.	M. N. Vargaftik, V. P. Zagorodnikov, I. I. Moiseev, *Kinetika I Kataliz (trans)* **1981**, *22*, 951 - 955.

66.	S. Nakamura, T. Yasui, *Journal of Catalysis* **1971**, *23*, 315-320.

67.	S. N. Reifsnyder, H. H. Lamb, *The Journal of Physical Chemistry B* **1998**, *103*, 321.

68.	D. R. Rainer, C. Xu, P. M. Holmblad, D. W. Goodman, *Journal of Vacuum Science and Technology A* **1997**, *15*,1653-1662.

69.	E. L. Kugler, M. Boudart, *Journal of Catalysis* **1979**, *59*, 201-210.

70.	T. Wei, J. Wang, D. W. Goodman, *The Journal of Physical Chemistry C* **2007**, *111*, 8781-8788.

71.	M. S. Chen, K. Luo, T. Wei, Z. Yan, D. Kumar, C. W. Yi, D. W. Goodman, *Catalysis Today* **2006**, *117*, 37.

72.	K. Luo, T. Wei, C. W. Yi, S. Axnanda, D. W. Goodman, *The Journal of Physical Chemistry B* **2005**, *109*, 23517.

73.	R. Haley, M. Tikhov, R. Lambert, *Catalysis Letters* **2001**, *76*, 125-130.

74.	E. A. Crathorne, D. Macgowan, S. R. Morris, A. P. Rawlinson, *Journal of Catalysis* **1994**, *149*, 254-267.

75.	D. Stacchiola, F. Calaza, L. Burkholder, W. T. Tysoe, *Journal of the American Chemical Society* **2004**, *126*, 15384-15385.

76.	D. Stacchiola, F. Calaza, L. Burkholder, A. W. Schwabacher, M. Neurock, W. T. Tysoe, *Angewandte Chemie International Edition* **2005**, *44*, 4572-4574.

77.	M. Neurock, *Journal of Catalysis* **2003**, *216*, 73.

78.	F. Calaza, D. Stacchiola, M. Neurock, W. T. Tysoe, *Journal of the American Chemical Society* **2010**, *132*, 2202-2207.

79.	D. D. Kragten, R. A. van Santen, M. Neurock, J. J. Lerou, *The Journal of Physical Chemistry A* **1999**, *103*, 2756-2765.

80.	R. N. Pandey, P. M. Henry, *Canadian Journal of Chemistry* **1974**, *52*, 1241-1247.

81.   R. N. Pandey, P. M. Henry, *Canadian Journal of Chemistry* **1975**, *53*, 1833-1841.

82.   D. P. Bancroft, F. A. Cotton, L. R. Falvello, W. Schwotzer, *Polyhedron* **1988**, *7*, 615-621.

83.   S. D. Kirik, R. F. Mulagaleev, A. I. Blokhin, *Acta Crystallogaphica Section C* **2004**, *60*, m449-m450

84.   N. Macleod, J. M. Keel, R. M. Lambert, *Applied Catalysis A: General* **2004**, *261*, 37-46.

85.   M.-M. Pohl, J. Radnik, M. Schneider, U. Bentrup, D. Linke, A. Brückner, E. Ferguson, *Journal of Catalysis* **2009**, *262*, 314.

86.   S. Koukiou, M. Konsolakis, R. M. Lambert, I. V. Yentekakis, *Applied Catalysis B: Environmental* **2007**, *76*, 101-106.

87.   V. Pitchon, M. Guenin, H. Praliaud, *Applied Catalysis* **1990**, *63*, 333-343.

88.   M. Gravelle-Rumeau-Maillot, V. Pitchon, G. A. Martin, H. Praliaud, *Applied Catalysis A: General* **1993**, *98*, 45-59.

89.   R. Pellegrini, G. Leofanti, G. Agostini, L. Bertinetti, S. Bertarione, E. Groppo, A. Zecchina, C. Lamberti, *Journal of Catalysis* **2009**, *267*, 40-49.

Chapter 2

Dynamic self-organization of supported Pd/Au catalysts during vinyl acetate synthesis

It is known that vinyl acetate monomer synthesis over bimetallic Pd_1Au_1 catalysts is highly structurally sensitive and that these structures are dynamically formed and disintegrated in reactant gas atmosphere. Here we show via a combination of bulk and surface sensitive methods that independent of their nominal composition, Pd/Au bimetallic particles undergo marked reconstruction and phase partition during vinyl acetate synthesis. While temperature-induced reorganization of SiO_2-supported Pd_xAu_y particles leads to all three thermodynamically metastable phases, i.e., Pd_3Au, Pd_1Au_1, $PdAu_3$, with mainly Au-enriched surface compositions, the reactive atmosphere induces selectively the formation of the Pd_1Au_1 phase and separated Pd particles. The Pd in the Pd_1Au_1 has higher specific activity and selectivity than the sole Pd nanoparticles, exemplifying the importance of changing its electronic nature. As the Pd_1Au_1 phase dominates the catalytic activity, novel tailored catalysts could be produced, limiting the presence of dispersed Pd.

2.1. Introduction

PdAu bimetallic catalysts supported on oxides such as SiO_2 and Al_2O_3 are used in a variety of important processes, including vinyl acetate monomer (VAM) synthesis from acetic acid (AcOH), ethylene (C_2H_4) and oxygen (O_2).[1,2] Au acts as promoter without being alone catalytically active for this reaction, leading to higher selectivity, activity, and especially stability.[3] This has been attributed to ligands and structural (ensemble) effects.[4] Similar positive effects were induced by Au to Pd for the benzyl alcohol oxidation.[5]

The impact of Au on the catalytically active Pd has been widely studied and led to contradictory models for the active ensembles.[3] Specifically, the dynamic reconstruction during VAM synthesis is still unclear, but the insight would provide essential guidelines for the optimization of the catalyst, the catalyst pretreatment and the operation conditions. The physicochemical properties (electronegativity, metal radii, number of valence electrons) of palladium and gold are similar.[6] The mixing enthalpies for Pd and Au are positive and similar; thus phase separation is not expected.[7,8] On the other hand, three ordered phases are reported. Okamoto and Massalski[9], for example, describe solid phases with compositions of Au_3Pd_1, Au_1Pd_3 and, below 200ºC, Au_1Pd_1.[10] The authors reported relatively high ordering temperatures for Au_3Pd_1 and Au_1Pd_3 of 850 and 870°C, respectively, which were challenged by Sluiter et al.[11] indicating order-disorder temperatures for Au_3Pd_1 and Au_1Pd_3 between 400 and 500°C and an order-disorder temperature of the Pd_1Au_1 phase of 150°C. Since other fcc-based systems with two ordered phases A_3B_1 and A_1B_3 type show order-disorder temperatures twice as high as the one of an intermediate A_1B_1 structure, the phase diagram proposed by Sluiter appears more probable.

Christensen et al.[12] used the surface free energies to construct a Pd-Au phase diagram for surface alloys. The calculated segregation energies for Pd on Au were positive and negative for Au on Pd. Thus, Pd is expected to preferentially diffuse into the bulk, whereas Au should remain in the surface layer. For evaluation of the mixing degree in the surface layer, the curvature of the surface energy per surface atom was used. The curvature exhibits positive values for Pd atoms on Au and for Au atoms on Pd. Thus surface intermixing is preferred in both cases. However for Pd atoms on Au the curvature

is higher than for Au atoms on Pd, resulting in higher tendencies towards surface intermixing for Pd atoms in a Au-rich surface. The surface intermixing of Pd and Au was confirmed by Soto-Verdugo and Metiu[13], who calculated the relative energies for Pd atoms in the surface layer and in the bulk using density functional theory. These calculations are in good agreement with the experimental data of Goodman et al.[14], describing neighboring Pd atoms in a low index surface plane as active sites for vinyl acetate synthesis. Studying the impact of the particle size, it was demonstrated that high activity was found for Pd-Au particles between 2 and 4 nm. For smaller particles the concentration of Pd atoms on low index surfaces was too low, while for larger particles the metal dispersion was not sufficient to reach a high activity.

However, the surface composition depends also on the particle size. Ferrer et al.[15] observed a weakly enriched Pd outer shell on a bimetallic core for particles smaller than 5 nm, while larger particles had high Pd concentrations in the core and the outer shell, separated by a Au rich layer. Concerning the temperature dependence of ordered phases, Jiang et al.[16] showed a shape and size effect on the disorder-order temperatures for the Pd_3Au_1, Pd_1Au_3 and the Pd_1Au_1 phases of supported metal particles. Brückner et al.[17] addressed the changes in the particle morphology of supported PdAu catalysts for VAM formation at 155°C - 190°C in order to explore reasons for catalyst deactivation. Besides sintering, surface enrichment in Pd was observed qualitatively by IR spectroscopy of adsorbed CO samples aged at 155, 170°C and 190°C.

In order to understand the consequences and causes of the potential rearrangement of the metal partners in the alloy, we explore the reactant induced formation and restructuring of PdAu bimetallic particles supported on SiO_2 during vinyl acetate synthesis at a reaction temperature of 150 °C. For evaluation of the alloy formation, catalysts with Pd/Au molar ratios of 1.1, 2.0 and 6.0 were prepared. Potassium was added to the catalyst as KOAc, crucial for reaching high conversion levels by enhancing the adsorption of acetic acid monomers on the catalytically active Pd sites[18]. Fresh catalysts and used samples after 120 h time-on-stream were characterized by low temperature CO adsorption, X-ray absorption spectroscopy and X-ray diffraction. Samples were also characterized after thermal treatments in reducing and inert atmosphere.

2.2. Experimental section

2.2.1. Synthesis

Pd−Au/SiO$_2$ catalysts with Pd to Au molar ratios of 1.1, 2.0, and 6.0 were prepared via incipient wetness impregnation of SiO$_2$ with an aqueous solution of HAuCl$_3$ and PdCl$_2$ according to DE102006058800 A1,[19] which includes a precipitation with carbonate and subsequent washing with aqueous ammonia to remove chlorides. The Pd−Au/SiO$_2$ catalysts were reduced in flowing H2 at 300 °C for 1 h with a heating rate of 3 °C/min. Total metal loading for bimetallic samples is 3.0 wt.- %.

A model catalyst Pd(OAc)$_2$−KOAc on SiO$_2$ was prepared via incipient wetness impregnation of an aqueous Pd(OAc)$_2$ solution with a final Pd concentration of 1.5 wt.-%. After freeze-drying, aqueous KOAc solution was added via incipient wetness impregnation (potassium loading 5 wt.-%). The catalyst was subsequently freeze-dried and applied to vinyl acetate synthesis without any further treatment.

2.2.2. X-ray absorption spectroscopy

X-ray absorption spectroscopy measurements were conducted at HASYLAB, DESY, Hamburg, Germany, on the beamlines X1 and C. The storage ring energy was 4.5 GeV and the current decay during a typical fill was from 110 to 90 mA. The θ goniometer was equipped with a Heidenhain encoder within a tolerance of 10−5 °. The intensity of the higher order reflections was minimized by detuning the second crystal of the monochromator to 60 % of the maximum intensity. The Au L$_{III}$ (11919 eV) edge was measured with a pair of Si(111) crystals. For the Pd K edge (24350 eV) the monochromator was equipped with a pair of Si(311) crystals. The samples were prepared as self-supporting wafers, having a total absorbance of 2.0. The samples were flushed with He inside the sample chamber and cooled to liquid N$_2$ temperature. Prior to measurements the samples were rereduced in flowing H$_2$ at 300 °C for 1 h with a heating rate of 5 °C/min. After reduction the samples were flushed with He for 15 min at 300 °C. For EXAFS analysis, the scattering contributions in the pre- and postedge background were removed from the X-ray absorption by a third-order polynomial function. The oscillations were weighted with k^2 and Fourier transformed within the limits

$k = 2.1-12$ Å^{-1} for the Pd K edge and $k = 2.8-12$ Å^{-1} for the Au L$_{III}$ edge. XAS data processing and EXAFS analysis were performed using IFEFFIT 150 20 with the Horae package[21] (Athena and Artemis). The amplitude S$_o^2$, was derived from EXAFS data analysis of known references with known coordination numbers and was fixed during analysis (S$_o^2$ was found to be 0.9 for Au and 1.0 for Pd). The multiple-edge fitting was carried out with the constraints 1-3.[22]

$$N_{AuPd} = N_{PdAu} * x_{Pd}/x_{Au} \qquad\qquad\qquad (1)$$

$$d_{AuPd} = d_{PdAu} \qquad\qquad\qquad (2)$$

$$\sigma_{AuPd} = \sigma_{PdAu} \qquad\qquad\qquad (3)$$

2.2.3. Low temperature CO adsorption

The infrared spectra were recorded on a Vertex 70 spectrometer from Bruker Optics at a resolution of 4 cm^{-1}. The samples were prepared as self-supporting wafers with a density of 10 mg/cm^2. Samples were first activated in vacuum (1.0×10^{-7} mbar or less) at 300 °C for 1 h with a heating rate of 5 °C/min, cooled to room temperature, and subsequently re-reduced in 20 mbar H$_2$ at 300 °C with a heating rate of 5 °C/min. After re-reduction, the samples were outgassed at 300 °C in a vacuum for 30 min. After pretreatment of the samples, the system was cooled to −150 °C with liquid nitrogen in 10 mbar He added to enhance the thermal conductivity. At −150 °C a spectrum was taken, the cell was evacuated, and 1 mbar CO was introduced. To increase thermal conductivity, 10 mbar He was again added to the system. All spectra during CO adsorption were taken at −150 °C.

2.2.4. X-ray diffraction

X-ray powder diffraction measurements were conducted on a Philips X'Pert Pro System using Cu Kα radiation (0.154056 nm) generated at 45 kV and 40 mA. The samples were mounted on a rotating powder holder. The XRD patterns were measured in a 2θ range of 5°−70° with a step size of 0.019°/s. Data analysis was performed with High Score Plus software.

2.2.5. Reactor setup for vinyl acetate formation

Activity tests were performed in a 6-fold reactor setup at a temperature of 150 °C and a gas composition of 60 vol % C_2H_4, 13 vol % AcOH, 4.5 vol % O_2, and balance N_2. SiC was used as inert diluent to maintain a constant temperature over the whole catalyst bed. The diluent/catalyst ratio was chosen to be 10/1. The product stream was analyzed using a GC (model 2014 from Shimadzu), equipped with a Haysep Q and a molecular sieve column and a TCD detector.

2.3. Results and discussion

2.3.1. Activity behavior with time on stream of Pd/Au Catalysts

In order to evaluate activity and selectivity behavior of bimetallic samples with different Pd/Au ratios, samples were tested in vinyl acetate synthesis for 120 h timeon- stream. Figure 2-1 shows the production rates of vinyl acetate (a) and selectivity levels (b) as function of time-on-stream for the bimetallic Pd/Au catalyst synthesized according to ref 19 with a palladium loading of 1.5 wt.-% and a Pd/Au molar ratio of 2.0. A pronounced increase in vinyl acetate production was found during the first 25 h time-on-stream. The initial decrease in selectivity can be related to the significant increase in activity; however, after the initial decrease, the selectivity continuously increased up to a constant value of approximately 97.0 %. Thus, in the presence of the reactant atmosphere a reconstruction of the bimetallic samples toward a more active and more selective ensemble takes place. The restructuring process and the final active state of the catalyst was identified via characterization of samples after 120 h time-on-stream. The reconstruction was monitored using bulk and surface sensitive methods for fresh and reactively aged samples and is discussed in the following sections.
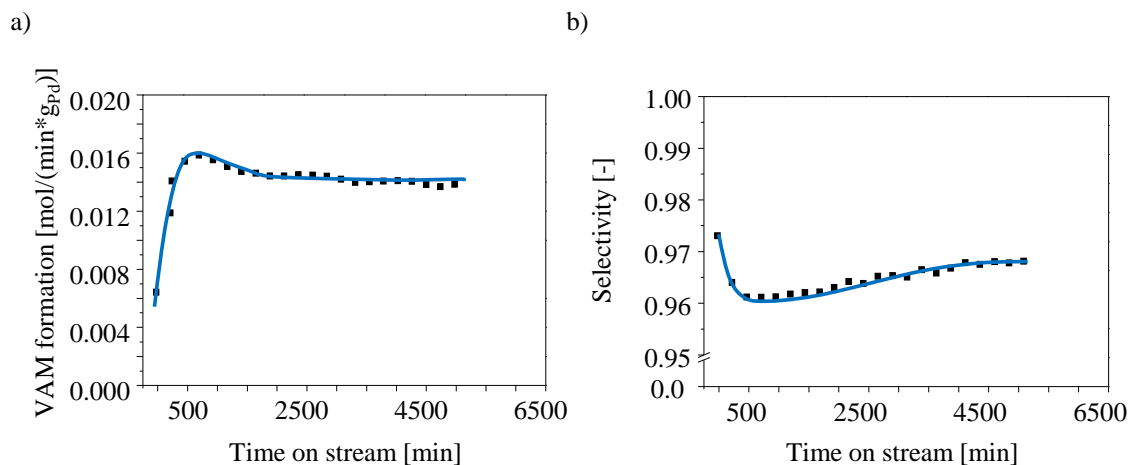
Figure 2-1: (a) Production rate and (b) selectivity with time-on-stream for Pd/Au 2.0−KOAc on SiO₂. Reaction conditions: 60 vol % C₂H₄, 13 vol % AcOH, 4.5 vol % O₂, balance N₂; total pressure, 8.8 bar; temperature, 150 °C.

2.3.2. X-ray diffraction

The X-ray diffraction patterns of fresh samples showed the presence of multiple Pd_xAu_y phases [Figure 2-2, fresh (green)], while after reaction at 150 °C for 120 h all catalysts showed only a single XRD reflection of a metal phase, specifically Pd_1Au_1 [Figure 2-2, used (blue)]. The phase compositions of the catalysts at steady state after 120 h on stream given in Table 2-2 were analyzed from XRD patterns by applying Vegard's law.[23] The phase compositions were averaged for the 111, 002, and 022 surface planes visible at 2θ = 38.3°−40.0°, 44.5°−46.7°, and 64.6°−67.9°. The deconvolution of the most distinct surface plane, the 111 surface, is shown in Figure 2-2. The differences between the phase compositions observed by XRD and the Pd/Au ratios used in the synthesis indicate that an X-ray amorphous Pd phase must be present after reaction. Its presence has also been postulated by Macleod et al.[24] The fraction of this highly dispersed Pd phase is given in Table 2-1 and was calculated on the basis of the chemical composition. We identified this monometallic phase as $Pd(OAc)_2$ phase via analysis of the water collected after washing the catalysts post usage. Because the formation of a Pd_1Au_1 phase and the concurrent formation of dispersed Pd were independent of the initially applied Pd/Au ratio, we conclude that the reconstruction occurs within a liquid surface layer consisting of acetic acid and water present under reaction conditions. Pd

atoms in Pd-rich particles are easier to be oxidized compared to Pd atoms in close proximity to Au.[25] Thus, especially in Pd-rich particles, the acetic acid environment formed Pd acetate, and Pd segregated to the surface and was subsequently dissolved.
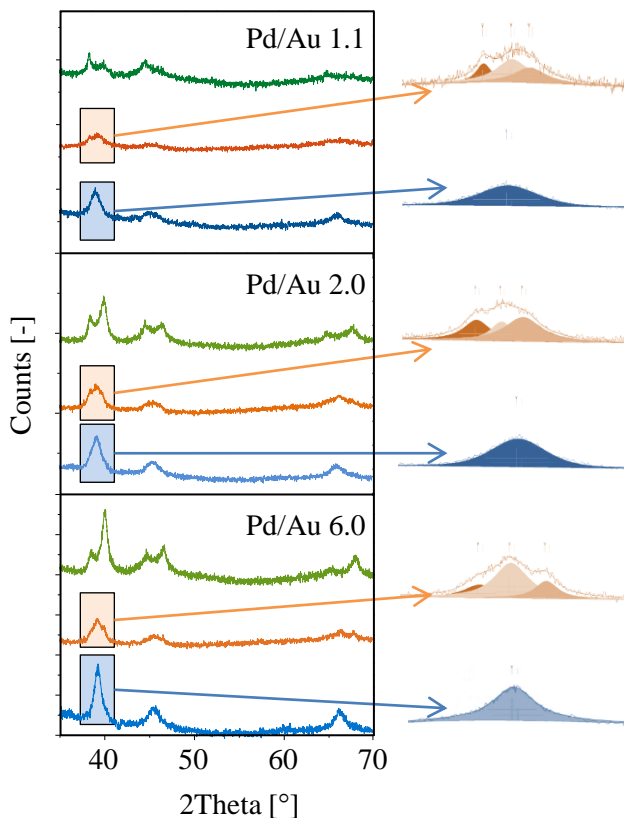
Figure 2-2: Left: X-ray diffraction profiles for fresh (green), thermally altered (orange), and used (blue) samples. Bimetallic phases of the corresponding planes are located in between those of the pure metals: Au(111) ($2\theta = 38.3°$), Pd(111) ($2\theta = 40.0°$), Au(002) ($2\theta = 44.5°$), Pd(002) ($2\theta = 46.7°$), Au(022) ($2\theta = 64.6°$), Pd(022) ($2\theta = 67.9°$). Right: deconvolution for the 111 surface plane of thermally altered (orange) and used (blue) samples.

Table 2-1: Concentrations of dispersed Pd after 120 hours on stream.

Pd/Au molar ratio	Fraction of dispersed Pd (Atom %)
1.1	3.8
2.0	39.4
6.0	70.9

The surface segregation of Pd in Pd_1Au_1 alloys induced by ligands favoring the interaction with Pd (e.g., CO) was already demonstrated by Soto-Verdugo and Metiu.[13] As soon as the surface of the bimetallic particle is highly intermixed, (electronic) effects of Au on Pd limit the oxidation of Pd, and thus, the dissolution of Pd from the bimetallic

particle is hindered. Moreover, the saturation of the liquid surface layer with $Pd(OAc)_2$ limits further dissolution of Pd. Both effects favor the formation of bimetallic particles with a bulk composition of Pd_1Au_1, which exhibits a high degree of surface intermixing. Please note that for initially less Pd-rich samples the composition of the bimetallic particles present during VAM synthesis can also be rich in Au due to additional removal of Pd from bimetallic particles with already high concentrations of Au. On the other hand, Pd can be deposited on Au-rich particles, e.g., via acetate bridges formed between dissolved Pd acetate and Pd in the surface layer of the bimetallic particle, and thus, a Pd-rich shell can be created. The increasing selectivity with time-on-stream (see Figure 2-1b) indicates that the bimetallic particles tend toward the formation of a more active ensemble, i.e., bimetallic particles of Pd_1Au_1 nature as discussed above. Among the three ordered bimetallic PdAu phases, the Pd_1Au_1 phase is the most selective for vinyl acetate formation. The Pd_3Au phase contains large surface ensembles of Pd atoms, which favor total oxidation of C_2H_4, while on the Au-rich $PdAu_3$ phase, too few Pd atoms in close proximity are present to form an appreciable concentration of the catalytically active ensembles.[2] To confirm that this specific reconstruction of the bimetallic particles toward a Pd_1Au_1 phase and a dispersed monometallic Pd phase occurred only under reaction conditions, the catalysts were subjected to a thermal treatment in He for 120 h. Changes in the composition of the bimetallic phase were not detected by XRD, which is attributed to the lower mobility of the metal atoms in the presence of partially oxidized Pd surface atoms formed during exposure to the (ambient) gas atmosphere. Without reduction of surface Pd−O species, the atoms in the bimetallic particles did not reconstruct.

In contrast, thermal treatment of the catalyst after reduction in H_2 led to the formation of three distinct intermetallic compounds (i.e., Au_1Pd_1, Au_3Pd, and $AuPd_3$), in agreement with the phase diagram discussed above.[9] In order to avoid Pd hydride formation, the thermal treatment in reducing atmosphere consisted of the reduction period (up to 300 °C) followed by flushing with He from 300 °C down to ambient temperature. This procedure decomposed the PdH phase formed during reduction in H_2 and yielded diffractograms with lattice parameters representing the respective Pd_1Au_1 alloy composition. Note that the presence of Pd hydride would expand the lattice of the metal

particles, leading to a shift of the X-ray diffraction peaks to lower angles. The relative fractions of the bimetallic phases present in the catalyst depend on the overall Pd/Au ratio of the catalyst and on the gas composition applied (Table 2-2).

Table 2-2: Alloy compositions determined by XRD of samples aged in reactant atmosphere and via thermal treatment.

Pd/Au molar ratio	Pd_xAu_y after 120 h on stream	Pd_xAu_y after thermal treatment in reducing atmosphere (with He flushing to remove Pd-H species)
1.1	$Pd_{0.42}Au_{0.58}$	$Pd_{0.17}Au_{0.83}$, $Pd_{0.51}Au_{0.49}$, $Pd_{0.81}Au_{0.19}$
2.0	$Pd_{0.47}Au_{0.53}$	$Pd_{0.12}Au_{0.88}$, $Pd_{0.52}Au_{0.48}$, $Pd_{0.80}Au_{0.20}$
6.0	$Pd_{0.51}Au_{0.49}$	$Pd_{0.20}Au_{0.80}$, $Pd_{0.48}Au_{0.59}$, $Pd_{0.81}Au_{0.19}$

2.3.3. Low-temperature CO adsorption

To characterize the surface composition of the bimetallic Pd−Au particles, the IR spectroscopy of CO adsorbed at −150 °C was used. Spectra of CO adsorbed on monometallic Au and Pd, as well as on the pure silica support can be found in the supporting information. Moreover pressure dependent CO adsorption on bimetallic samples ranging from 0.005 mbar to the maximum coverage at 1 mbar are shown in the Supporting Information. Before reaction, IR spectra showed two bands representing CO adsorbed linearly on Pd and two bands representing CO adsorbed linearly on Au (see Figure 2-3i). The band at 2090 cm^{-1} is attributed to CO adsorbed on Pd in larger monometallic domains (linear CO on Pd next to Pd). The band at 2060− 2040 cm^{-1} corresponds to CO adsorbed on Pd in close proximity to Au (linear CO on Pd next to Au). The exact peak position is dependent on the degree of intermixing between Pd and Au. CO linearly adsorbed on Au led to adsorption features between 2130 and 2100 cm^{-1}. Herein CO on Au that is mainly surrounded by Au (linear CO on Au next to Au) is found at 2100 cm^{-1} and CO adsorbed on Au that is in close contact to Pd is located at higher frequencies around 2130 cm^{-1}. On monometallic samples CO was found to adsorb linearly at 2098 cm^{-1} on Au and at 2094 cm^{-1} on Pd, which is in good agreement with literature.[26,27]

The frequency region below 2000 cm^{-1} represents CO that is adsorbed in multifold positions (bridged and 3-fold-hollow) on palladium. The intensity of the multifold adsorption features is dependent on the degree of surface mixing. For larger Pd

ensembles the probability of CO to adsorb in a multifold position is enhanced and thus the relative intensities of linear to multifold adsorbed CO are a direct measure for the degree of surface intermixing of palladium and gold.[27]
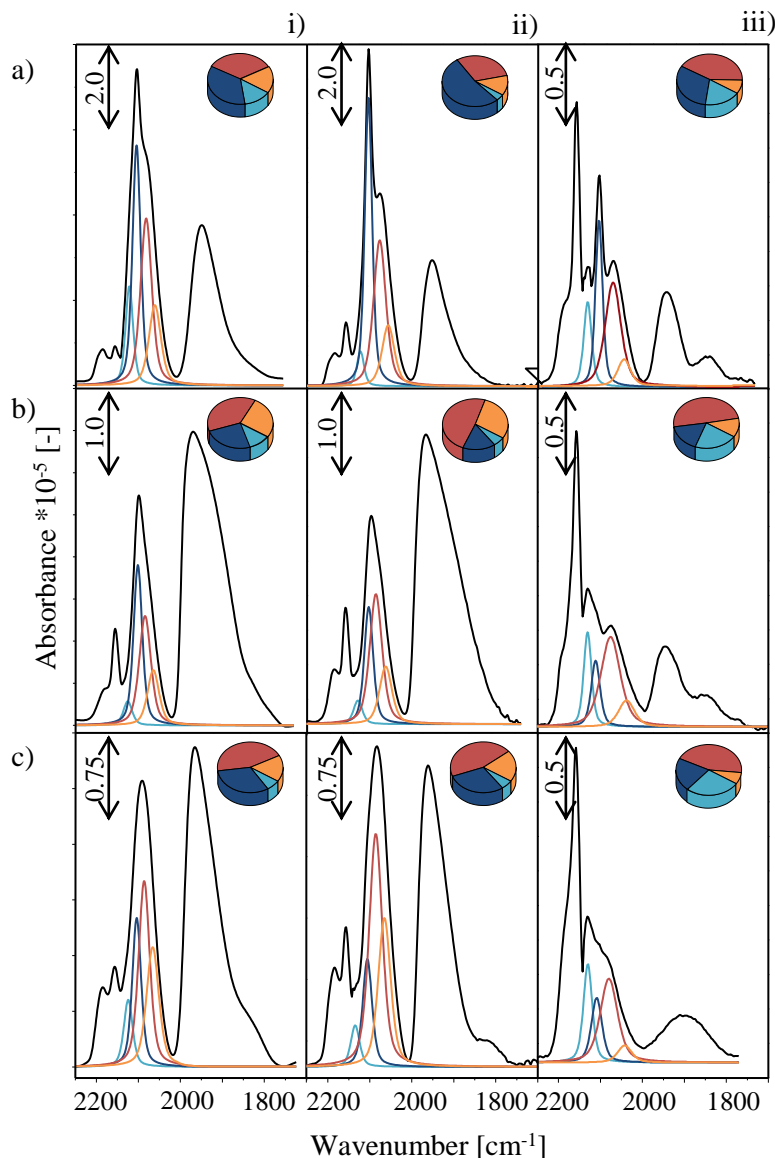
Figure 2-3: IR spectra of adsorbed CO at −150 °C and 1 mbar partial pressure of CO on Pd/Au molar ratios of (a) 1.1, (b) 2.0, and (c) 6.0. Blue lines represent CO on gold, and red lines CO on palladium. (i) Fresh samples, (ii) thermally reconstructed samples, and (iii) reactively reconstructed samples. Pie charts represent intensities of the respective CO species.

The assignments of the linear CO species on Au and Pd are supported by calculations by Liu and Nørskov[28], estimating that the change in adsorption energy reflects changes in the d band level of Pd resulting from an increasing number of Au atoms in contact with

Pd. Due to an electron transfer from Au to Pd, an increased back-donation from the d-level electrons of Pd to the antibonding π*-orbitals of the adsorbed CO takes place.[29] This leads to a red-shift of the CO stretching frequency adsorbed on Pd influenced by Au. Back-donation to the antibonding CO orbitals is reduced for electronically altered Au, which leads to shifts to higher wavenumbers. The respective extent of the blue- or red-shift with regard to the pure metal depends on the degree of intermixing. The adsorption of CO on the silica support led to bands at 2156−2185 cm^{-1}, which are attributed to the interaction of CO with terminal hydroxyl groups and cations.[30,31] For reasons of clarity, however, we will only show and discuss the deconvolution of metal related features of the CO adsorption.

To study the catalysts after VAM synthesis by IR spectroscopy, the KOAc promoter had to be removed by washing the catalyst with deionized water. The subsequent analysis of the washing water indicated the removal of Pd from the dispersed Pd phase in the form of Pd(OAc)$_2$ as describe above. To confirm that palladium is not removed from the bimetallic particles, the IR spectra of CO on a freshly reduced catalyst, which was first loaded with KOAc and subsequently washed, and on the fresh catalyst without KOAc impregnation were compared. As both spectra were identical, we conclude that Pd is not removed from bimetallic particles during washing. As CO does not form bridged species between Pd and Au,[27] the linearly adsorbed CO species are predominantly found on alloyed surfaces, where the Pd atoms are separated by Au. The spectra of CO adsorbed on the catalysts before reaction are shown in Figure 2-3i. The ratios of the intensities from CO linearly adsorbed on Pd or Au are compiled in Table 2-3. Before contact with reactants this ratio varies with the Pd/Au ratio used for catalyst synthesis, while a correlation with the initially applied metal ratios was not found. For example, the ratio for "Au next to Pd"/"Au next to Au" slightly increased from 0.4 to 0.5 for Pd/Au molar ratios of 1.1 and 2.0 but decreased to 0.2 for a Pd/Au molar ratio of 6.0 (see Table 2-3). In agreement with XRD data, this suggests that on fresh samples several bimetallic compositions and surface ensembles of Pd and Au are present. The blue-shifts, with regard to CO adsorbed on pure Au (2098 cm^{-1}), for CO adsorbed on Au next to Au and "Au next to Pd" species were similar for all samples before reaction. The shifts are in a range of 5 cm^{-1} for "Au next to Au" species and of 25 cm^{-1} for highly intermixed

"Au next to Pd" species. As expected, the ratio in the intensities of linear to bridged adsorbed CO (two-fold and 3-fold hollow sites) decreased with increasing Pd content, because a smaller fraction of the Pd was incorporated into bimetallic particles.[32] Comparing fresh and reactively restructured samples (Figure 2-3i,iii) it is evident that the intensity of CO species adsorbed on Pd increased with respect to the fraction of CO adsorbed on Au. This indicates that the reaction induced surface enrichment in Pd results from a reconstruction or an oxidative leaching of Pd from the core of the bimetallic particles. By this process large surface ensembles of Au were removed and a highly intermixed metallic surface was created.

Table 2-3: Ratios of neighbor pair types from IR of adsorbed CO species on fresh catalysts.

Pd/Au molar ratio	'Au next to Pd'/'Au next to Au'	'Pd next to Au'/'Pd next to Pd'	linear/bridged
1.1	0.4	0.5	0.8
2.0	0.5	0.7	0.4
6.0	0.2	0.4	0.2

Table 2-4: Ratios of neighbor pair types from IR of adsorbed CO species on catalysts thermally reconstructed.

Pd/Au molar ratio	'Au next to Pd'/'Au next to Au'	'Pd next to Au'/'Pd next to Pd'	Linear/bridged
1.1	0.1	0.4	0.9
2.0	0.4	0.6	0.7
6.0	0.2	0.5	0.3

Table 2-5: Ratios of neighbor pair types from IR of adsorbed CO species on catalysts reconstructed in reactant atmosphere.

Pd/Au molar ratio	'Au next to Pd'/'Au next to Au'	'Pd next to Au'/'Pd next to Pd'	Linear/bridged
1.1	0.6	0.2	0.9
2.0	1.3	0.2	0.9
6.0	1.3	0.2	1.4

While not including the effects of a reactive atmosphere, thermodynamic calculations by Christensen et al.[12] predict a pronounced Au surface enrichment, suggesting that for bimetallic Pd_1Au_1 particles Pd diffuses into the bulk phase, while Au forms a surface layer on the Pd-rich bulk phase. This is in agreement with the IR data obtained for fresh and thermally altered samples, where intensive adsorption bands for CO on Au were observed (see Figure 2-3i,ii, 2130−2100 cm^{-1}). Thus, low-temperature CO adsorption

supports that the reconstruction induced by reactant gases is significantly different from thermodynamic predictions.

In agreement with the present study, Brückner et al.[17] observed surface depletion of Au for catalysts treated at 190, 170, and 155 °C applying total pressures of 9 bar and a gas composition close to industrial applications.[33] Their CO adsorption data showed that the ratio of linear to bridged adsorbed CO decreased significantly for samples after application to VAM synthesis.

We observed, in contrast, a significantly higher degree of alloying on bimetallic particles of samples after 120 h time-on stream. The blue-shift with respect to pure Au was found to be about 8 cm^{-1} for CO on Au next to Au species and increased up to 30 cm^{-1} for Au next to Pd. For CO adsorbed on palladium we observed a red-shift with respect to pure Pd of 20 and 45 cm^{-1} for "Pd next to Pd" and "Pd next to Au" species, respectively. The increased shift for Pd compared to Au is attributed to the presence of residual potassium on the catalyst surface, which is known to cause a red-shift and a significant peak broadening of vibrations of CO adsorbed on Pd.[34,35] Since Pd is the active metal and, thus, must be in close contact to the promoter metal potassium, the influence of residual potassium is mainly observed for Pd after reaction and the peak broadening is more pronounced for samples with higher Pd concentrations. Within the Pd species ("Pd next to Pd" and "Pd next to Au"), peak broadening is enhanced for the "Pd next to Pd" species. This can be attributed to potassium remaining as a Pd−K mixed phase[36] formed during the reduction of KOAc and Pd(OAc)$_2$ in close proximity. Peak broadening and peak shifts were more pronounced for Pd-rich samples, since the concentration of the dispersed Pd phase was higher (compare Table 2-1). Residual potassium is also responsible for the increase in intensity of the band around 2155 cm^{-1}. Montanari et al.[30] found that the bands of CO adsorbed on potassium cations and on terminal hydroxyl groups overlap. Table 2-5 summarizes the ratios of the intensities for the bands of CO adsorbed on used catalysts. The degree of alloying is significantly enhanced after contact to the reactant atmosphere. The ratios between the intensities of linearly adsorbed CO species on Au ("Au next to Pd"/"Au next to Au") are strongly increased. The slightly lower "Au next to Pd"/"Au next to Au" ratio for the more Au rich sample with a Pd/Au molar ratio of 1.1 can be explained by the presence of small, highly

Au-rich clusters. The restructuring process is more pronounced on palladium-rich particles, since the restructuring is based on the formation of Pd(OAc)$_2$ and the subsequent Pd leaching from the particle surface. For Au-rich particles the restructuring and subsequent surface enrichment in palladium is not as pronounced, and thus, the surface of Au-rich particles remains Au-rich during reaction. The ratios between the intensities of linearly adsorbed CO species on Pd ("Pd next to Au"/"Pd next to Pd") are equal for all three samples, but are lower compared to fresh samples. This is due to the more pronounced broadening of CO linearly adsorbed on the "Pd next to Pd" species caused by residual potassium compared to linearly bound CO on "Pd next to Au" species as discussed above. Thus, we conclude that all bimetallic particles on the catalysts studied had similar surface concentrations of Au and Pd after application in vinyl acetate synthesis.

In contrast, low-temperature CO adsorption on samples thermally aged under reducing atmosphere did not show significant shifts in wavenumbers. Noteworthy is the fact that increasing shifts in absorption frequencies were found for CO adsorbed on "Au next to Pd" species in highly Pd-rich samples and "Pd next to Au" species in the more Au-rich sample with an atomic ratio of Pd/Au 1.1. This is attributed to an increase in the degree of alloying. The restructuring of the surface, however, was less pronounced, as found for samples after reaction. Comparing parts i and ii of Figure 2-2 shows that the intensity of the absorption features assigned to CO adsorbed on Au (light blue and dark blue peaks) and on Pd (red and orange peaks) are similar. However, small variations in the peak ratios of CO adsorbed on Au ("Au next to Pd"/"Au next to Au") and on Pd ("Pd next to Au"/"Pd next to Pd") are detected. Thermal reconstruction of as synthesized particles is highly dependent on the respective compositions of the metallic particles, as it can only occur within the particle, and thus, surface changes are less evident than for samples after reaction (compare Tables 2-3, 2-4 and 2-5).

2.3.4. X-ray absorption spectroscopy

Evidence for the above discussed formation of a Pd−K phase was also found in the EXAFS. Samples after reaction showed a significant expansion of the Pd−Pd distance of about 0.05 Å compared to the distance in fresh catalysts (compare Tables 2-6 and 2-7).

Table 2-6: Results of the EXAFS analysis for Au L$_{III}$ edge and Pd K edge of fresh samples.

Pd/Au molar ratio	Au-Pd		Au-Au		Pd-Au		Pd-Pd	
	d / nm	N	d / nm	N	d / nm	N	d / nm	N
1.1	0.277	4.0	0.279	7.8	0.277	4.5	0.275	4.7
2.0	0.277	4.5	0.279	7.3	0.277	2.2	0.275	7.9
6.0	0.276	5.4	0.280	6.5	0.276	1.1	0.275	9.3

Table 2-7: Results of the EXAFS analysis for Au L$_{III}$ edge and Pd K edge of reactively reconstructed samples.

Pd/Au molar ratio	Au-Pd		Au-Au		Pd-Au		Pd-Pd	
	d / nm	N	d / nm	N	d / nm	N	d / nm	N
1.1	0.278	6.5	0.279	4.6	0.278	5.9	0.281	4.5
2.0	0.277	7.4	0.278	3.9	0.277	4.1	0.280	5.9
6.0	0.277	7.2	0.279	3.8	0.277	1.2	0.281	8.8

The analysis of the EXAFS of fresh and reactively reconstructed samples confirms the formation of a single Pd$_1$Au$_1$ phase under reaction conditions. The EXAFS at the Au L$_{III}$ edge of all reactively reconstructed samples indicated an ordered phase with an alloy composition of approximately Pd$_1$Au$_1$. An ordered 1:1 phase in a fcc lattice leads to a ratio of 2:1 for the coordination numbers of the mixed contributions relative to the monometallic ones, which was found at the Au L$_{III}$ edge.[37] In contrast, randomly distributed Pd$_1$Au$_1$ alloys with a molar composition of 1:1 should show similar coordination numbers for both adsorbing and back-scattering pairs.[38] XRD and low temperature CO adsorption showed slightly Au-rich bimetallic particles after reaction for

the Pd/Au 1.1 sample. This is confirmed via EXAFS analysis. N_{AuPd}/N_{AuAu} is slightly lower than observed for the Pd/Au 2.0 and 6.0 samples (see Table 2-7). Since the alloy compositions derived from XRD data are consistent with the one obtained from EXAFS analysis, we conclude that all Au is incorporated into a Pd_1Au_1 phase forming bimetallic particles. The EXAFS at the Pd K edge after reaction showed high coordination numbers for Pd−Pd neighbors, which resulted from the additional contribution of the monometallic Pd phase on the silica surface. Note that the coordination number of Pd includes both the (bimetallic) neighbors from the Pd_1Au_1 phase and the atoms from the monometallic Pd phase. Since the samples were rereduced before the XAS measurements, the dispersed Pd phase, present in the form of Pd acetate species after reaction, was reduced to monometallic Pd particles. The increase in the distances between the metal atoms in the samples after reaction (2.75 − 2.80 Å) was assigned to a Pd−K mixed phase formed from dispersed $Pd(OAc)_2$ and KOAc (not removed for the XAS experiments), as discussed above.

2.3.5. Activity behavior with time on stream for model catalyst $Pd(OAc)_2$ on SiO_2

To confirm that the observed activity and selectivity increase (compare Figure 2-1) observed for bimetallic samples is due to the reconstruction of the bimetallic particle, $Pd(OAc)_2$ was impregnated onto SiO_2 in order to simulate the second species present besides the bimetallic Pd_1Au_1 phase. Total palladium loading was chosen to be 1.5 wt %, and additional KOAc impregnation (potassium loading 5 wt %) was performed. Activity tests illustrated in Figure 2-4 showed that this catalyst rapidly deactivates under reaction conditions and, in contrast to the bimetallic Pd_1Au_1 catalyst, does not show an initiation period (see Figure 2-1ii). Moreover, the selectivity of this catalyst was constant over the entire reaction time studied. Thus, we can conclude that the second palladium species (i.e.,Pd acetate species) present during reaction is neither responsible for the pronounced activity increase nor for the observed selectivity increase and thus relate the observed behavior with time-on-stream to the reconstruction of Pd_xAu_y particles toward Pd_1Au_1 particles in reaction atmosphere.
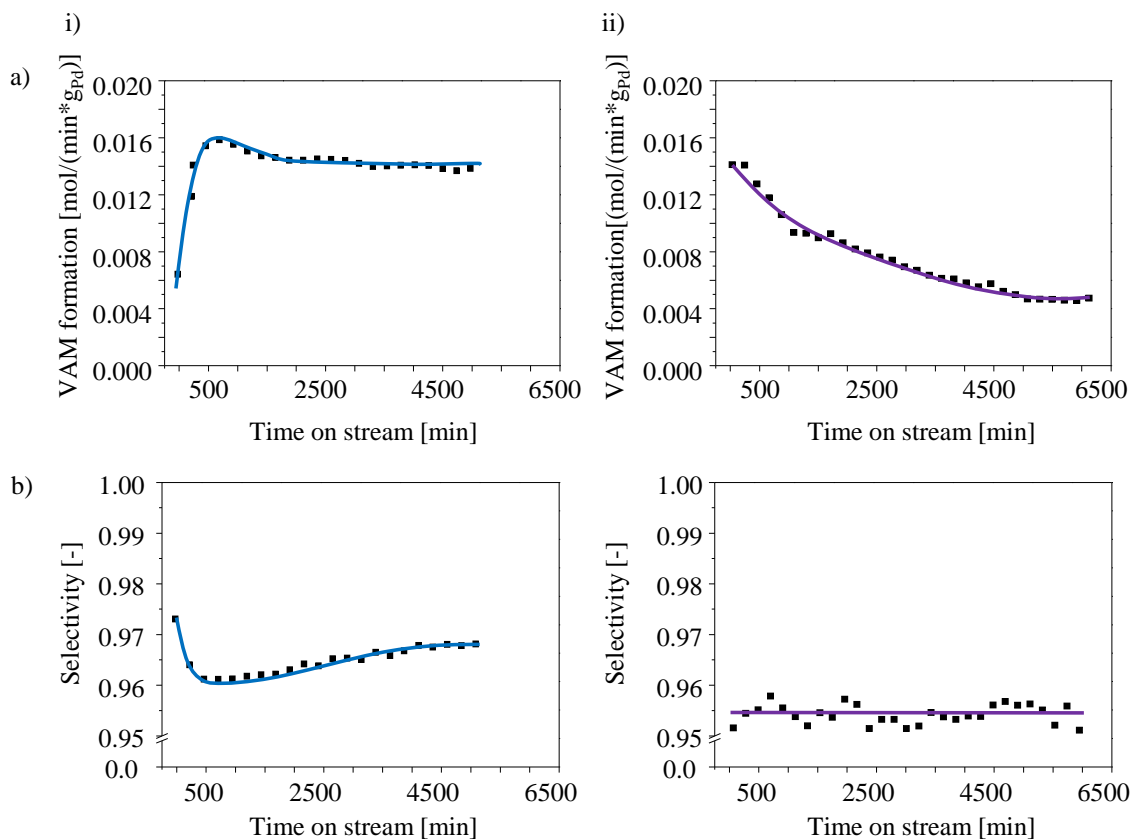
Figure 2-4: (a) VAM formation and (b) selectivity with time-on-stream for Pd/Au 2.0−KOAc on SiO₂ (i) and Pd(OAc)₂−KOAc on SiO₂ (ii), both with 1.5 wt % Pd and 5 wt % K. Reaction conditions: 60 vol % C₂H₄, 13 vol % AcOH, 4.5 vol % O₂, N₂ balance; total pressure, 8.8 bar; temperature, 150 °C.

Moreover, the steady-state activity level per gram of palladium for the model catalyst Pd(OAc)₂ on SiO₂ is similar to the activity per gram of palladium found for bimetallic samples with high Pd/Au molar ratios, i.e., high concentrations of dispersed palladium (see Figure 2-5). Thus, the presence of a monometallic palladium phase in the form of a palladium acetate species is supported. Moreover, the activity levels normalized to the respective palladium content (Figure 2-5b) reflect the presence of a highly active and selective Pd_1Au_1 phase together with a less active monometallic palladium phase. For high Pd concentrations, a high amount of dispersed monometallic palladium is present on the catalyst surface. Since palladium in this monometallic palladium acetate species is less active compared to palladium in the bimetallic particle, the activity normalized to palladium is lower for Pd-rich samples. Since the concentration of palladium in the monometallic palladium phase is similar for samples with high palladium concentrations,

the activity levels normalized to the respective palladium concentration is similar for samples with high Pd/Au molar ratios.
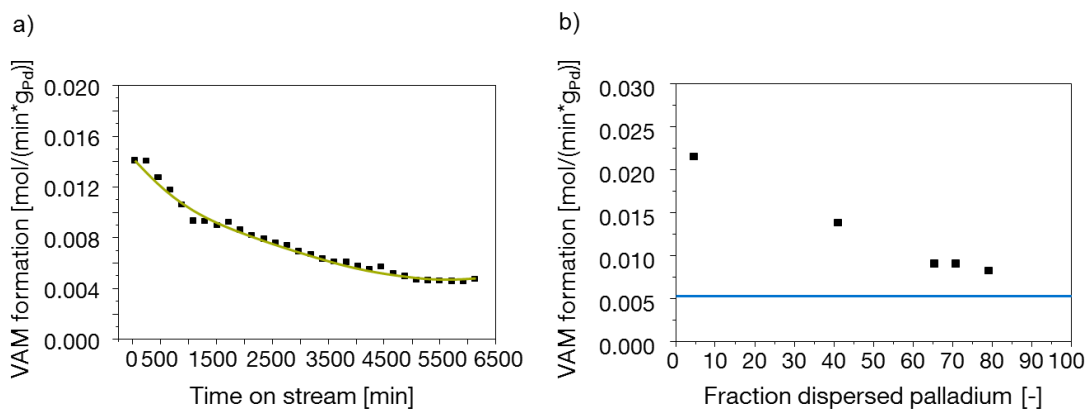
Figure 2-5: (a) VAM formation rate over Pd(OAc)$_2$−KOAc on SiO$_2$ vs. time on stream. (b) Fraction of dispersed palladium phase (calculated on the basis of the chemical composition) vs. VAM formation rate. Reaction conditions: 60 vol % C$_2$H$_4$, 13 vol % AcOH, 4.5 vol % O$_2$, N$_2$ balance; total pressure, 8.8 bar; temperature, 150 °C.

2.4. Conclusions

In summary, reactive reconstruction of Pd-Au bimetallic particles was detected by surface and bulk sensitive methods. While thermal treatment of the bimetallic particles led to the formation of bimetallic particles with Pd/Au of compositions in agreement to the PdAu phase diagram, in the presence of the reactant gases during vinyl acetate synthesis a single Pd-Au phase close to the equimolar composition was formed. Besides this single equimolar phase, Pd dispersed as Pd(OAc)$_2$ species or as a highly dispersed monometallic Pd phase was present, independent of the initial Pd/Au ratio. The reconstruction process is attributed to the oxidation of Pd^0 (present in larger Pd ensembles), the formation of Pd(OAc)$_2$ by a reaction with the reactant and subsequent extraction from the bimetallic particle into the liquid phase consisting of AcOH and H$_2$O. The phase composition of the bimetallic particles was identified to have a large impact on the activity for VAM formation. We expect that the observed formation of the bimetallic surface phase independently of the Pd/Au ratio and the presence of the isolated Pd are the key to understand the relation of the structural properties of bimetallic catalysts and the kinetic data observed for VAM synthesis. As the Pd$_1$Au$_1$ phase dominates the catalytic activity, novel tailored catalysts could be produced limiting the presence of dispersed Pd.

2.5. Acknowledgements

2.6. References

1.   Y. F. Han, D. Kumar, D. W. Goodman, *Journal of Catalysis* **2005**, *230*, 353.

2.   R. Renneke, S. McIntosh, V. Arunajatesan, M. Cruz, B. Chen, T. Tacke, H. Lansink-Rotgerink, A. Geisselmann, R. Mayer, R. Hausmann, P. Schinke, U. Rodemerck, M. Stoyanova, *Topics in Catalysis* **2006**, *38*, 279-287.

3.   M. Chen, D. Kumar, C.-W. Yi, D.W. Goodman, *Science* **2005**, *310*, 291-293.

4.   G. A. Somorjai, Y. Li, *Introduction to Surface Chemistry and Catalysis*, *2 ed.*, John Wiley and Sons, New York, **1994**.

5.   C. Evangelisti, E. Schiavi, L. A. Aronica, A. M. Caporusso, G. Vitulli, L. Bertinetti, G. Martra, A. Balerna, S. Mobilio, *Journal of Catalysis* **2012**, *286*, 224-236.

6.   H. P. Myers, L. Walldén, Å. Karlsson, *Philosophical Magazine* **1968**, *18*, 725-744.

7.   P. Weinberger, C. Blaas, B. I. Bennett, A. M. Boring, *Physical Review B* **1993**, *47*, 10158-10163.

8.   P. Weinberger, J. Kudrnovsky, J. Redinger, B.. I. Bennett, A. M. Boring, *Physical Review B* **1993**, *48*, 7866-7871.

9.   H. Okamoto, T. Massalski, *Journal of Phase Equilibria* **1985**, *6*, 229-235.

10.   T. Mohri, S. Takizawa, K. Terakura, *Journal of Physics: Condensed Matter* **1993**, *5*, 1473.

11.   M. H.-F. Sluiter, C. Colinet, A. Pasturel, *Physical Review B* **2006**, *73*, 174204.

12.   A. Christensen, A. V. Ruban, P. Stoltze, K. W. Jacobsen, H. L. Skriver, J. K. Nørskov, F. Besenbacher, *Physical Review B* **1997**, *56*, 5822-5834.

13.   V. Soto-Verdugo, H. Metiu, *Surface Science* **2007**, *601*, 5332-5339.

14.   M. S. Chen, D. W. Goodman, *Catalysis Today* **2006**, *111*, 22-33.

15.   D. Ferrer, A. Torres-Castro, X. Gao, S. Sepúlveda-Guzmán, U. Ortiz-Méndez, M. José-Yacamán, *Nano Letters* **2007**, *7*, 1701-1705.

16.   X. Jiang, M. Jiang, M. Zhao, *Physica B: Condensed Matter* **2011**, *406*, 4544-4546.

17.   Q. Smejkal, D. Linke, U. Bentrup, M. M. Pohl, H. Berndt, M. Baerns, A. Brückner, *Applied Catalysis A* **2004**, *268*, 67-76.

18. E. A. Crathorne, D. Macgowan, S. R. Morris, A. P. Rawlinson, *Journal of Catalysis* **1994**, *149*, 254-267.

19. H.-J. Eberle, R. Heidenreich, J. Weis (Wacker-Chemie GmbH), *DE 10200605800 A1* Germany, **2008**.

20. M. J. Newville, *Journal of Synchrotron Radiation* **2001**, *8*, 322.

21. B. Ravel, M. J. Newville, *Journal of Synchrotron Radiation* **2005**, *12*, 537-541

22. G. H. Via, K. F. Drake, G. Meitzner, F. W. Lytle, J. H. Sinfelt, *Catalysis Letters* **1990**, *5*, 25-33.

23. L. Vegard, *Zeitschrift für Physik.* **1921,** *5*, 17-26.

24. N. Macleod, J. M. Keel, R. M. Lambert, *Applied Catalysis A* **2004**, *261*, 37-46.

25. L. Hilaire, P. Légaré, Y. Holl, G. Maire, *Surface Science* **1981**, *103*, 125-140.

26. F. Boccuzzi, A. Chiorino, *The Journal of Physical Chemistry B* **2000**, *104*, 5414-5416.

27. E. L. Kugler, M. Boudart, *Journal of Catalysis* **1979**, *59*, 201-210.

28. P. Liu, J. K. Norskov, *Physical Chemistry Chemical Physics* **2001**, *3*, 3814-3818.

29. K. Hadjiivanov, J. C. Lavalley, J. Lamotte, F. Maugé, J. Saint-Just, M. Che, *Journal of Catalysis* **1998**, *176*, 415-425.

30. T. Montanari, L. Castoldi, L. Lietti, G. Busca, *Applied Catalysis A* **2011**, *400*, 61-69.

31. T. Montanari, R. Matarrese, N. Artioli, G. Busca, G. *Applied Catalysis B* **2011**, *105*, 15-23.

32. J. W. Niemantsverdriet, *Spectroscopy in Catalysis: An Introduction*. Wiley-VCH Verlag GmbH, Weinheim, **2000**.

33. M. J. Baker, T. C. Bristow, R. W. Clarke, S. J. Kitchen, B. L. Williams (BP Chemical Limited), *US 6225496*, **2001**.

34. B. E. Hayden, A. W. Robinson, P. M. Tucker, *Journal of Electron Spectroscopy and Related Phenomena* **1987**, *44*, 297-304.

35. P. A. J. M. Angevaare, H. A. C. M. Hendrickx, V. Ponec, *Journal of Catalysis* **1988**, *110*, 11-17.

36. R. Pellegrini, G. Leofanti, G. Agostini, L. Bertinetti, S. Bertarione, E. Groppo, A. Zecchina, C. Lamberti, C. *Journal of Catalysis* **2009**, *267*, 40-49.

37.   A. Jentys, *Characterization of Bimetallic Pt/Ni Catalysts by X-ray Absorption Spectroscopy*, Technische Universität Wien, Wien, **1991**.

38.   A. M. Beale, B. M. Weckhuysen, *Physical Chemistry Chemical Physics* **2010**, *12*, 5562-5574.

2.7. Supporting Information

Results of the EXAFS analysis

The results of the EXAFS analysis for the Pd/Au samples before and after reaction are listed in Table 2-S1.

Table 2-S1: EXAFS fit results for Pd/Au samples before reaction (b.r.) and after reaction (a.r)

	Au-Pd		Au-Au		Pd-Au		Pd-Pd		$E_0(Au)$	$\sigma^2(AuAu)$	$E_0(Pd)$	$\sigma^2(PdPd)$	$\sigma^2(PdAu)=$ $\sigma^2(AuPd)$	R-factor
	N	d/nm	N	d/nm	N	d/nm	N	d/nm						
1.1 b.r	4.0	0.277	7.8	0.279	4.5	0.277	4.7	0.275	3.0	0.009	-6.2	0.006	0.007	0.002
1.1 a.r.	6.5	0.278	4.6	0.279	5.9	0.278	4.5	0.281	3.0	0.002	-6.8	0.004	0.001	0.015
2.0 b.r.	4.5	0.277	7.3	0.280	2.2	0.277	7.9	0.275	3.8	0.009	-3.7	0.004	0.005	0.008
2.0 a.r	7.4	0.277	3.9	0.278	4.1	0.277	5.9	0.280	2.5	0.001	-8.2	0.003	0.005	0.012
6.0 b.r.	5.4	0.276	6.5	0.280	1.1	0.276	9.3	0.275	5.1	0.009	-4.7	0.003	0.005	0.006
6.0 a.r	7.2	0.277	3.8	0.279	1.2	0.277	8.8	0.281	3.1	0.009	-4.9	0.004	0.008	0.012

CO adsorption on reference samples

Figure 2-S1 shows the transmission infrared spectra of CO adsorbed at -150 °C on a series of reference samples and a bimetallic Pd/Au sample with a Pd/Au molar ratio of 0.8. The low Pd/Au ratio was chosen as example in order to provide equally pronounced linear adsorption on both metals. Spectra were taken at 1 mbar CO partial pressure. On the monometallic Pd sample, CO adsorbs predominantly in multifold mode (2000-1700 cm^{-1}). Linearly adsorbed CO is found at a wavenumber of approximately 2095 cm^{-1}.

CO adsorbed on monometallic Au is exclusively present in linear adsorption mode and was detected at wavenumbers around 2098 cm^{-1}. No multifold adsorbed CO species were found.

For bimetallic samples, the linear adsorption mode is more dominant as it was found for monometallic palladium sample. As well known in literature[1,2], the introduction of Au to

monometallic palladium leads to a shift towards lower wavenumbers for adsorption features representing CO on Pd. The adsorption features of Au are less affected in terms of wavenumber shifts, however small shifts towards higher wavenumbers are distinguishable.
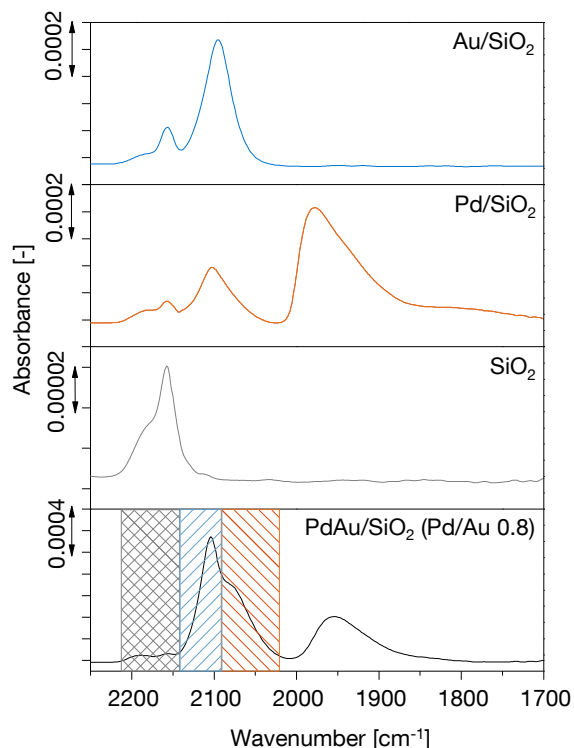
Figure 2-S1: FTIR spectra of CO adsorbed at -150 °C at maximum coverage (1 mbar) on Au/SiO$_2$, Pd/SiO$_2$, pure SiO$_2$ and a bimetallic sample with a Pd/Au molar ratio of 0.8. Dashed regions in grey, blue and orange account for CO adsorption on the support, Au and Pd.

At -150 °C CO also adsorbs on the silica support. Two adsorption features are evident. CO adsorbed on OH-groups is found at a wavenumber of approximately 2153 cm^{-1}, which is in good agreement to literature.[3,4] CO adsorption at surface impurities leads to a weaker adsorption feature at higher wavenumbers ($\sim$2180cm^{-1}).

Dashed regions in Figure 2-S1 represent the wavenumber regions for CO on Pd, which is electronically altered by Au and CO on Au, which frequencies are shifted due to close neighborhood to Pd. The deconvolution of the FTIR spectra of CO adsorbed on the bimetallic samples is shown and discussed in the main part of this work.

Pressure dependence of CO adsorption

Figure 2-S2 shows the pressure dependence of the adsorption of CO for Pd/Au 2.0 in a CO partial pressure range of 0.005 mbar – 1.000 mbar.

With increasing coverage the intensity of the multifold adsorption feature at 1968 cm^{-1} is intensified, whereas relative to this feature the shoulder around 1900 cm^{-1} shows only small variations. Similar behavior with increasing partial pressure of CO was found by McKenna and Anderson[5] on monometallic palladium. The adsorption features representing linearly adsorbed CO on Pd and Au ($\sim$ 2120-2015cm^{-1}) show pronounced variations until the maximum coverage is reached. For low coverages CO adsorbs predominately on Pd and only low intensities for the adsorption of CO on Au are found (> 2100 cm^{-1}). With increasing partial pressure (and increasing coverage), CO adsorption on Au is favored and the adsorption features representing CO on Au increase in intensity.

The adsorption of CO on the support also shows pressure dependency. At low partial pressures, the adsorption of CO on OH-groups ($\sim$ 2153 cm^{-1} at maximum coverage) is weak. With increasing partial pressures the adsorption of CO on OH-groups is enhanced. The adsorption on cationic surface impurities ($\sim$ 2180 cm^{-1}) is weak and less effected by an increasing CO partial pressure. The pressure dependence of the CO adsorption on the support is in perfect agreement to studies of Busca et al.[3,4].
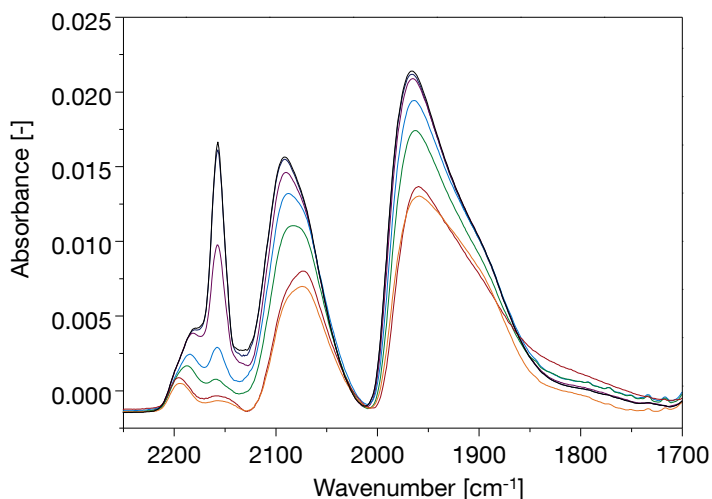
Figure 2-S2: FTIR spectra of CO adsorbed at -150 °C at increasing pressures. 0.005 mbar – 0.010 mbar – 0.050 mbar – 0.100 mbar – 0.500 mbar – 0.750 mbar – 1.000 mbar.

1.   E. L. Kugler, M. Boudart, *Journal of Catalysis* **1979**, *59*, 201-210.

2.   Y. Soma-Noto, W. M. H. Sachtler, *Journal of Catalysis* **1974**, *32*, 315-324.

3.   T. Montanari, L. Castoldi, L. Lietti, G. Busca, *Applied Catalysis A: General* **2011**, *400*, 61-69.

4.   T. Montanari, R. Matarrese, N. Artioli, G. Busca, *Applied Catalysis B: Environmental* **2011**, *105*, 15-23.

5.   F.-M. McKenna, J. A. Anderson, *Journal of Catalysis* **2011**, *281*, 231-240.

Chapter 3

Temperature dependent evaluation of two active species for heterogeneously operated vinyl acetate synthesis: Part I - physicochemical characterization

SiO_2 supported Pd-Au catalysts were synthesized with Pd/Au molar ratios varying from 0.8 to 7.0 using the chloride salts as precursors and were used in vinyl acetate synthesis under industrial conditions at 150°C and 180°C. Aging at 150°C led to the formation of the Pd_1Au_1 phase, while the remaining Pd atoms were present as a dispersed phase formed under reaction conditions via palladium leaching in form of Pd acetate species. The presence of these two spatially separated phases was observed by EXAFS studies of aged catalysts combined with modeling of the coordination numbers for the respective bimetallic clusters. Temperature dependent *in-situ* XRD and *in-situ* XAS experiments as well as high resolution TEM of the reduced samples in inert atmosphere showed a pronounced phase separation into a palladium rich and a gold rich phase at elevated temperatures (>160°C). Low temperature CO adsorption and X-ray diffraction of samples after vinyl acetate formation at 180°C showed that the phase separation also takes place during vinyl acetate synthesis at elevated temperatures. The pronounced temperature dependency of the morphology and surface composition of the bimetallic Pd-Au catalysts studied is related to the selectivity, activity and especially stability levels for vinyl acetate synthesis.

3.1. Introduction

Bimetallic noble metal catalysts are key to many catalytic processes, including palladium catalyzed oxidation or acetoxylation processes. The acetoxylation of ethylene to vinyl acetate is formally an oxidative esterification (Equation 3-1) and industrially performed over SiO_2 or SiO_2/Al_2O_3 supported bimetallic Pd/Au catalysts.[1,2,3]

$$CH_3COOH + C_2H_4 + \frac{1}{2} O_2 \rightarrow CH_3COOCHCH_2 + H_2O \qquad \text{Equation 3-1}$$

Little consensus exists on the details of the reaction mechanism and active species, despite over 30 years of ongoing research.[4] The addition of the catalytically inactive Au to the Pd based catalyst led to a pronounced increase in both activity and stability.[5,6] The reaction has been found to be highly structure sensitive, i.e., the catalytic properties strongly depend on the local structure and chemical composition,[7] which has been linked to the presence of isolated Pd atoms in a specific configuration. The formation of these ensembles depends subtly on the reaction conditions and it appears that the structure is dynamically formed and disintegrated during the reaction.[8] The Pd-Au phase diagram (see Figure 3-1) by Okamoto and Massalski[9] shows three ordered solid phases with compositions of Pd_3Au_1, Pd_1Au_3 and at lower temperatures an equimolar Pd_1Au_1 phase.
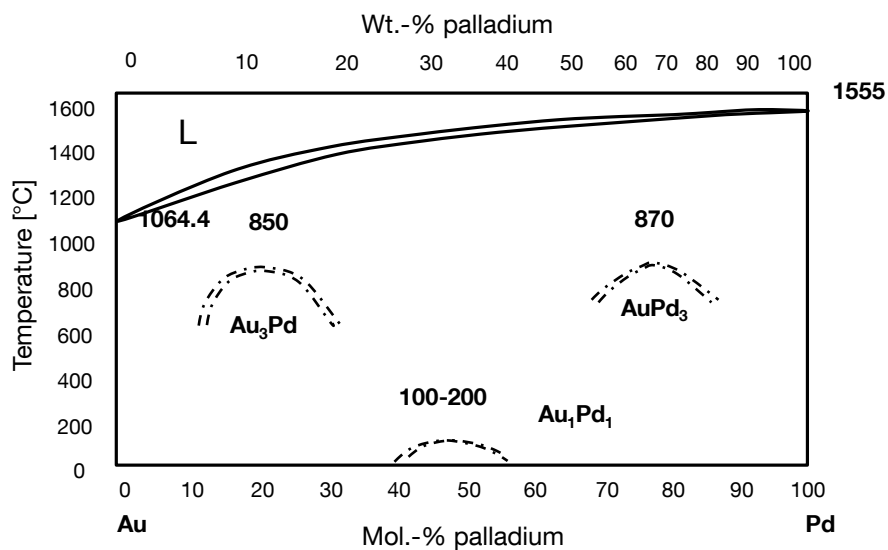

Figure 3-1: Pd-Au phase diagram reprinted from Okamoto and Massalski.

Zhu and Hou[10] investigated the role of mechanical stress, induced by an inhomogeneous stress field at equilibrium, in the chemical ordering of Pd Au nanoalloys for 309 and 561

atom clusters. Three stable phases in good agreement to the Pd-Au phase diagram were identified, which correspond to well defined plateaus in the chemical potential as a function of the Pd fraction present. It was stated that the formation of ordered phases is predominantly driven by thermodynamic forces. Similar ordered phases were found by Atanasov and Hou[11] for 923 atom clusters. For these cuboctahedral clusters the formation of ordered phases was found to be driven by the negative mixing enthalpy, while the stress field which would lead to disordering does not overcome the mixing enthalpy resulting from the ordering of the phases. Since the stability of these two phases is temperature sensitive, a pronounced temperature dependency of the selectivity for vinyl acetate synthesis can be expected.

The catalyst activity varies indeed in a complex pattern, in which the catalyst activity initially increases during the first 20 - 30 h time on stream, followed by a very slow deactivation over the following 110 h time on stream.[12] To stabilize the catalysts over longer time periods it is essential to understand and carefully tailor the structural properties of the catalyst surface. Regarding activity levels, it has been stated that the controlled growth of the metallic particles to sizes of about 2-3 nm is required to obtain improved catalysts,[13] because particles in the sub nm range exhibit mainly edges and corner sites on the surface and the surface planes present are too small to create the catalytically active ensembles of two Pd monomers in direct neighborhood.

Under reaction conditions the surface of the catalysts is covered with a multilayer of acetic acid[14] and water, the latter being formed in the reaction (see Equation 3-1). The amount of adsorbed acetic acid increases significantly with the introduction of potassium acetate, which is added as promoter and significantly enhances the adsorption of acetic acid by the formation of dimeric species with acetic acid.[15]

In our previous study[12] we showed that a bimetallic Pd_1Au_1 phase and a highly dispersed monometallic palladium phase in the form of palladium acetate are present under working conditions, both only formed when the catalyst is exposed to the reactants. In contrast, thermal treatment, under reducing as well as inert atmosphere, led to a different structure of the bimetallic particles compared with the restructuring under reactant atmosphere.

In [12] we attributed the restructuring of the bimetallic particles under working conditions to the formation of palladium acetate, predominantly on the larger palladium assembles, followed by the subsequent dissolution of palladium from the bimetallic Pd_xAu_y core. Under reaction conditions the fraction of palladium dissolved in the acidic acid is present as acetate on the SiO_2 support. In this study we will focus on the temperature dependency of the restructuring process under a reactive atmosphere. A combination of bulk sensitive methods, such as EXAFS and XRD, with the (surface sensitive) sorption of CO will be applied to obtain a detailed characterization of the (bi)metallic particle structure. By applying either a reactive or a non-reactive atmosphere over a wide temperature range, we will describe the formation of mono and bimetallic phases. The catalyst properties described will be correlated to catalytic properties reported in the second part of this work.

3.2. Experimental

3.2.1. Synthesis

Pd/Au-SiO_2 catalysts with molar ratios starting from Pd rich samples with a molar Pd/Au ratio of 7.0 to Au rich samples with a molar Pd/Au ratio of 0.8 were prepared via incipient wetness impregnation with an aqueous solution of $HAuCl_3$ and $PdCl_2$ according to DE102006058800 A1.[16] The synthesis procedure includes precipitation and washing steps to remove chloride from the catalyst. The series of catalysts was prepared with a constant total metal loading of 3 wt.-%. WACKER HDK with a surface area of ~200 m^2/g was used as SiO_2 support. The Pd/Au-SiO_2 catalysts were reduced in flowing H_2 at 300 °C for 1 hour with a heating rate of 3 °C/min. The samples with Pd/Au ratios of 6.0, 2.0 and 1.1 are shown exemplarily in the paper.

3.2.2. Atomic absorption spectroscopy (AAS)

The concentrations of palladium, gold and potassium were determined via atomic absorption spectroscopy using a UNICAM 939 AA-Spectrometer. Typically 30 mg of the sample were dissolved in a mixture of hydrofluoric acid and nitro-hydrochloric acid.

Samples were dried before dissolution at a temperature of 473 K. Standard solutions with 15, 30, 50 and 100 ppm palladium or gold were used.

3.2.3. Low temperature CO adsorption

The samples were prepared as self-supporting wafers with a density of approximately 10 mg/cm^{-2}. The samples were first activated in vacuum (better than $1.0*10^{-7}$ mbar) at 300 °C for 1 hour with a heating rate of 5 °C/min, cooled to room temperature and subsequently re-reduced in H_2 at 300 °C with a heating rate of 5 °C/min. After re-reduction, the samples were outgassed at 300 °C for 30 minutes. After pretreatment, the samples were cooled in 10 mbar He (added for thermal conductivity reasons) to -150 °C and a spectrum was taken. Subsequently the cell was evacuated and 1 mbar CO was introduced. To increase thermal conductivity, 10 mbar He were added and the spectra were collected at -150 °C. The infrared spectra were recorded on a Vertex 70 spectrometer from Bruker Optics with a resolution of 4 cm^{-1} and an accumulation of 128 interferrograms. The spectra were background corrected and difference spectra of the activated sample and after adsorption of 1 mbar CO (both at -150 °C and 10 mbar He) were created. The difference spectra were deconvoluted using GRAMS AI 9.0 R2. Peak positions and values for the half width at half height were fixed within a range of 4 cm^{-1} for samples before reaction. For samples after reaction, values for CO on palladium were allowed to vary within a range of 20 cm^{-1}, due to peak broadening and peak shifts originating from residual potassium.

3.2.4. X-ray powder diffraction

X-ray powder diffraction measurements were conducted on a "Philips X'Pert Pro System" using Cu-Kα radiation of 0.154056 nm (45 kV and 40 mA). The experiments were carried out on a rotating sample holder in a 2Θ range of 5° to 70° with a step size of 0.019°/s. Temperature dependent in-situ measurements were performed in an Anton Paar HTK 1200 oven under flowing H_2, respectively He, with a heating rate of 3 °C/min and a cooling rate of 2 °C/min. For preventing the formation of palladium hydrides, the gas

atmosphere was changed to helium at maximum temperature. Deconvolution of the diffraction profiles were performed using High Score Plus 3.0 a. Before deconvolution the range of the diffractogram was reduced to a 2Θ range of $35°$ to $70°$.

3.2.5. X-ray absorption spectroscopy

X-ray absorption spectroscopy measurements of aged samples were conducted at HASYLAB, DESY, Germany on beamline X1 and C. The storage ring energy was 4.5 GeV and the current decay during a typical fill was from 110 mA to 90 mA. Temperature dependent in-situ X-ray absorption spectroscopy measurements were performed at the European Synchrotron Radiation Facility (ESRF) in Grenoble, France on the BM 26 – DUBBLE – Dutch-Belgian Beamline. The storage ring was filled in 16 bunch mode.

The samples were prepared as self-supporting wafers, having a total absorbance of 1.5 for the Au-L_{III} edge and 2.0 for the Pd-K egde. A total absorbance of 2.0 for the Pd edge was necessary since the maximum on placeable amount of sample was exceeded for a total absorbance of 1.5. The samples were flushed with He inside the sample chamber and cooled to liquid N_2 temperature for ex-situ measurements. In-situ measurements were conducted with the same temperature program as used for in-situ XRD measurements.

For EXAFS analysis, the scattering contributions in the pre- and post- edge background were removed from the X-ray absorption spectra by a third-order polynomial spline function. The oscillations were weighted with k^2 and fitted in k-space within the limits k=2.1-12 $Å^{-1}$ for the Pd-K edge and k=2.8-12 $Å^{-1}$ for the Au-L_{III} edge. XAS data processing and EXAFS analysis were performed using IFEFFIT[17] with the Horae package[18] (Athena and Artemis). The amplitude, i.e. S_o^2, was derived from EXAFS data analysis of known references with known coordination numbers and was fixed during analysis. S_o^2 was found to be 1.0 for Au and 1.0 for Pd. The multiple-edge fitting in k-space was carried out using the constraints (1)-(3).[19]

(1) $N_{AuPd} = N_{PdAu} * x_{Pd}/x_{Au}$

(2) $r_{AuPd} = r_{PdAu}$

(3) $\sigma_{AuPd} = \sigma_{PdAu}$

The mean interatomic distances, variances (Debye-Waller (D-W) factor) and coordination numbers were first determined using the correlated Einstein model[20,21] by using the $ein(T, \Theta)$-function in Artemis, in order to account for the temperature dependence of the D-W-factor. It was shown that the neglection of the anharmonic term at elevated temperatures leads to a nonphysical decrease in interatomic distances.[22] Since odd cumulants contribute to the EXAFS phase, while even ones influence the EXAFS function, the third cumulant C3 has to be taken into account for temperature dependent measurements.[23] Thus after having determined the amplitude dependent parameters, the third cumulants C3, together with R and ΔE_0 were refined, whereas all other parameters were fixed. ΔE_0 was allowed to float freely; since ΔE_0 accounts for an overall phase shift between the experimental and calculated spectra it is also correlated to C3.[24]

3.2.6. Modeling of the local environment of the atoms in the particles

To support the analysis of the EXAFS data of the first shell coordination numbers for Pd and Au in various potential particles, structures ranging from fully ordered phases to fully random ensembles were generated based on an FCC lattice structure using Accelrys Material Studio 6.0. The particle size used for bimetallic particles was 2 nm (corresponding to 1985 metal atoms). The highly dispersed palladium phase was modeled by additional monometallic particles with a size of 0.5 nm (43 atoms). The particle sizes were chosen based on TEM measurements of catalysts after reaction. The particle size of 0.5 nm for the monometallic palladium phase was used, since particles were re-reduced before EXAFS measurements and thus monometallic palladium particles were formed from the dispersed palladium species (in form of palladium acetate) present on the catalysts after reaction. The (first shell) coordination numbers for the metal atoms in the model clusters were calculated based on the particle geometry.

3.2.7. Aging under industrial reaction conditions

Aging under industrial conditions was performed in a 6-fold reactor set-up at temperatures of 150 °C and 180 °C. The gas composition consisted of 60 vol.-% C_2H_4, 13 vol.-% AcOH, 4.5 vol.-% O_2 and N_2 balance. The reactors were filled in a way that for all Pd/Au ratios the amount of Pd was constant in the catalyst bed. SiC was used as inert diluent to ensure an isothermal temperature over the catalyst bed. The diluent to catalyst ratio was 10/1. The product stream was analyzed using a GC 2014 from Shimadzu, equipped with a Haysep Q and a mol sieve column and a TCD detector.

3.3. Results

3.3.1. Particle morphology

The results of the analysis of the EXAFS for the bimetallic Pd-Au particles before and after vinyl acetate synthesis at 150 °C are summarized in Table 3-1 (the complete results of the EXAFS analysis are given in the supplementary material):

Table 3-1: EXAFS fit results for Pd/Au samples before reaction (b.r.) and after reaction at 150 °C (a.r)

Pd/Au molar ratio	Au-Pd		Au-Au		Pd-Au		Pd-Pd	
	N	r/nm	N	r/nm	N	r/nm	N	r/nm
1.1 b.r	4.0	0.277	7.8	0.279	4.5	0.277	4.7	0.275
1.1 a.r.	6.5	0.278	4.6	0.279	5.9	0.278	4.5	0.281
2.0 b.r.	4.5	0.277	7.3	0.280	2.2	0.277	7.9	0.275
2.0 a.r	7.4	0.277	3.9	0.278	4.1	0.277	5.9	0.280
6.0 b.r.	5.4	0.276	6.5	0.280	1.1	0.276	9.3	0.275
6.0 a.r	7.2	0.277	3.8	0.279	1.2	0.277	8.8	0.281

As discussed in [12], samples after reaction show a N_{AuPd}/N_{AuAu} ratio of close to 2.0, which accounts for an ordered Pd_1Au_1 phase. However, the N_{PdAu}/N_{PdPd} ratio before reaction is significantly smaller than 2.0 and varies with the Pd/Au molar ratio of the catalyst. This discrepancy was assigned to the formation of a monometallic dispersed palladium phase during reaction via leaching of Pd from the Pd rich particles until an equimolar ratio of Pd and Au was reached in the remaining bimetallic particles.

In order to support the assumption from the analysis of the EXAFS that bimetallic particles with a composition of Pd_1Au_1 together with a monometallic palladium phase (in form of palladium acetate under reaction conditions) are formed during vinyl acetate synthesis, models of ordered and randomly arranged bimetallic particles together with different fractions of monometallic dispersed palladium particles were generated and the average coordination numbers of the atoms were calculated. The correlation between the coordination numbers and the degree of ordering within the bimetallic particle is shown in Figure 3-2. For full ordering (i.e. formation of the Pd_1Au_1-phase) a ratio of 2 would be expected for N_{AuPd}/N_{AuAu} and N_{PdAu}/N_{PdPd}, whereas for a fully random arrangement of the Pd and Au atoms the ratio would be 1. Note that in the presence of an additional monometallic phase the correlations shown in Figure 3-2 can only be applied for the metal incorporated only into the bimetallic particles. For homogenously distributed bimetallic particles, the sum of $N_{PdAu} + N_{PdPd}$ and $N_{AuPd} + N_{AuAu}$ would be equal, which is not observed from the EXAFS analysis (compare Table 3-1). The fraction of the monometallic phase can be estimated from the deviation of these ratios for the metal atoms being preset in excess. In the case of the Pd/Au particles studied here, gold is only preset in the bimetallic particles, while Pd forms an additional monometallic phase, which can be seen from the differences in the coordination numbers of the Pd and Au neighbors.
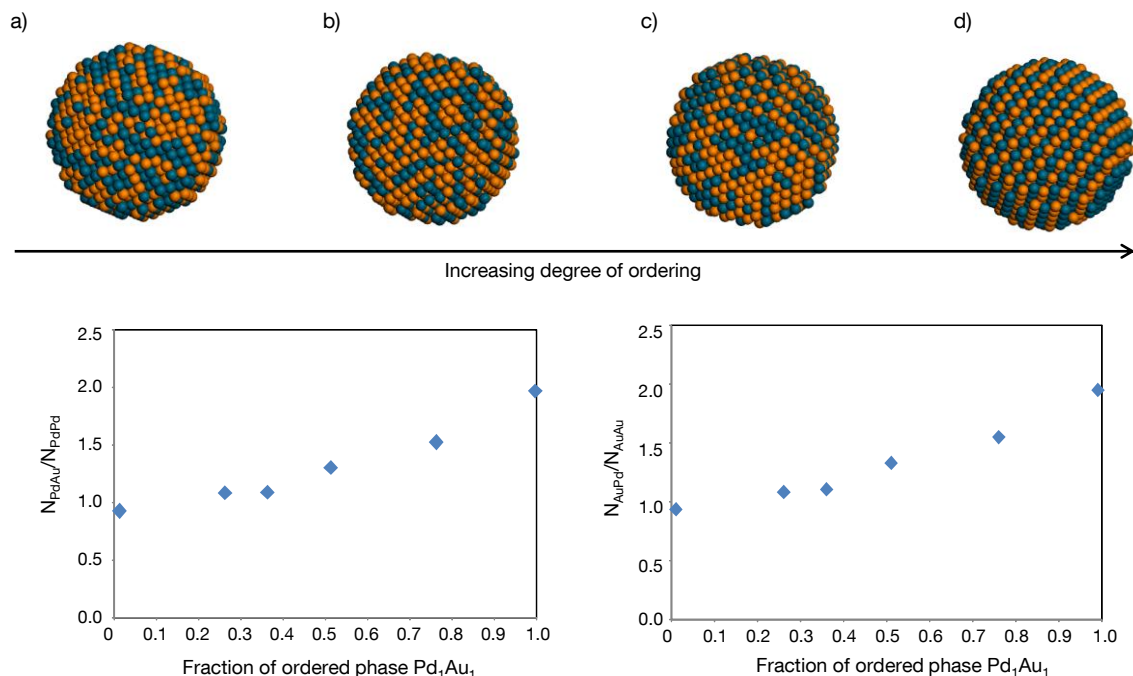
Figure 3-2: Modeled particles with different concentrations of ordered Pd$_1$Au$_1$ phase. a) 0 % b) 25 % c) 75 % d) 100 % of ordered Pd$_1$Au$_1$ phase. i) Correlation of N$_{PdAu}$/N$_{PdPd}$ and the concentration of ordered Pd$_1$Au$_1$ in the particle. ii) Correlation of N$_{AuPd}$/N$_{AuAu}$ and the concentration of ordered Pd$_1$Au$_1$ in the particle.

Depending on the degree of ordering in the bimetallic phase, the additional palladium phase has a different effect on the coordination numbers. Figure 3-3 shows the ratio of N$_{PdAu}$/N$_{PdPd}$ as a function of the concentration of the dispersed monometallic palladium phase present. For an increasing fraction of dispersed palladium phase present, both the ratio N$_{PdAu}$/N$_{PdPd}$ and N$_{total}$ (i.e., N$_{PdAu}$+N$_{PdPd}$) decrease (see Figure 3-3). Applying the correlations presented in Figure 3-2 and 3-3 on the results of the EXAFS analysis, the fraction of dispersed palladium and the type of bimetallic phase can be determined by the following steps.

From the ratio of N$_{AuPd}$/N$_{AuAu}$, which is around 2 for all samples after reaction, the presence of an ordered 1:1 phase can be assumed, which is in agreement to literature.[25] Using the ratio N$_{PdAu}$/N$_{PdPd}$, which includes contributions from the bimetallic and the monometallic particles, in the second step the fraction of isolated Pd particles can be estimated. The results are summarized in Table 3-2 and compared to the concentration of dispersed palladium phase calculated on the basis of the chemical composition of the respective sample and the presence of a Pd$_1$Au$_1$ phase.
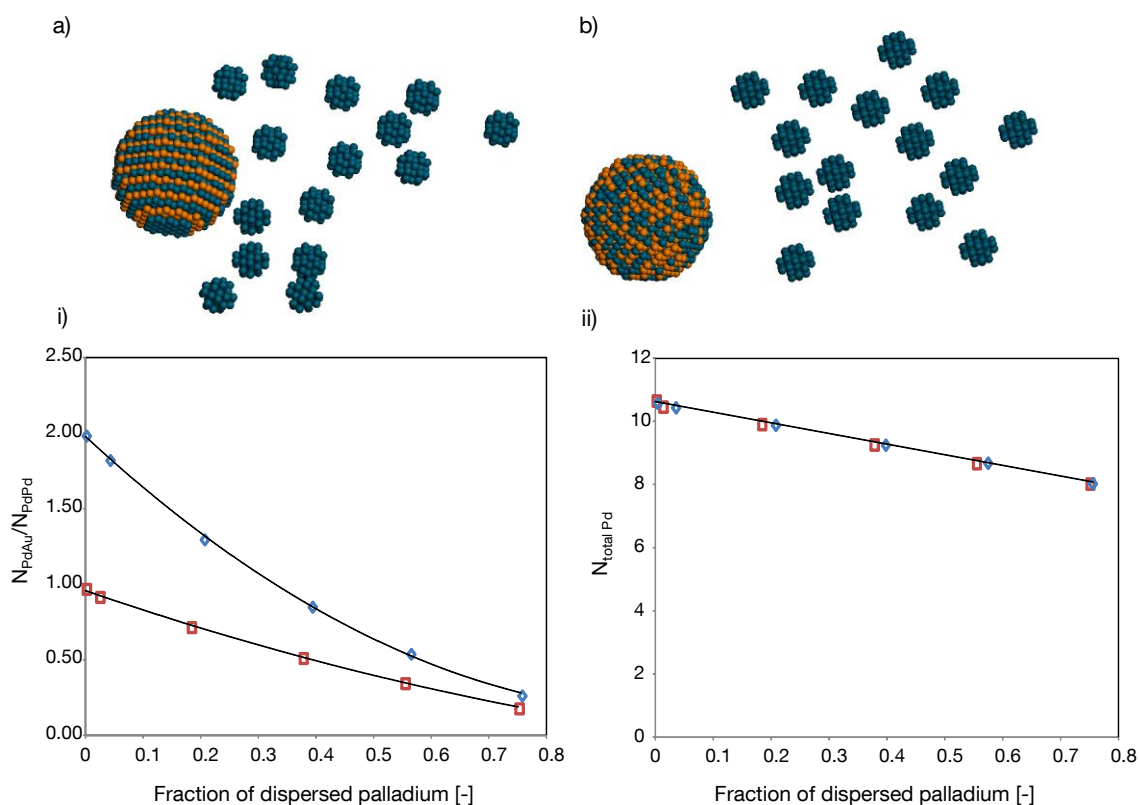
Figure 3-3: Bimetallic particles modeled with additional monometallic palladium phase. a) Ordered Pd$_1$Au$_1$ phase with 55 % dispersed palladium. b) Random Pd$_1$Au$_1$ phase with 55 % dispersed palladium. i) Correlation of N$_{PdAu}$/N$_{PdPd}$ and the fraction of dispersed palladium for fully random and fully ordered Pd$_1$Au$_1$. ii) Correlation of N$_{total}$ and the fraction of dispersed palladium for fully random and fully ordered Pd$_1$Au$_1$. □ 100 % random bimetallic particle, ◇ 100 % ordered bimetallic particle. Fraction of dispersed palladium is calculated based on the total content of palladium in the sample.

Table 3-2: Fraction of dispersed palladium (in respect to the total palladium concentration) calculated on the basis of the chemical composition and according to the correlations found via particle modeling.

Pd/Au molar ratio	Fraction of dispersed palladium calculated on the basis of the chemical composition [-] *	Fraction of dispersed palladium calculated as average value of the fractions determined according to the correlation based on N$_{PdAu}$/N$_{PdPd}$ and N$_{Pd\,total}$ found via particle modelling [-]
1.1	0.04	0.12
2.0	0.39	0.40
6.0	0.71	0.62

*calculated according to: f(dispersed Pd) = [c(Pd total) - c(Pd in Pd$_1$Au$_1$ phase)]/c(Pd total)

3.3.2. Temperature dependent phase separation followed by X-ray diffraction

The temperature dependent formation of bimetallic PdAu particles was investigated by in-situ XRD measurements. The experiments were carried out in H_2, because preliminary tests showed that surface PdO, formed during storage of the catalysts in air, strongly restricts the mobility of the metal atoms within the particles. In order to avoid hydride formation on Pd (Pd-H is only stable below approximately 150 °C, in situ XRD data sets in reducing atmosphere are shown in the supplementary information) at lower temperatures, H_2 was replaced by He before cooling to room temperature after the reduction.

Under reducing conditions a pronounced phase separation towards a Pd-rich Pd_3Au_1 and a Au-rich Pd_1Au_3 phase was found with increasing temperature. The changes during temperature treatment for Pd/Au 1.1, Pd/Au 2.0 and Pd/Au 6.0 are shown Figure 3-4. A further change in the presence of bimetallic phases was not found at the maximum temperature of 300 °C both in H_2 and He, while during cooling to 170 °C in He, ordered phases were formed according to the Pd-Au phase diagram[9]. The phase segregation process during the heating period started at a temperature of approximately 160 °C, which is slightly higher as proposed in the phase diagram[9], where the Pd_1Au_1 phase is described to be stable up to 100 °C. The degree of phase separation was found to be more pronounced for Pd-rich samples (see Figure 3-4, Temperature dependent XRD patterns are exemplarily shown for Pd/Au 1.1, 2.0 and 6.0). The composition of the alloy phases at the end of the temperature treatment are summarized in Table 3-3.
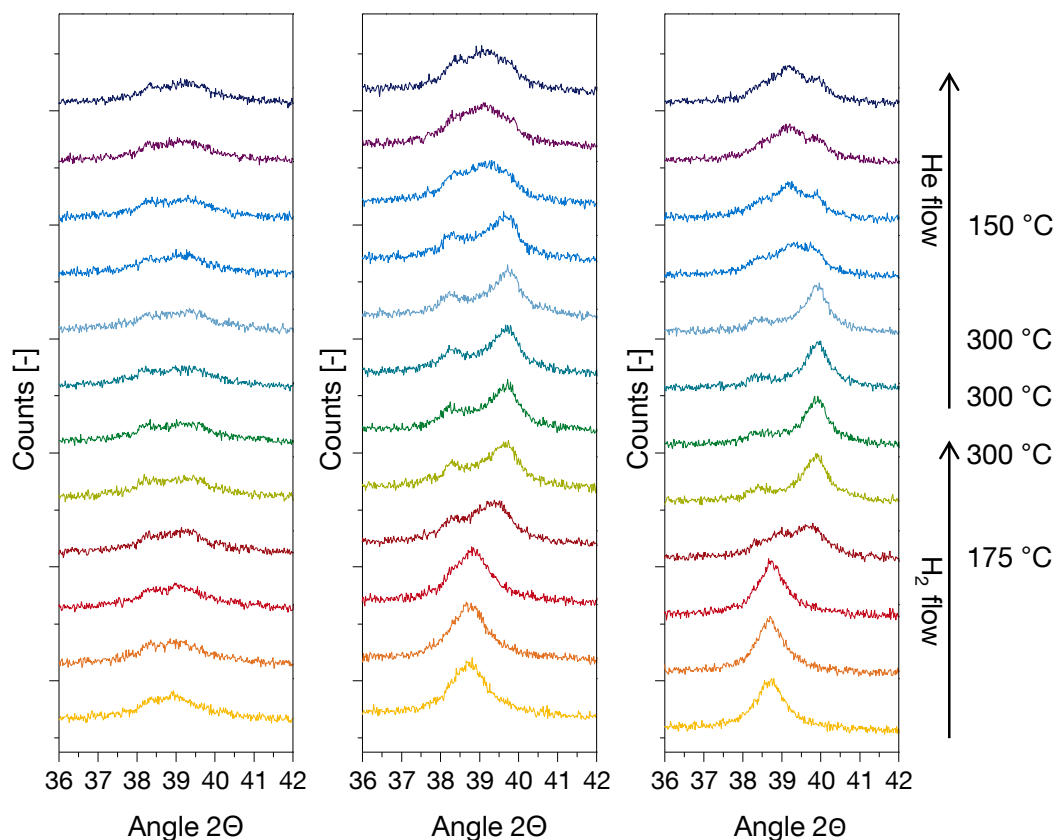
Figure 3-4: Temperature dependent XRD patterns for the reflection at the 111 plane of bimetallic particles for a) Pd/Au 1.1, b) Pd/Au 2.0 and c) Pd/Au 6.0. Temperature increases from bottom to top. 2Θ = 38.3 ° represents pure Au, 2Θ = 40.1 ° represents pure Pd phases.

Table 3-3: Alloy compositions determined by XRD of samples aged via thermal treatment. Compositions were obtained via deconvolution of the XRD profiles after the thermal treatment.

Pd/Au molar ratio	Pd_xAu_y phases present after thermal treatment in reducing atmosphere (with He flushing to remove Pd-H species)
1.1	$Pd_{0.17}Au_{0.83}$, $Pd_{0.51}Au_{0.49}$, $Pd_{0.81}Au_{0.19}$
2.0	$Pd_{0.12}Au_{0.88}$, $Pd_{0.52}Au_{0.48}$, $Pd_{0.80}Au_{0.20}$
6.0	$Pd_{0.20}Au_{0.80}$, $Pd_{0.48}Au_{0.59}$, $Pd_{0.81}Au_{0.19}$

3.3.3. Temperature dependent phase separation followed by X-ray absorption spectroscopy

X-ray absorption spectroscopy was applied in order to verify the temperature dependent phase separation found via XRD. The samples were subjected to the same temperature treatment and gas atmosphere as for the temperature dependent X-ray diffraction studies. As mentioned above, the phase separation at elevated temperatures was more pronounced for samples with high concentrations of palladium, thus a bimetallic sample with a Pd/Au molar ratio of approximately 5 was studied via *in-situ* XAS. Figure 3-5 shows the normalized X- ray absorption near-edge structure (XANES) at the Au L_{III} edge. At the Au L_{III} edge p to d electronic transitions are observed and thus the electron density in the d states is reflected by the intensity of the white line. As a reference, the monometallic sample Au/SiO_2 is presented in orange.
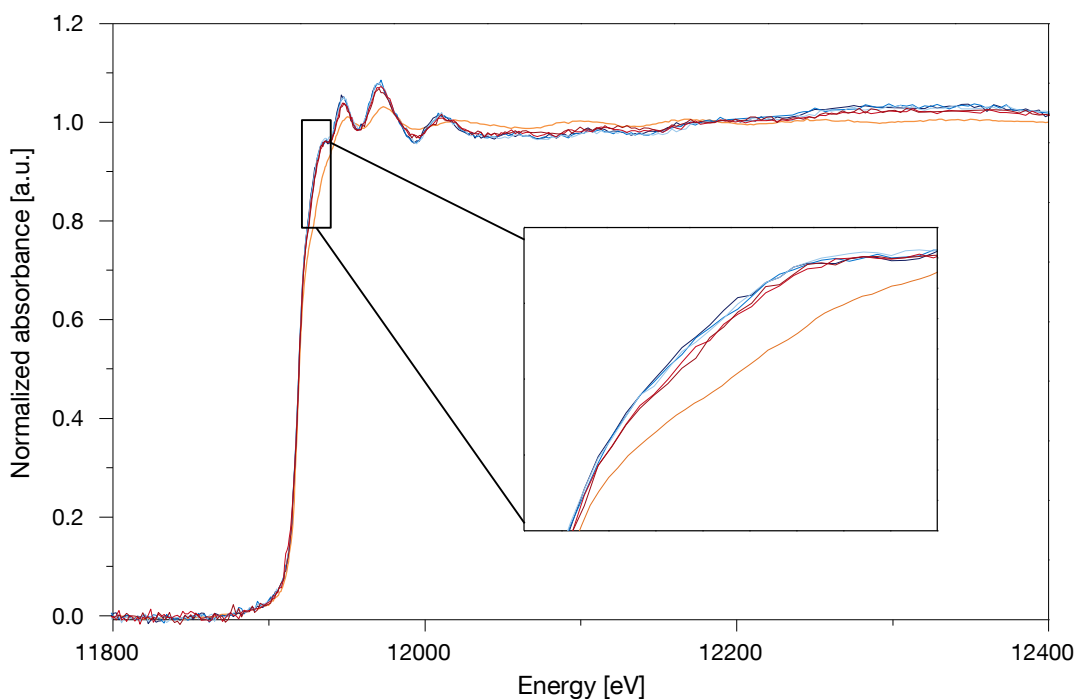
Figure 3-5: Normalized XANES at the Au L_{III} edge in He at 588 K of Au/SiO_2 and Pd-Au/SiO_2 during temperature treatment. — **Au/SiO_2,** — **Pd-Au/SiO_2 (50 °C),** — **Pd-Au/SiO_2 (100 °C),** — **Pd-Au/SiO_2 (150 °C),** — **Pd-Au/SiO_2 (250 °C),** — **Pd-Au/SiO_2 (300 °C).**

All XANES measured on the bimetallic Pd-Au/SiO_2 sample show higher white line intensities compared with the monometallic Au/SiO_2 sample, which indicates the presence of an electron deficient Au phase. Note that for Pd the K-edge was investigated,

which results from a s-to-p transition and thus shows only minor effects on the electron density in the d-bands of Pd.

The EXAFS at both the Au L_{III} edge and the Pd K edge were used to further characterize the temperature dependent reconstruction in bimetallic PdAu particles. Table 3-4 summarizes the structural parameters at the different temperatures. Coordination numbers and interatomic distances were calculated from the analysis of the EXAFS in *k* space. The temperature dependence of the EXAFS was accounted for by using the correlated Einstein model and by including the third cumulant C3 in the fit procedure. Thus the observed changes in coordination numbers and interatomic distances reflect the structural changes in the particles as function of the temperature treatment. Since EXAFS is a volume average method, pronounced changes in coordination numbers originating from reconstruction within bimetallic particles are not expected. However, two temperature regimes with respect to coordination numbers were found. Values found for N_{AuAu} in the low temperature range ($\leq$ 150 °C) are lower than those found at elevated temperatures. N_{AuPd} in contrast is higher at lower temperatures and decreases with increasing temperatures. The ratio of N_{AuPd}/N_{AuAu} is illustrated in Figure 3-6a. Due to the large excess of palladium, the values on the Pd-edge are less affected, however a slight change in average coordination numbers for temperatures above 150 °C is observed, too (compare Figure 3-6b).

Table 3-4: Results of the EXAFS analysis for PdAu/SiO$_2$ at different temperatures during temperature dependent EXAFS measurements.

Temperature	Au-Pd		Au-Au		Pd-Au		Pd-Pd	
	N	r/ Å	N	r/ Å	N	r/ Å	N	r/ Å
50 °C	4.94	2.80	4.80	2.86	0.99	2.80	5.68	2.82
100 °C	4.55	2.81	4.20	2.86	0.91	2.81	5.67	2.81
150 °C	4.71	2.78	4.90	2.84	0.94	2.78	5.51	2.77
200 °C	4.63	2.78	5.90	2.84	0.92	2.78	5.71	2.76
250 °C	4.40	2.77	6.01	2.84	0.88	2.77	5.85	2.77
300 °C	4.43	2.77	5.90	2.85	0.89	2.77	5.66	2.76

a)

b)
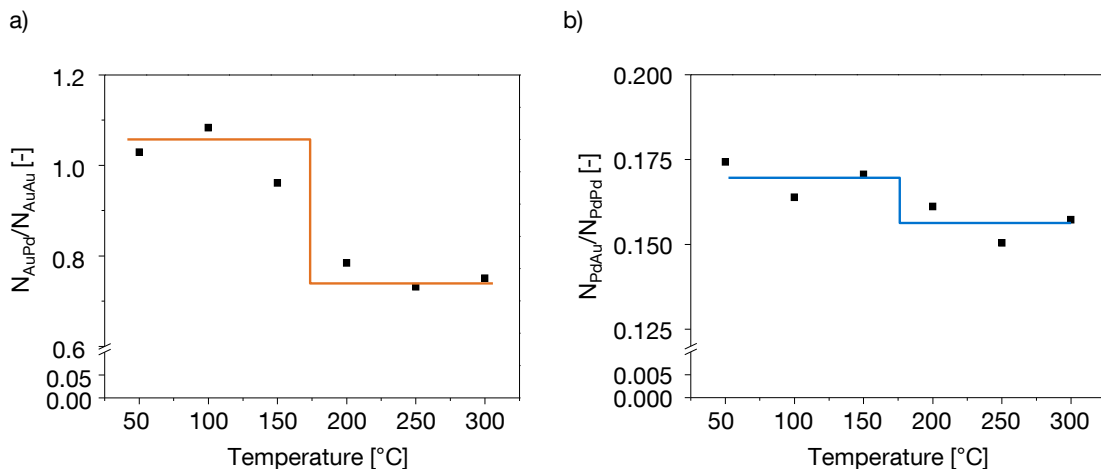
Figure 3-6: a) Ratio of the coordination numbers at the Au-edge (N_{AuPd}/N_{AuAu}) and b) at the Pd edge (N_{PdAu}/N_{PdPd}) with temperature. Orange and blue lines are a guideline for the eye.

a)   b)   c)
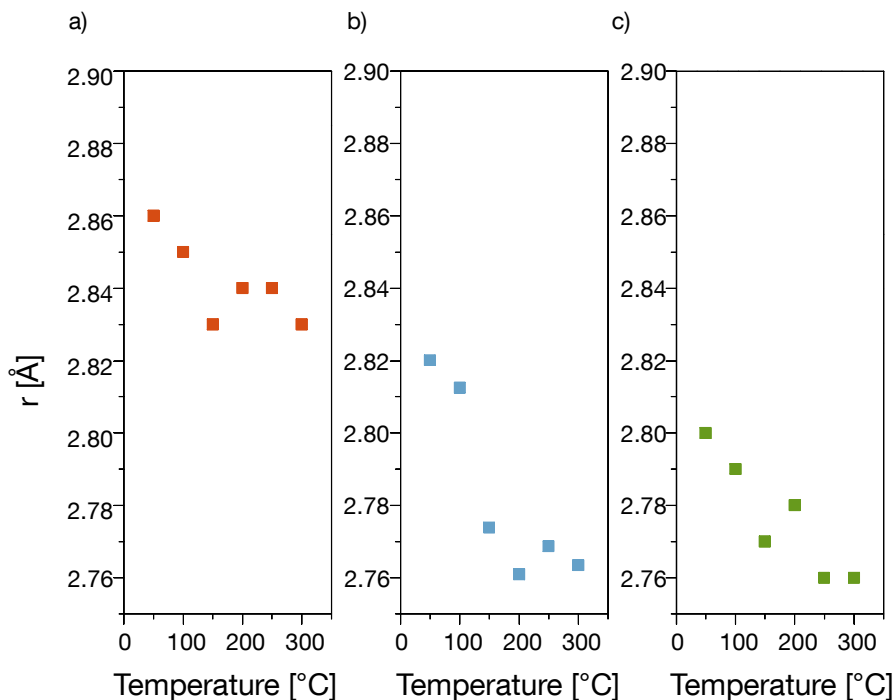
Figure 3-7: Temperature dependence of interatomic distances for a) Au-Au, b) Pd-Pd and c) Pd-Au, respectively Au-Pd.

Since the elevated temperatures were accounted for in the fit procedure by applying the correlated Einstein model and, in a second step, by including the third cumulant in the fitting procedure, the interatomic distances represent the actual situation in the bimetallic particles. Figure 3-7 shows the temperature dependence of the interatomic distances. The Au-Au distance only shows deviations from the ideal distance which are within the

measurement and fitting inaccuracy. However the Pd-Pd distances are enlarged at lower temperatures (50 and 100 °C). This originates from the formation of low-temperature stable Pd-hydrides. The effect is less pronounced for the mixed distances Pd-Au, respectively Au-Pd. At 150 °C Pd-H decomposition starts and the interatomic distance of Pd-Pd converges toward the ideal distance of 2.73 Å. The decomposition of bulk Pd-H at a temperature of 150 °C is in agreement to *in-situ* XRD measurements in reducing atmosphere. A clear shift toward higher 2Θ with respect to as prepared Pd/SiO_2 was observed for Pd/SiO_2 in flowing H_2 at low temperatures. For temperatures above 150 °C the 2Θ position was similar to the as synthesized sample. Treatment in inert atmosphere did not cause a shift in 2Θ position. Data sets of in-situ measurements of Pd/SiO_2 can be found in the supporting information. The Pd-Au distances show a simultaneous change in interatomic distances at 150 °C which is again attributed to the decomposition of Pd-H. Since gold does not form bulk hydrides, the enlargement is less pronounced for the mixed distances.

In temperature dependent XAS measurements, the Debye-Waller factors typically increase linearly with increasing temperature in the temperature range (> 100 K) studied here.[26,27,28] The EXAFS analysis yielded a temperature dependence of σ^2 which is in good agreement to these previously published data sets, including studies of Au bulk materials. Thus the correlated Einstein model provides valuable fit results for bimetallic supported particles. The temperature dependent Debye-Waller factors are shown in the supporting information. The EXAFS analysis of the third cumulant C3 yielded a non-linear increase with temperature, which is in good accordance to literature.[26,27] The temperature dependence of C3 as well as detailed results of the complete EXAFS analysis are provided in the supporting information.

Moreover the total coordination number of palladium is smaller than the total coordination number of Au. Both, palladium and gold exhibit cubic face centered lattices where the coordination number on the surface is around 6 for edges and corners and 9 for (111) surface planes, whereas it is 12 for the inner core of the metal particle. Thus low coordination numbers of Pd can originate from small monometallic particles or a surface enrichment within a bimetallic particle, while higher total coordination numbers of Pd suggest a preferred location in the core of the bimetallic particle.

3.3.4. High resolution transmission electron microscopy

In order to further support the temperature dependent phase separation within the bimetallic Pd-Au particles, high resolution electron microscopy was applied on thermally reconstructed samples. Following the thermal reconstruction *in-situ* was not possible, due to potential beam damage with extended exposure time. Figure 3-8 shows HRTEM images of a bimetallic PdAu/SiO$_2$ sample with a Pd/Au molar ratio of 1.1. Within the bimetallic particle different intermetallic regions with varying lattice distances were detected.
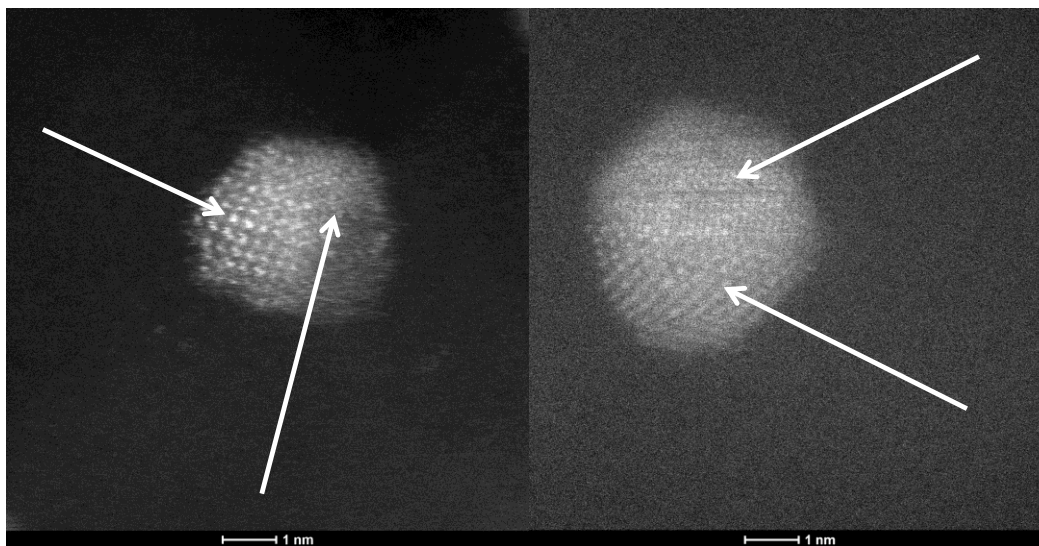
Figure 3-8: HRTEM images of Pd/Au 1.1 after thermal treatment reducing and inert atmosphere. Arrows point towards different intermetallic regions on two different particles.

3.3.5. Temperature dependent phase formation during VAM synthesis

A single Pd$_1$Au$_1$ phase was found after vinyl acetate synthesis at 150 °C with a degree of ordering close to 100 %.[12] In order to further investigate the temperature dependent restructuring during VAM synthesis, samples aged at 180 °C under reaction atmosphere were analyzed. All samples showed three distinct XRD reflections after exposure to the reactant gases at 180 °C for 120 hours, which can be assigned to bimetallic phases with compositions close to the three stable ordered phases of PdAu alloys. The reflections for the 111 plane of the samples after reaction at 150 °C and 180 °C are shown in Figure 3-9. Table 3-5 summarizes the alloy compositions found after 120 hours on stream at reaction temperatures of 150 and 180 °C, which were calculated according to Vegard's law.[29]

Please note that alloy compositions of samples aged at 180 °C are affected by the slow cooling rate (necessary to purge the AcOH from the system), which caused a reformation of the Pd_1Au_1 phase that is only stable at lower temperatures.
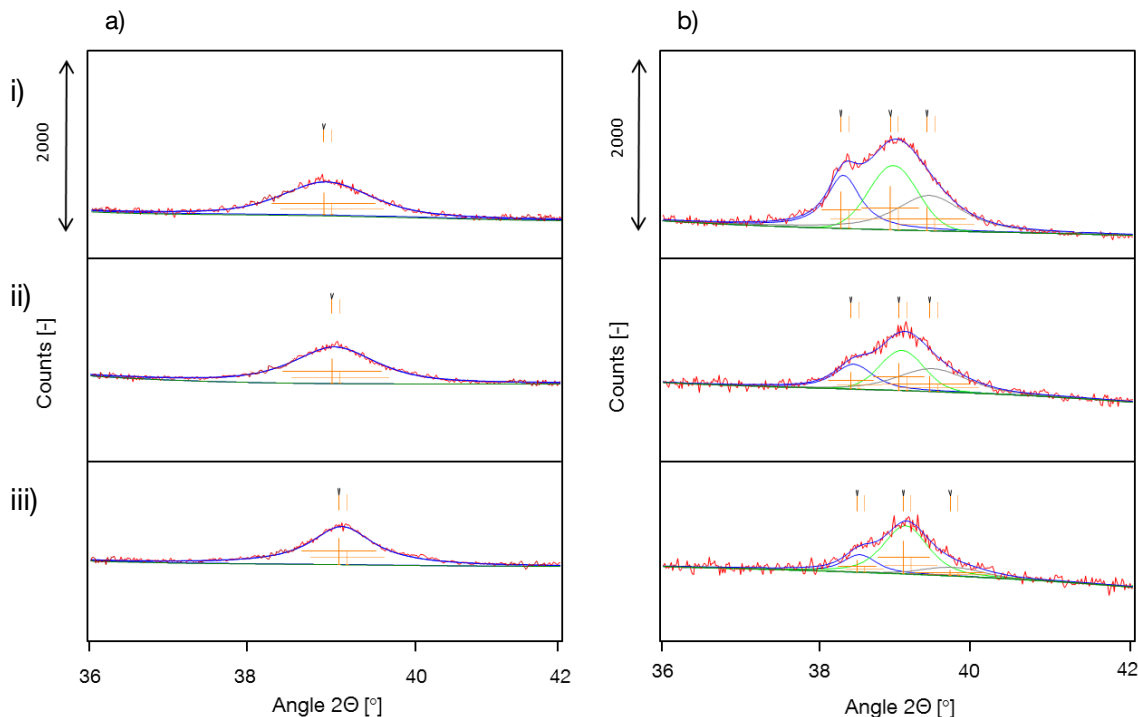
Figure 3-9: XRD profiles for the 111 reflection of bimetallic particles after 120 hours on stream at a) 150 °C and b) 180 °C for i) Pd/Au 1.1, ii) Pd/Au 2.0 and iii) Pd/Au 6.0.

In general the full width at half maximum height of the reflections is higher for the sample Pd/Au 1.1, while the XRD of the palladium rich samples Pd/Au 2.0 and 6.0 showed broader reflections for all three phases after reaction at 180 °C, (i.e., a highly Au-rich phase, a highly palladium rich phase and a nearly equimolar phase). The reflection corresponding to the Pd-rich phase exhibits the smallest full width at half maximum for all samples investigated.

The more Au is present in the sample, the higher the fraction of Au in the bimetallic phase present after reaction at 150 °C. For samples aged at 180 °C, the Pd-rich and the Au-rich bimetallic phases showed lower palladium concentrations compared with the thermal treatment in inert atmosphere (compare Table 3-3 with Table 3-5). Table 3-5 summarizes the compositions obtained by fitting of the XRD profiles of samples after vinyl acetate formation at 150 and 180 °C.

Table 3-5: Alloy compositions after 120 hours on stream for reaction temperatures of 150 and 180 °C, obtained by XRD profile fitting.

Pd/Au molar ratio	Pd_xAu_y phase compositions after 120 h on stream at a reaction temperature of 150 °C	Pd_xAu_y phase compositions after 120 h on stream at a reaction temperature of 180 °C
1.1	$Pd_{0.42}Au_{0.58}$	$Pd_{0.02}Au_{0.96}$, $Pd_{0.45}Au_{0.55}$, $Pd_{0.79}Au_{0.21}$
2.0	$Pd_{0.47}Au_{0.53}$	$Pd_{0.08}Au_{0.92}$, $Pd_{0.51}Au_{0.49}$, $Pd_{0.67}Au_{0.33}$
6.0	$Pd_{0.51}Au_{0.49}$	$Pd_{0.06}Au_{0.94}$, $Pd_{0.45}Au_{0.55}$, $Pd_{0.89}Au_{0.11}$

3.3.6. Low temperature CO adsorption on catalyst reactively aged at 150 °C and 180 °C

In order to evaluate the effect of temperature during reaction on the surface composition of the catalysts after exposure to the reactants, low temperature CO adsorption was applied on catalysts aged at 180 °C. In our previous work[12] we showed that samples aged at 150 °C exhibit bimetallic particles with similar surface compositions and that the surface is highly intermixed after reaction. The results for samples aged at 150 °C and 180 °C are compared in Table 3-6. CO adsorbed on Au, which is electronically altered by a close contact to Pd is named CO on 'Au next to Pd' species. CO adsorbed on 'Au next to Au' represents CO on Au atoms, which are mainly surrounded by Au. The corresponding nomenclature is used to assign the bands for CO adsorbed on palladium. The assignments of the linear CO species on Au and Pd are supported by Liu and Nørskov[30]. The change in frequency of the CO stretching vibration reflects changes in the electron density of the Pd d-band states, which result from an increasing number of Au atoms in contact with Pd.

The IR spectra after adsorption of CO at -150 °C on the sample with a Pd/Au molar ratio of 6.0 aged at 150 °C and 180 °C are shown in Figure 3-10. The comparison of samples after reaction at 150 °C and 180 °C of the remaining samples is shown in the supporting information. The bands at 2156 - 2185 cm^{-1} are assigned to the interaction of CO with terminal hydroxyl groups on the support and cations (e.g. K^+).

Table 3-6: Ratios of the IR intensities of CO species adsorbed on Pd and Au in catalysts reconstructed in reactant atmosphere at 150 °C and 180 °C.

Pd/Au molar ratio	Reaction temperature [°C]	Au next to Pd/ Au next to Au	Pd next to Au/ Pd next to Pd	Linear/ multi-fold on Pd
1.1	180 °C	0.7	2.8	1.0
	150°C	0.6	0.2	0.9
2.0	180 °C	0.7	0.5	5.4
	150°C	1.3	0.2	0.9
6.0	180 °C	0.7	0.8	6.2
	150°C	1.3	0.2	1.4

CO linearly adsorbed on Pd (on 'Pd next to Pd' and 'Pd next to Au') can be observed in the region of 2090 cm^{-1} and 2040 cm^{-1}. Multi fold adsorbed CO on Pd is located at wavenumbers below 2000 cm^{-1}, the intensity of these bands is dependent on the degree of surface mixing.[31] CO linearly on 'Au next to Pd' and 'Au next to Au' is located between 2130 cm^{-1} and 2094 cm^{-1}. The shift in wavenumbers with respect to CO on pure Pd (2094 cm^{-1}) and Au (2098 cm^{-1}) depends on the electronic interaction between the metallic components in the bimetallic phase. The close contact between Pd and Au results in an electron transfer from Au to Pd[30], leading to an increase in the occupation of the Pd d-states and in an enhanced back donation from the d-level electrons of Pd to the π*-orbitals of CO. In the same way the back donation for electronically altered Au to CO is reduced. These changes in back-donation result in a red-shift of the CO stretching vibration on Pd and a blue-shift on Au, the extend of both being dependent on the surface intermixing.

a)   b)
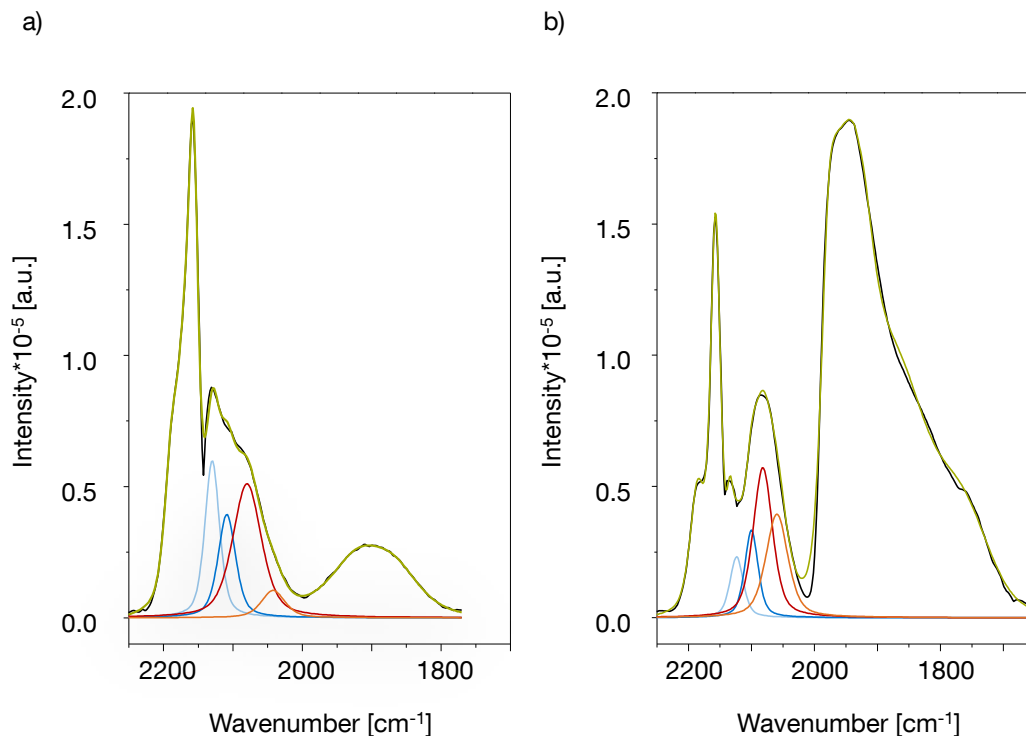
Figure 3-10: IR spectra of adsorbed CO at -150 °C and 1 mbar partial pressure of CO on PdAu/SiO₂ with a Pd/Au molar ratio of 6.0. a) After 120 hours time on stream at 150°C, b) after 120 hours time on stream at 180°C. Blue lines represent CO on gold (light blue shifted to higher wavenumbers by interaction with Pd), red on palladium (lighter red shifted to lower wavenumbers by interaction with Au). Black lines represent measured data sets, green lines the sum deconvolution.

The main difference between samples aged at 150 °C and 180 °C is the ratio in intensity of linear to multi-fold bound CO on palladium. This ratio is enhanced by a factor of up to 5 for samples aged at 180 °C, indicating that after reaction at 180 °C the bimetallic surface is less intermixed compared to samples after reaction at 150 °C. Since multifold bound CO is only present on palladium, the effect is more pronounced for Pd rich catalysts. Samples with low Pd/Au ratios, e.g Pd/Au 1.1, exhibit high concentrations of Au-rich phases, where multifold adsorption was not observed.

The ratio of CO on 'Au next to Pd'/'Au next to Au' was found to be similar for all samples studied after ageing at 150 °C and 180 °C. In general samples aged at 180 °C show lower 'Au next to Pd'/'Au next to Au' ratios compared to samples aged at 150 °C. This indicates that the surfaces were found to be more intermixed after reactions performed at 150 °C. Moreover the overall intensity of CO adsorbed on Au compared to Pd decreases on samples aged at 180 °C, while the surface concentration of palladium is

significantly enhanced (compare intensities of blue peaks with respect to red peaks in Fig. 3-10 a and b). Samples after reaction at 150 °C showed a similar surface composition for the Au-rich phase (represented by 'Au next to Pd'/'Au next to Au'), independent of the applied Pd/Au ratio. A similar behavior was found for samples after 180 °C, however, as mentioned above, with lower 'Au next to Pd'/'Au next to Au' ratios.

The ratio of bands assigned to CO adsorbed on Pd ('Pd next to Au'/'Pd next to Pd') was highly affected by the presence of residual potassium, which remained on the metal particles after reaction and caused a pronounced broadening of the CO bands adsorbed on Pd.[32,33] Thus values of 'Pd next to Au'/'Pd next to Pd' cannot be used as a direct measure for the degree of surface intermixing between palladium and gold. Less potassium was found on samples after reaction at 180 °C as the features representing CO on K^+ (bands in the region 2156 – 2185 cm^{-1}) are less pronounced in Figure 3-10 b than in Figure 3-10 a.[34,35]

An additional measure for the degree of alloying is the shift in the frequency of the CO bands assigned to 'Au next to Pd', and 'Pd next to Au' compared to the monometallic samples. In general the shifts in the peak positions induced by electronic interactions were less pronounced for samples aged at 180 °C (i.e., 10 cm^{-1}) compared to the ones treated at 150 °C (i.e., 15 cm^{-1}), which indicates that the bimetallic surface is less intermixed for samples treated at elevated temperatures. As mentioned above, shifts found for palladium were not only affected by the interaction between Pd and Au, but also by the presence of residual potassium and thus cannot be directly assigned to a certain degree of surface intermixing. In general the effect of residual potassium is more pronounced for samples with higher palladium contents, since these samples exhibit higher amounts of dispersed palladium in close contact to potassium.

3.3.7. Leaching of Pd from the bimetallic particles

In order to verify that Pd is leached from the bimetallic particles in the presence of acetic acid[12], a fully reduced catalyst (Pd/Au 5.0) was dispersed in acetic acid at 25 °C and stirred for 72 hours. The AcOH solution and the catalyst before and after the AcOH

treatment were analyzed using AAS, results are given in Table 3-7. The acetic acid was removed via centrifugation and exhibited a yellow-orange color. AAS analysis revealed that only palladium was removed from the sample, while the concentration of gold found in the AcOH solution after the treatment was negligible and the deviations in Au concentration of the catalysts are within the measurement inaccuracies.

Table 3-7: Concentrations of palladium and gold of a catalyst before and after AcOH treatment for 72 hours.

Sample	Pd concentration	Au concentration
Catalyst before AcOH treatment	1.75 wt.-%	0.68 wt.-%
Catalyst after AcOH treatment	0.70 wt.-%	0.66 wt.-%
AcOH solution after treatment	400 ppm	0.4 ppm

3.4. Discussion

3.4.1. Temperature dependent phase separation in bimetallic particles

In-situ XRD indicated that under He atmosphere a pronounced phase separation towards a palladium rich and a gold rich phase occurs at approximately 160 °C. This phase separation was more pronounced for samples with high palladium concentrations. During cooling to room temperature bimetallic Pd-Au phases with compositions close to 3:1, 1:1 and 1:3 were formed. These phases are in accordance to the Pd-Au phase diagram presented.[9] The less pronounced phase separation for gold rich samples can be explained by the higher Au concentration in the bimetallic particles, which limits the formation of the palladium rich Pd_3Au_1 phase and thus the separation towards a Pd-rich phase is not as visible in XRD as for the palladium rich samples. Before reaction the phase composition of the bimetallic particles reflect the overall chemical composition. Under reaction conditions at 150 °C all samples self-assemble during the first 20-30 hours time-on-stream towards the equimolar Pd_1Au_1 phase, which results in higher activity and selectivity levels. The reconstruction in reactant atmosphere is based on the formation of

palladium acetate species followed by a leaching into the liquid surface layer consisting of AcOH and water under reaction conditions. In contrast, under inert atmosphere the temperature dependent reconstruction does not involve a leaching process, but the reconstruction takes place within the bimetallic particle.

This temperature dependent phase separation within the particle was also followed via *in-situ* X-ray absorption spectroscopy studies. The XANES at the Au L_{III} edge showed a lower electron density for Au in the bimetallic $PdAu/SiO_2$ sample compared to the Au/SiO_2 sample, which implies an increase in the electron deficiency in the Au d-band by alloying with Pd. The white line heights show that the temperature has only a slight effect on the electronic state of Au. In agreement with *in-situ* XRD, a temperature increase above 160 °C led to a phase separation towards the Pd-rich Pd_3Au_1 and the Au-rich Pd_1Au_3 phases. Since XAS data average over the volume, clusters with a larger number of Au atoms are weighted more than clusters with fewer Au atoms.[22] Thus both for white line intensities and coordination numbers, the Au-rich phase has a more pronounced influence. Therefore the slight decrease in white line intensity for higher temperatures can be assigned to the formation of the Au-rich phase, which is less alloyed and thus exhibits a lower electron deficiency in the d-band of Au. The phase separation at elevated temperatures is also visible in the coordination numbers. Above a temperature of 150 °C the Au-Au coordination number increases and simultaneously the Au-Pd coordination number deceases. Taking into account that the sample studied is Pd-rich (Pd/Au molar ratio ≈ 5) the formation of a Pd_3Au_1 phase is favored. However, since bimetallic particles with various compositions were present after synthesis, some particles are likely to be rich in Au, which leads to the additional formation of the Au-rich Pd_1Au_3 phase. Note that a homogenous distribution of the elements in the particles would lead to the formation of the Pd-rich Pd_3Au_1 phase, in which Au-Au neighbors are non-existent ($N_{Au-Au}=0$). As mentioned above, Au-rich regions have a pronounced impact on the overall coordination numbers. Changes in the coordination numbers of palladium are less evident than for the gold, since the reconstruction in the mainly palladium rich particles does not cause severe changes in the environment of the palladium atoms. The high concentration of the Pd_3Au_1 phase is also visible in the interatomic distances of Pd-Au and Au-Pd at temperatures above 150 °C. The Pd-Au, respectively Au-Pd distances are

more on the side of the Pd-Pd distance, which is due to the low concentration of Au within the Pd_3Au_1 phase. Since only few Au-Au neighbors are expected to be present in a bimetallic alloy mainly consisting of an ordered Pd_3Au_1 phase, a lattice distortion induced by Au located within the Pd lattice occurs only to a minor extent.

Moreover, the phase separation towards a Pd-rich and Au-rich phase was also observed in high resolution TEM images. Two or more regions with different lattice spacing were found within one particle. The thermal treatment, performed under similar conditions as during *in-situ* XRD and *in-situ* XAS studies, led to a phase separation within the bimetallic particle. Thus HRTEM images confirmed that a thermal reconstruction took place within the bimetallic particle and led to particles with regions of different (intermetallic) phase composition within a single particle.

3.4.2. Metal clusters present after reaction

Combining the analysis of the EXAFS with modeling of the local arrangement of the atoms inside the bimetallic particle directly confirms the proposed restructuring of the metal phase under reaction conditions at 150 °C. All samples showed the same ratio for the Au neighbors (N_{Au-Pd}/N_{Au-Au}) of approximately 2.0, which results from the presence of bimetallic particles with ordered Pd_1Au_1 morphology. The concentration of the dispersed palladium phase, obtained from the palladium related coordination numbers (see Fig. 3-3), are in good agreement to those calculated on the basis of the chemical composition, taking possible inaccuracies in measurement and data fitting into account. Values for the concentration of dispersed palladium derived from the modeling can be estimated by using the correlation based on the total coordination number of palladium ($N_{Pd\ total}$) or using the correlation based on the N_{Pd-Au}/N_{Pd-Pd} ratio. For example, varying concentrations of the dispersed palladium phase are a possible source for discrepancies in the concentration of the monometallic phase calculated according to the chemical composition and according to the correlations derived from EXAFS analysis. The higher the concentration of dispersed palladium, the larger are the monometallic palladium particles formed during re-reduction. This leads to an increase in the Pd-Pd coordination number, and thus to, e.g., a lower ratio of N_{Pd-Au}/N_{Pd-Pd} which is used to estimate the fraction of dispersed Pd (compare Figure 3-3 b).

XRD as well as the analysis of the EXAFS support the assumption that Au is fully incorporated into the equimolar bimetallic phase. The restructuring mechanism via dissolution of palladium from the particles via formation of palladium acetate species was confirmed by treating a reduced catalyst in AcOH for 72 hours, where about 60 % of the palladium present was dissolved in acetic acid, whereas Au was not removed from the reduced sample. This restructuring mechanism via leaching assumes a high affinity of acetic acid to palladium, while the interaction with gold has to be very weak. A pronounced AcOH induced segregation of Pd to the bimetallic surface was also found by Owens et al.[36], who studied the adsorption and thermal decomposition of acetic acid on deposited Au on Pd 111. A similar segregation effect was found for the adsorption of formic acid on PdAu/ɣ-Al_2O_3, where the surface concentration of Pd increased after contact to 2.2 vol.-% gaseous formic acid.[46,37]

3.4.3. Temperature dependent self-organization during VAM formation

In [12] we showed that the initiation period observed for bimetallic Pd/Au-SiO_2 samples can be related to the dynamic self-assembling of the bimetallic particles at reaction temperatures close to 150 °C.[38] Here we showed that at higher temperatures a phase separation towards a palladium-rich phase and a gold-rich phase occurs, which either leads to palladium-rich or gold-rich surfaces. Both resulted in a lower selectivity, as large palladium assembles promote the total oxidation of C_2H_4 to CO_2, the main byproduct of the reaction. On Au-rich surfaces with a gold fraction of higher than 0.7, C_2H_4 primarily adsorbs on Au, which also favors the combustion of C_2H_4 to CO_2.[39]

The XRD profiles of samples aged at 180 °C showed the presence of three alloy phases after reaction, while in contrast on samples aged at 150 °C only one distinct Pd_1Au_1 phase was observed. The three phases found after reaction at 180 °C exhibit compositions close to the three ordered phases predicted by the PdAu phase diagram.[9] Temperature dependent *in-situ* XRD and *in-situ* XAS studies indicated that the phase separation of the Pd_1Au_1 phase starts at temperatures above 160 °C, therefore, we can assume that the Pd_1Au_1 phase in not stable during reactions at 180 °C. However all three phases were found after reaction, which suggests that the Pd_1Au_1 phase is preferentially formed via reactant induced self-assembling during VAM synthesis. Both the Pd-rich and Au-rich

phase were found to have lower concentrations of palladium compared with the respective sample after thermal treatment in an inert atmosphere. This can be explained by the leaching of palladium from the bimetallic particle by the acetic acid present under reaction conditions via formation of palladium acetate. Due to the higher concentration of palladium within the Pd-rich phase, the formation of palladium acetate is favored and leads to a depletion of palladium in the Pd_3Au_1 phase. For the Pd_1Au_3 phase already small extents of palladium leaching lead to a pronounced decrease in the overall concentration of palladium within the Au-rich domain.

Low temperature CO adsorption also confirms the phase separation at higher reaction temperatures. CO adsorption at -150 °C for samples aged at 150 °C showed only low amounts of multifold adsorbed CO (ratio linear/multi-fold ≈0.9). For samples treated at 180 °C, an up to 5-fold increase in the ratios between linear and bridged adsorbed CO was found. This clearly supports the assumption of the formation of a Pd rich and a Au-rich phase at higher temperatures. The surface of the Pd rich phase is significantly less intermixed than the surface of an equimolar phase. Since multi-fold adsorption of CO on palladium is favored for large palladium ensembles, the high ratio of linear/multi-fold CO indicates the formation of a Pd rich phase at a reaction temperature of 180 °C, which has to be accompanied by the formation of an Au rich phase, resulting from the phase separation discussed above. The low ratios for CO adsorbed on Au in close neighborhood to Pd ('Au next to Pd') and CO adsorbed on Au without Pd neighbors ('Au next to Au') (see Table 3-6) for samples after reaction at 180°C are again supporting the phase separation at higher temperatures. The ratio 'Au next to Pd'/'Au next to Au' can be used as a measure for the degree of surface intermixing between Pd and Au. High values represent high degrees of surface intermixing as a phase separation towards a palladium rich and a gold rich phase leads to a decrease in the number of Pd and Au atoms in close neighborhood, while the low values found for samples after reaction at 180 °C result from a low degree of intermixing. The values for the ratio 'Au next to Pd'/'Au next to Au' are similar for all bimetallic Pd/Au catalysts studied within one reaction temperature, which implies that the Au containing surfaces are similar after reaction. For a reaction temperature of 150 °C the surface is similar, since only equimolar bimetallic particles are present. For a reaction temperature of 180 °C, the Au containing surfaces within the

Au-rich bimetallic phase exhibit similar degrees of intermixing, implying that independent of the Pd/Au ratio present in the catalyst one specific Au-rich phase, the Pd_1Au_3 phase, is formed as identified via XRD.

The elevated reaction temperature led to a surface enrichment in palladium, compared to a reaction temperature of 150 °C. This surface enrichment in palladium can promote the leaching of palladium from the bimetallic particle under reaction conditions and could provide an explanation for the differences in deactivation behavior at different temperatures as reported in the literature e.g. by Brückner et al.[40]

3.5. Conclusions

A series of Pd-Au catalysts supported on amorphous SiO_2 were synthesized via incipient wetness impregnation, including a precipitation and washing step to remove chloride. The synthesis procedure led to bimetallic particles with various Pd_xAu_y compositions. Thermal treatment in H_2-He atmosphere revealed severe phase separation towards a palladium rich and a gold rich phase at elevated temperatures. This separation occurs at a temperature of approximately 160°C. The phase separation was additionally followed by *in-situ* XAS studies and also observed by HRTEM of thermally restructured samples. Slow cooling rates in inert atmosphere lead to the (re-)formation of three bimetallic phases, Pd_3Au_1, Pd_1Au_1 and Pd_1Au_3. These compositions are in agreement with the stable ordered phases according to the Pd/Au phase diagram. Dynamic self-assembling under reactant atmosphere at 150°C led to the formation of the Pd_1Au_1 phase, the remaining Pd was present as a monometallic dispersed palladium phase. Via particle modeling and comparison with EXAFS data, the Pd_1Au_1 phase was identified to be highly ordered and the existence of the dispersed palladium phase was confirmed. The presence of dispersed palladium was further verified by exposure of a reduced sample to acetic acid, where Pd was removed from the bimetallic particles in form of palladium acetate. Characterization via XRD and low temperature CO adsorption of samples after vinyl acetate formation at 180°C showed that the phase separation found for the temperature treatment in H_2-He also took place in reactant atmosphere. However, the presence of the Pd_1Au_1 phase was more pronounced for reactively aged samples at 180°C compared to samples treated at

elevated temperatures in inert atmosphere. Elevated reaction temperatures promote the surface enrichment of palladium, which is a possible explanation for the temperature dependence of deactivation rates.

3.6. Acknowledgments

3.7. References

1.   I. I. Moiseev, M. N. Vargaftic, Y. K. Syrkin, *Doklady Akademii Nauk SSSR* **1960**, *133*, 377

2.   T. C. Bissot (E. I. Du Pont de Nemours and Company), *US 4048096*, **1977**.

3.   D. Kumar, M. S. Chen, D. W. Goodman, *Catalysis Today* **2007**, *123*, 77-85.

4.   S. Nakamura, T. Yasui, *Journal of Catalysis* **1970**, *17*, 366.

5.   M. Chen, D. Kumar, C.-W. Yi, D. W. Goodman, *Science* **2005**, *310*, 291-293.

6.   Y. F. Han, J. H. Wang, D. Kumar, Z. Yan, D. W. Goodman, *Journal of Catalysis* **2005**, *232*, 467.

7.   M. S. Chen, K. Luo, T. Wei, Z. Yan, D. Kumar, C. W. Yi, D. W. Goodman, *Catalysis Today* **2006**, *117*, 37.

8.   K. Luo, T. Wei, C. W. Yi, S. Axnanda, D. W. Goodman, *The Journal of Physical Chemistry B* **2005**, *109*, 23517.

9.   H. Okamoto, T. Massalski, *Journal of Phase Equilibria* **1985**, *6*, 229-235.

10.   B. Zhu, M. Hou, *The European Physical Journal D* **2012**, *66*, 63.

11.   I. S. Atanasov, M. Hou, *The European Physical Journal D* **2009**, *52*, 51-54.

12.   S. Simson, A. Jentys, J. A. Lercher, *The Journal of Physical Chemistry C* **2013**, *117*, 8161-8169.

13.   V. N. Kalevaru, A. Benhmid, J. Radnik, M. M. Pohl, U. Bentrup, A. Martin, *Journal of Catalysis* **2007**, *246*, 399.

14.   E. A. Crathorne, D. Macgowan, S. R. Morris, A. P. Rawlinson, *Journal of Catalysis* **1994**, *149*, 254-267.

15.   W. M. Haynes, *Handbook of Chemistry and Physics Vol. 91*, CRC Pr Inc, Cleveland **2010-2011**.

16.   H.-J. Eberle, R. Heidenreich, J. Weis (Wacker-Chemie GmbH), *DE 10200605800 A1* Germany, **2008**.

17.   M. J. Newville, *Journal of Synchrotron Radiation* **2001**, *8*, 322.

18.   B. Ravel, M. J. Newville, *Journal of Synchrotron Radiation* **2005**, *12*, 537-541

19.   G. H. Via, K. F. Drake, G. Meitzner, F. W. Lytle, J. H. Sinfelt, *Catalysis Letters* **1990**, *5*, 25-33.

20.   L. L. Araujo, P. Kluth, G. de M. Azevedo, M. C. Ridgway, *Physical Review B* **2006**, *74*, 184102.

21.   M. Vaccari, P. Fornasini, *Journal of Synchrotron Radiation* **2006**, *13*, 321-325.

22.   A. I. Frenkel, *Chemical Society Reviews* **2012**, *41*, 8163-8178.

23.   M. Bauer, H. Bertagnolli, *The Journal of Physical Chemistry B* **2007**, *111*, 13756-13764.

24.   E. Bus, J. T. Miller, A. J. Kropf, R. Prins, J. A. van Bokhoven, *Physical Chemistry Chemical Physics* **2006**, *8*, 3248-3258.

25.   A. Jentys, *Characterization of Bimetallic Pt/Ni Catalysts by X-ray Absorption Spectroscopy*, Technische Universität Wien, Wien, **1991**.

26.   M. Okube, A. Yoshiasa, O. Ohtaka, H. Fukui, Y. Katayama, W. Utsumi, *Solid State Communications* **2002**, *121*, 235-239.

27.   R. Giulian, et al., *Journal of Physics: Condensed Matter* **2009**, *21*, 155302.

28.   B. Joseph, A. Iadecola, L. Malavasi, N. L. Saini, *Journal of Physics: Condensed Matter* **2011**, *23*, 265701.

29.   L. Vegard, *Zeitschrift für Physik* **1921**, *5*, 17-26.

30.   P. Liu, J. K. Norskov, *Physical Chemistry Chemical Physics* **2001**, *3*, 3814-3818.

31.   E. L. Kugler, M. Boudart, *Journal of Catalysis* **1979**, *59*, 201-210.

32.   B. E. Hayden, A. W. Robinson, P. M. Tucker, *Journal of Electron Spectroscopy and Related Phenomena* **1987**, *44*, 297-304.

33.   P. A. J. M. Angevaare, H. A. C. M. Hendrickx, V. Ponec, *Journal of Catalysis* **1988**, *110*, 11-17.

34.   T. Montanari, L. Castoldi, L. Lietti, G. Busca, *Applied Catalysis A: General* **2011**, *400*, 61-69.

35.   T. Montanari, R. Matarrese, N. Artioli, G. Busca, *Applied Catalysis B: Environmental* **2011**, *105*, 15-23.

36.   T. G. Owens, T. E. Jones, T. C. Q. Noakes, P. Bailey, C. J. Baddeley, *The Journal of Physical Chemistry B* **2006**, *110*, 21152-21160.

37.   D. A. Bulushev, S. Beloshapkin, P. E. Plyusnin, Y. V. Shubin, V. I. Bukhtiyarov, S. V. Korenev, J. R. H. Ross, *Journal of Catalysis* **2013**, *299*, 171-180.

38. M.-M. Pohl, J. Radnik, M. Schneider, U. Bentrup, D. Linke, A. Brückner, E. Ferguson, *Journal of Catalysis* **2009**, *262*, 314.

39. F. Calaza, F. Gao, Z. Li, W. T. Tysoe, *Surface Science* **2007**, *601*, 714-722.

40. Q. Smejkal, D. Linke, U. Bentrup, M. M. Pohl, H. Berndt, M. Baerns, A. Brückner, *Applied Catalysis A: General* **2004**, *268*, 67-76.

3.8. Supporting information

Temperature dependent X-ray absorption spectroscopy

Figure 3-S1 shows the temperature dependence of the Debey-Waller factor for the Au L_{III} and the Pd K edge. A linear increase with temperature is found for σ^2 of both edges, which is in good agreement to literature.[1,2,3]
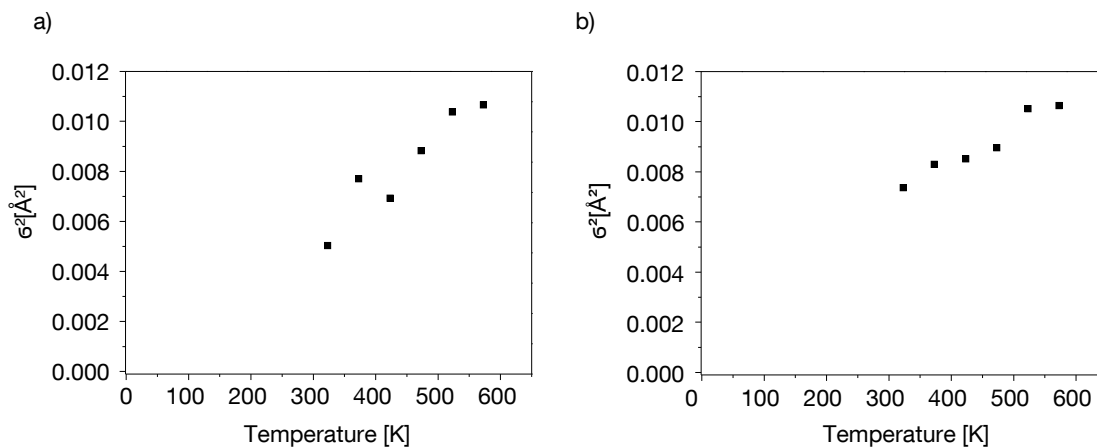

Figure 3-S1: Temperature dependence of the σ^2 for a) the Au-edge and b) the Pd-edge.

Table 3-S1 lists the complete results of the EXAFS analysis for PdAu/SiO$_2$ with a Pd/Au molar ratio of five at different temperatures, including the values for the third cumulant C3.

Table 3-S1: Results of the EXAFS analysis for PdAu/SiO$_2$ at different temperatures during temperature dependent EXAFS measurements.

T [K]	Au-Pd		Au-Au		Pd-Au		Pd-Pd		E$_0$(Au)	σ²(AuAu)	E$_0$(Pd)	σ²(PdPd)	σ²(AuPd)=σ²(PdAu)	C3(PdPd)	C3(PdAu)=C3(AuPd)	C3(AuAu)	R-factor
	N	r/ Å	N	r/ Å	N	r/ Å	N	r/ Å	[eV]	[Å²]	[eV]	[Å²]	[Å²]	[Å³]]	[Å³]	[Å³]	[-]
323	4.94	2.80	4.80	2.86	0.99	2.80	5.68	2.82	4.11	0.00557	-2.44	0.00750	0.00406	0.00015	0.00020	0.00016	0.029
373	4.56	2.81	4.20	2.85	0.91	2.79	5.64	2.81	4.36	0.00734	-1.62	0.00846	0.00342	0.00018	0.00019	0.00020	0.055
423	4.72	2.78	4.90	2.83	0.94	2.77	5.51	2.77	3.37	0.00693	-2.88	0.00852	0.00526	0.00025	0.00049	0.00029	0.032
473	4.67	2.78	6.06	2.84	0.93	2.78	5.74	2.76	3.25	0.00815	-2.52	0.00958	0.00595	0.00034	0.00057	0.00066	0.152*
523	4.40	2.77	6.01	2.84	0.88	2.76	5.81	2.77	2.11	0.01006	-3.23	0.01046	0.00803	0.00046	0.00073	0.00094	0.042
573	4.43	2.76	5.90	2.83	0.89	2.76	5.66	2.76	3.22	0.01050	-3.19	0.01051	0.00673	0.00070	0.00082	0.00105	0.046

*reason for high R-factor: severe glitches in Au L$_{III}$ edge spectrum

Low temperature CO adsorption on catalysts reactively aged at 150 °C and 180°C

Figure 3-S2 and 3-S3 show the FTIR spectra of CO adsorbed at -150 °C on Pd/Au 2.0 and Pd/Au 1.1 after reaction at 150 °C and 180 °C. Samples aged at 180 °C exhibit strong adsorption features representing multifold adsorbed CO (below 2000 cm^{-1}). Above 160 °C, phase separation towards a Pd-rich and a Au-rich phase occurs within the bimetallic particles, leading to larger Pd domains and thus to multifold CO adsorption. This effect is more distinct for Pd-rich samples (also compare Figure 3-10 in the main contribution). In samples with low Pd/Au ratios, Pd-rich phases formed via phase separation at elevated temperatures (T > 160 °C) are subject to massive Pd leaching. In samples with high Pd/Au ratios, high concentrations of the dispersed Pd phase within the liquid surface layer present under reaction conditions slow down the leaching process and thus larger Pd domains are stabilized.
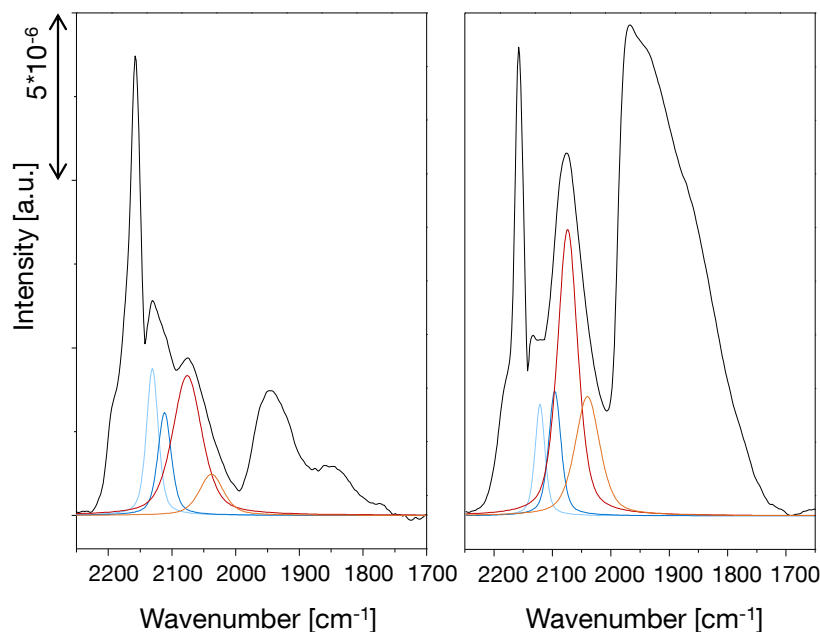
Figure 3-S2: IR spectra of adsorbed CO at -150 °C and 1 mbar partial pressure of CO on PdAu/SiO$_2$ with a Pd/Au molar ratio of 2.0. a) After 120 hours time on stream at 150°C, b) after 120 hours time on stream at 180°C. Blue lines represent CO on gold (light blue peak shifted to higher wavenumbers by interaction with Pd), red on palladium (light red peak shifted to lower wavenumbers by interaction with Au). Black lines represent measured data sets.

Thus for low Pd/Au ratios, bimetallic particles after vinyl acetate formation at elevated temperatures exhibit few monometallic palladium domains leading to less pronounced multi-fold CO adsorption.

Besides the increased fraction of multifold adsorbed CO, which represents larger monometallic Pd domains, less Au is present on the surface of the bimetallic particles. The ratio of 'CO adsorbed on Pd'/'CO adsorbed on Au' is higher for samples aged at 180 °C (compare intensity of red and blue peaks in Figure 3-S2 and 3-S3). Via the formation of Pd-acetate species and the subsequent dissolution out of the bimetallic particle the surface concentration of Pd is enhanced.
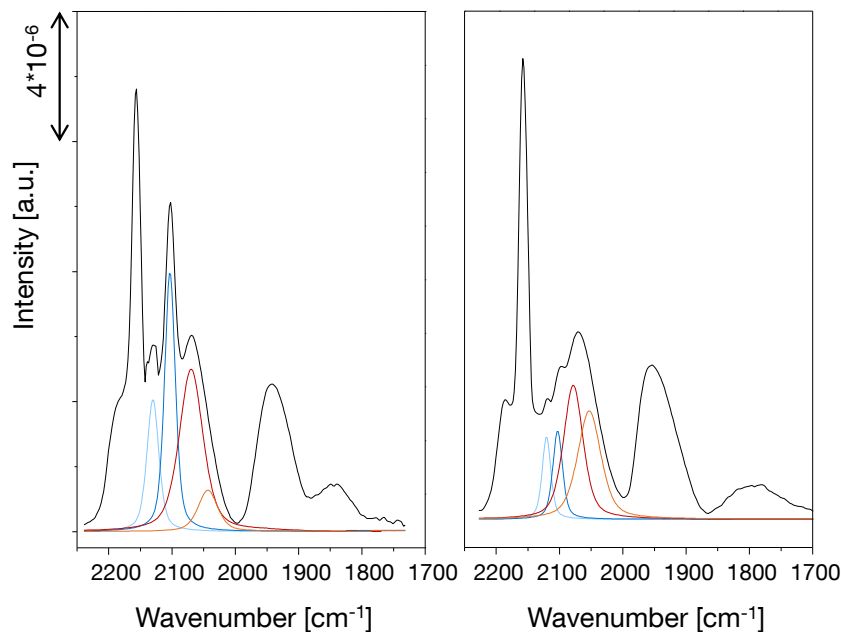

Figure 3-S3: IR spectra of adsorbed CO at -150 °C and 1 mbar partial pressure of CO on PdAu/SiO$_2$ with a Pd/Au molar ratio of 1.1. a) After 120 hours time on stream at 150°C, b) after 120 hours time on stream at 180°C. Blue lines represent CO on gold (light blue peak shifted to higher wavenumbers by interaction with Pd), red on palladium (light red peak shifted to lower wavenumbers by interaction with Au). Black lines represent measured data sets.

Temperature dependent Pd-H decomposition followed by *insitu*-XRD

Figure 3-S4 shows the temperature dependent Pd-H decomposition for a monometallic Pd/SiO$_2$ sample. At low temperatures (up to 150 °C), Pd forms Pd-H in the presence of H$_2$. The reflection is shifted to lower 2Θ values, caused by a widening of the lattice by the incorporation of hydrogen. At temperatures above 150 °C Pd-H decomposes, even in the presence of H$_2$, and the reflections of pure Pd at 2Θ = 40.1° are detected.
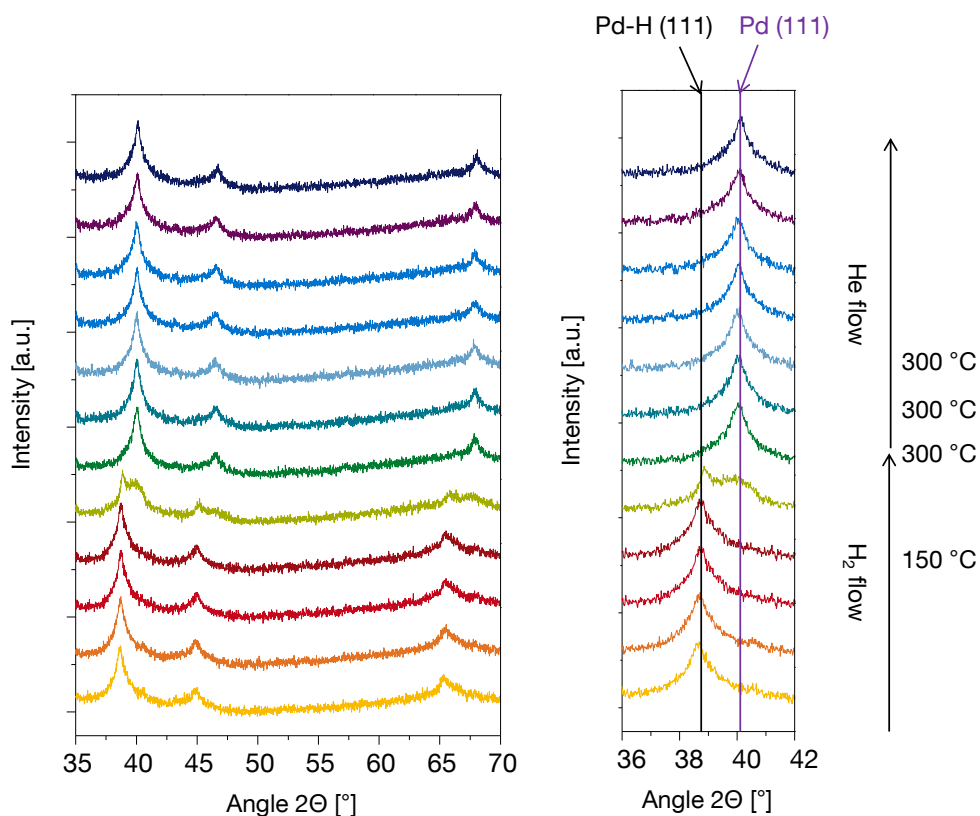
Figure 3-S4: Temperature dependent XRD patterns for the reflection at the 111, 002 and 022 plane (left) and close up of the 111 plane (right) of monometallic palladium on Pd-SiO$_2$, 3.0 wt.-% Pd. Temperature increases from bottom to top. 2Θ = 40.1 ° represents pure Pd phases.

1. M. Okube, A. Yoshiasa, O. Ohtaka, H. Fukui, Y. Katayama, W. Utsumi, *Solid State Communications* **2002**, *121*, 235-239.

2. R. Giulian, et al., *Journal of Physics: Condensed Matter* **2009**, *21*, 155302.

3. B. Joseph, A. Iadecola, L. Malavasi, N. L. Saini, *Journal of Physics: Condensed Matter* **2011**, *23*, 265701.

Chapter 4

Temperature dependent evaluation of two active species for vinyl acetate synthesis over Pd/Au-SiO$_2$ catalysts: Part II - structure activity correlation

The activity and selectivity of SiO$_2$ supported bimetallic catalysts for vinyl acetate synthesis with Pd/Au molar ratios ranging from 0.8 to 7.0 was studied over two series of materials, one containing total metal loading of 3.0 wt.-% and the other with a constant Pd-loading of 0.5 wt.-%. Monometallic reference samples impregnated on SiO$_2$ were investigated in order to evaluate the role of the Pd species formed during reaction. The leaching of Pd under reaction conditions in the layer of condensed acetic acid in form of palladium acetate present on the catalyst surface at a reaction temperature of 150 °C led to the formation of an equimolar bimetallic PdAu phase together with highly dispersed monometallic Pd species. Pd present in the bimetallic Pd$_1$Au$_1$ phase is approximately five times more active than Pd in the dispersed monometallic phase. For high Au concentrations a pronounced selectivity loss was observed with time-on-stream, which originates from the depletion of Pd in the already Au rich bimetallic particles through leaching. The resulting Au-rich surface favors the combustion of C$_2$H$_4$ to CO$_2$ over the formation of the vinyl acetate monomer (VAM). Activation energies determined over equimolar and Au-rich samples exhibit two selectivity regimes. For temperatures lower than 160 °C, the selectivity towards VAM increases with temperature, whereas above 160 °C a severe loss in selectivity towards VAM is observed. Highly Pd-rich samples show higher activation energies to CO$_2$ formation compared to vinyl acetate over the whole temperature range, resulting in a continuous decrease in selectivity with increasing temperature. For equimolar and Au-rich samples the phase separation towards a Pd-rich and Au-rich phase was identified to be the reason for the change in activation energies

with respect to both products (VAM and CO_2) at elevated temperatures. The depletion of Pd in the bimetallic phase via leaching was identified as main reason for long time deactivation. High concentrations of Pd within the liquid surface layer slow down the leaching and thus enhance the long time stability of the catalysts. Combining the structural information about the catalysts reactively aged at different temperatures discussed in part I with the kinetic results presented in this part, we will describe the role of the temperature on the restructuring of the bimetallic particles and the role of the additional monometallic Pd phase on the activity for vinyl acetate synthesis.

4.1. Introduction

Polyvinyl acetate is a widely used polymer in numerous applications based on the outstanding adhesive, optical, electrical and fiber-forming properties of the material. Nowadays polyvinyl acetate accounts for approximately 50 % of the global vinyl acetate monomer (VAM) consumption, followed by PVOH as the second largest end-use category.[1]

The oldest industrial process for vinyl acetate monomer synthesis is the gas-phase acetoxylation of acetylene over a zinc acetate catalyst, typically supported on carbon that allowed to reach yields ranging from 92 to 98 %.[2] Later Moiseev[3] and Smidt[4] reported a homogeneous liquid phase process using palladium salts such as $Pd(OAc)_2$ and co-catalysts (e.g. $CuCl_2$) for the acetoxylation of ethylene. This reaction uses ethylene, which is both cheaper and easier available than acetylene. In this process, vinyl acetate is formed via the reaction of C_2H_4 with palladium acetate in acetic acid. During this reaction Pd^{2+} is reduced to Pd^0 and reoxidized by e.g. $CuCl_2$, which itself is then subsequently reoxidized by oxygen. This process was further developed by Hoechst[5] and Bayer[6] into a heterogeneous gas phase process. Nowadays vinyl acetate is produced on a large scale via a gas-phase acetoxylation procedure over bimetallic Pd/Au catalysts.[7,8] Typical reaction conditions are $413 – 453\,K$ and pressures between 5 and 10 atm with the strongly exothermic reaction being performed in multi-tubular reactors. Supported Pd/Au catalysts with potassium acetate as promoter are used for the gas phase acetoxylation of ethylene. The introduction of the catalytically inert gold into the metallic phase leads to a pronounced increase in activity, which was mainly attributed to the formation of isolated Pd sites in the bimetallic phase, which are particularly active for vinyl acetate synthesis[9,10]. The presence of isolated Pd atoms in a suitable geometry strongly depends on the reaction conditions and it appears that the structures are dynamically formed and disintegrated under reaction conditions. Regarding the active species for vinyl acetate formation Moiseev[3] postulated that Pd^0 is the active site. In contrast, Nakamura[11] suggests a Pd^{1+}-acetate species to be the active intermediate, whereas Augustine and Blitz[12] observed Pd^{2+}-acetate on the surface of palladium crystallites. Reilly and Lerou[13] speculated that a liquid layer of the reactant phase is present on the surface of the

working catalyst, which was also observed by Crathorne et al.[14] who detected via temperature programmed desorption experiments that approximately three monolayers of adsorbed acetic acid are present on the catalyst surface. However this technique is known to underestimate the level of retained acetic acid by up to 60 % and it is thus more likely that under working conditions approximately five monolayers of acetic acid are present on the catalyst surface. Moreover the amount of adsorbed acetic acid increases significantly with the introduction of potassium acetate, acting as promoter which significantly enhances the adsorption of acetic acid by the formation of a dimeric species.[15]

We have shown previously that supported PdAu particles undergo severe restructuring during vinyl acetate synthesis.[16] Palladium leaching in form of palladium acetate leads to two active ensembles on the catalyst surface at a reaction temperature of 150 °C. On the one hand bimetallic particles with a composition of Pd_1Au_1 were identified as highly active species. The other species are highly dispersed palladium species formed from palladium acetate present on the SiO_2 surface under reaction conditions, which were also found to be active in vinyl acetate synthesis.

In this part we will focus on the catalytic activity of the bimetallic Pd_1Au_1 phase and the monometallic dispersed palladium phase for the vinyl acetate formation over supported catalysts with various Pd/Au ratios. The activity tests and kinetic evaluation, together with characterization data shown in part I, will provide comprehensive information on the active ensembles in vinyl acetate synthesis and the impact of both active species on the activity. Moreover temperature dependent studies and the characterization of various samples after reaction will outline possible reasons for deactivation. With temperature and Pd-Au composition dependent evaluation of deactivation behavior, tailoring of catalyst towards high stability levels will be discussed.

4.2. Experimental

4.2.1. Synthesis

The preparation of the bimetallic catalysts with a total metal loading of 3 wt.-% and varying Pd/Au ratios is presented in part I. A second series of bimetallic catalysts with a

constant Pd loading of 0.5 wt.-% and varying Au loadings was prepared according to DE102006058800 A1.[17] The total metal loadings were in a range of 0.6 wt.-% up to 2.5 wt.-% and are summarized in Table 4-S1 in the supplementary information. All samples were additionally impregnated with 5 wt.-% K in form of KOAc.

4.2.2. Activity tests

Deactivation studies were performed in a 6-fold reactor set-up, whereas kinetic investigations were conducted in a single reactor to achieve a sufficiently high time resolution of the measurements. To be close to the industrial conditions a temperature of 150 °C and a gas composition of 60 vol.-% C_2H_4, 13 vol.-% AcOH, 4.5 vol.-% O_2 and N_2 balance were applied. For activity tests with samples containing a constant total metal loading of 3 wt.-%, the catalyst weight was chosen in a way that for all Pd/Au ratios a similar amount of Pd was present in the catalyst bed. For catalysts with constant palladium content of 0.5 wt.-%, catalyst amount was chosen to reach conversion levels of approximately 40 % (similar to the catalysts of series one). SiC was used as inert diluent (diluent/catalyst ratio was 10/1) to ensure constant temperature over the whole catalyst bed. The rates were calculated after reaching a stable region in the conversion (after at least 100 hours time-on-stream). Kinetic measurements were performed under 8.8 bar. Activation energy measurements were performed in a temperature range of 140 °C - 190 °C. Kinetic measurements were performed at conversion levels < 10 % with respect to O_2 being the limiting reactant. Product stream analysis was done using a GC 2014 by Shimadzu, equipped with a Haysep Q and a molsieve column and a TCD detector.

4.3. Results

### 4.3.1. Catalytic activity of PdAu bimetallic catalysts supported on SiO_2

The catalytic behavior of bimetallic PdAu catalysts varies with the applied Pd/Au ratio. The rate of vinyl acetate formation normalized to the palladium concentration over samples with 3 wt.-% total metal loading is shown in Figure 4-1. An initiation period of

10 - 30 hours was observed over all samples. After this period, similar VAM formation rates per gram Pd were found on catalysts with high Pd content. With decreasing Pd concentrations the VAM formation rates per gram Pd increased. The highest Pd reactivity was found for the slightly Pd rich sample Pd/Au = 1.1, whereas the Au rich sample Pd/Au 0.8 showed a lower activity originating from severe deactivation. However the initial activity after the short intiation period was the highest over Pd/Au 0.8.

The initiation period observed originates from a restructuring of the bimetallic particles towards a Pd_1Au_1 phase and a dispersed Pd phase. The concentration of the dispersed Pd phase depends on the excess of Pd above the molar ratio of Pd/Au 1/1 in the catalyst. The fractions of Pd present within the dispersed palladium phase (calculated on the basis of the chemical composition and the alloy composition derived via XRD) for the Pd-rich catalysts are listed in Table 4-1. Catalysts with Pd fractions of above 60 % within the dispersed monometallic Pd phase exhibited a similar and only minor (or no) deactivation, while the VAM formation over the Au rich catalyst (Pd/Au 0.8) severely decreased with time-on-stream. The selectivity to VAM as function of time-on-stream is illustrated in figure in Figure 4-2. After the initiation period an increase in selectivity was found for all Pd rich samples until a steady level was reached after approximately 100 hours time-on-stream. In contrast, the Au-rich sample Pd/Au 0.8 shows a severe loss in selectivity with time on stream, being the main reason for the decrease in the VAM formation rate.

The length of the intiation period (minutes until maximum conversion was reached) is dependent on the Pd/Au ratio as shown in Figure 4-3. The gold rich sample Pd/Au 0.8 exhibited the shortest initiation period, while samples with more than 60 % of dispersed palladium showed similar initiation periods. For catalysts with low Pd/Au ratios, initiation periods were shorter than observed over palladium rich samples.
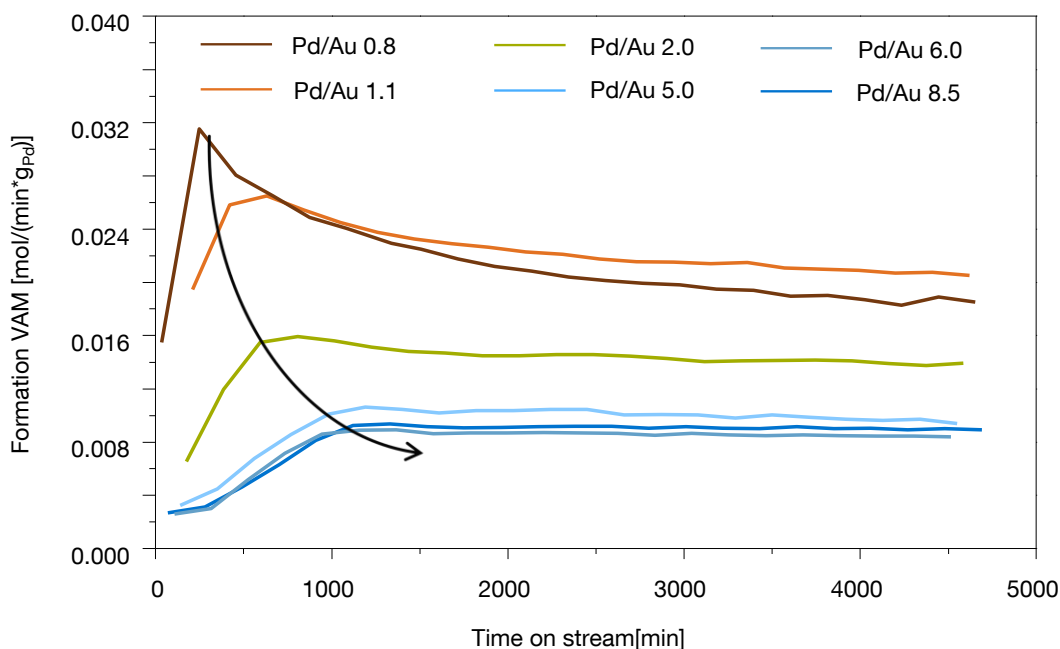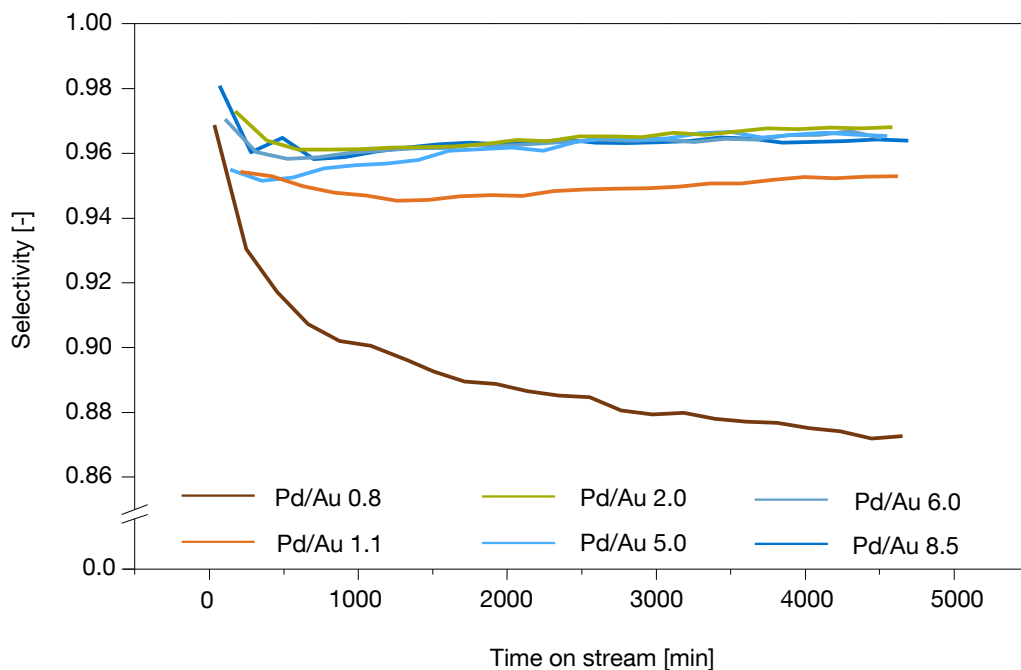
Figure 4-1: Time-on-stream behavior of bimetallic samples with total metal loading of 3 wt.-% and 5 wt.-% KOAc. Reaction conditions: 60 vol.-% C_2H_4, 13 vol.-% AcOH, 4.5 vol.-% O_2, N_2 balance; 8.8 bar total pressure; temperature: 150 °C.

Table 4-1: Fraction of dispersed palladium (in respect to the total palladium concentration) calculated on the basis of the chemical composition and according to the correlations found via particle modeling.

Pd/Au molar ratio	Fraction of dispersed palladium calculated on the basis of the chemical composition and the alloy composition after reaction derived via XRD [-] *
1.1	0.04
2.0	0.39
5.0	0.68
6.0	0.71
8.5	0.79

*calculated according to: f(dispersed Pd) = [c(Pd total) - c(Pd in PdAu phase after reaction at 150 °C)]/c(Pd total)

Figure 4-2: Selectivity for VAM with time on steam of bimetallic samples with total metal loading of 3 wt.-% and 5 wt.-% KOAc. Reaction conditions: 60 vol.-% C_2H_4, 13 vol.-% AcOH, 4.5 vol.-% O_2, N_2 balance; 8.8 bar total pressure; temperature: 150 °C.
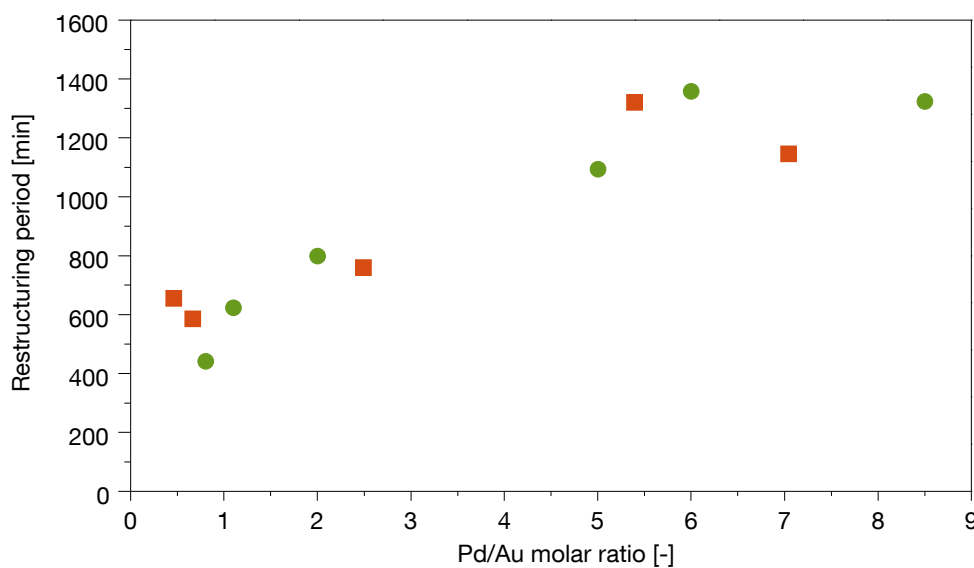

Figure 4-3: Initiation periods for bimetallic catalysts with (●) a constant total metal loading of 3 wt.-% and (■) a constant palladium loading of 0.5 wt.-%.

The vinyl acetate formation rate as function of the concentration of accessible palladium is shown in Figure 4-4. VAM formation rates were taken from steady state levels after 100 hours time-on-stream. Fractions of accessible palladium were calculated according to Equation 4-1 and are listed in Table 4-2.
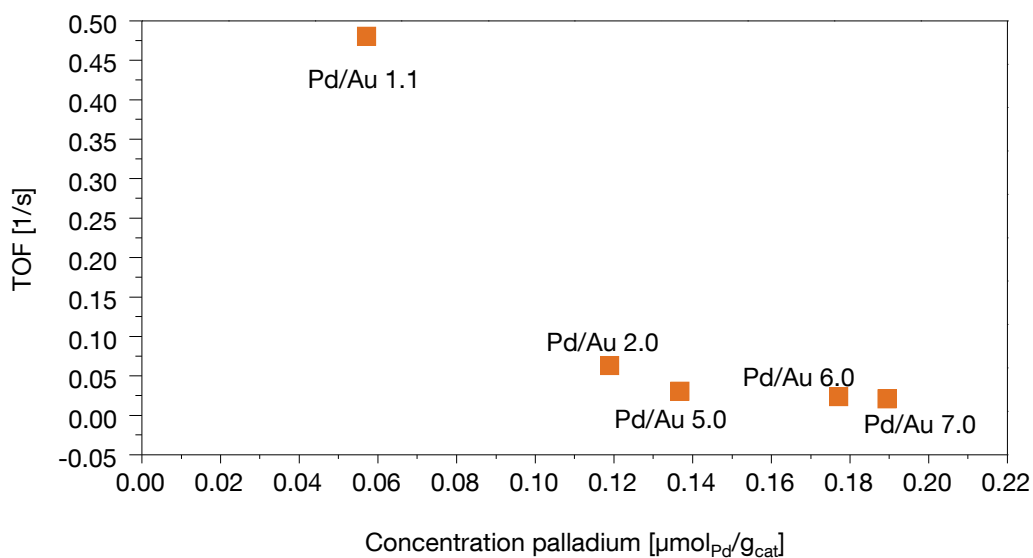
$f(Pd_{acc})=c(Pd_{total})*f(Pd_{dis}) + c(Pd_{total})*(1-f(Pd_{dis}))*D$ Equation 4-1

with $f(Pd_{acc})$ = fraction of accessible Pd

$c(Pd_{total})$ = total concentration of Pd

$f(Pd_{dis})$ = fraction of dispersed Pd (assuming a Pd dispersion in this phase of 100%)

D = Dispersion of metal particles (calculated on the basis of 2.2 nm particles)

Figure 4-4: Formation rates of vinyl acetate normalized to the concentration of accessible Pd atoms as function of the total Pd concentration for samples with constant total metal loading of 3 wt.-% and 5 wt.-% K. Reaction conditions: 60 vol.-% C_2H_4, 13 vol.-% AcOH, 4.5 vol.-% O_2, N_2 balance; 8.8 bar total pressure; temperature: 150 °C.

The highest activity per accessible palladium was observed for the sample Pd/Au 1.1. The Au-rich sample (Pd/Au 0.8) was not included due to the pronounced loss in activity and selectivity with time-on-stream.

Table 4-2: Fraction of accessible palladium calculated according to Equation 1.

Pd/Au molar ratio	Fraction of accessible palladium [-]
1.1	10.7
2.0	44.9
5.0	70.6
6.0	77.2
8.5	78.2

In order to exclude effects of different concentrations of palladium per gram support on the particle morphology, a series of catalysts with constant palladium loading of 0.5 wt.-% was prepared. The activity and selectivity as function of time-on-stream were similar to the catalyst series with a constant total metal loading of 3 wt.-% (data sets are shown in the supplementary information Figures 4-S1 and 4-S2).

4.3.2. Catalytic activity of palladium acetate impregnated onto SiO$_2$

In order to evaluate the contribution of the dispersed palladium phase on the catalytic properties, the support was impregnated with palladium acetate and potassium acetate via incipient wetness impregnation. Total loading of Pd was 1.5 wt.-% and the K loading was 5 wt.-%. The VAM formation rate and the selectivity to VAM for Pd(OAc)$_2$-SiO$_2$ without and promoted with potassium acetate are shown in Figure 4-5 a and b. The addition of KOAc led to an activity enhancement of a factor of two and a significant stabilization of the selectivity towards vinyl acetate. The time-on-stream behavior of a typical bimetallic catalyst (with 5 wt.-% K) is compared to Pd(OAc)$_2$/SiO$_2$ with KOAc in Figure 4-6.
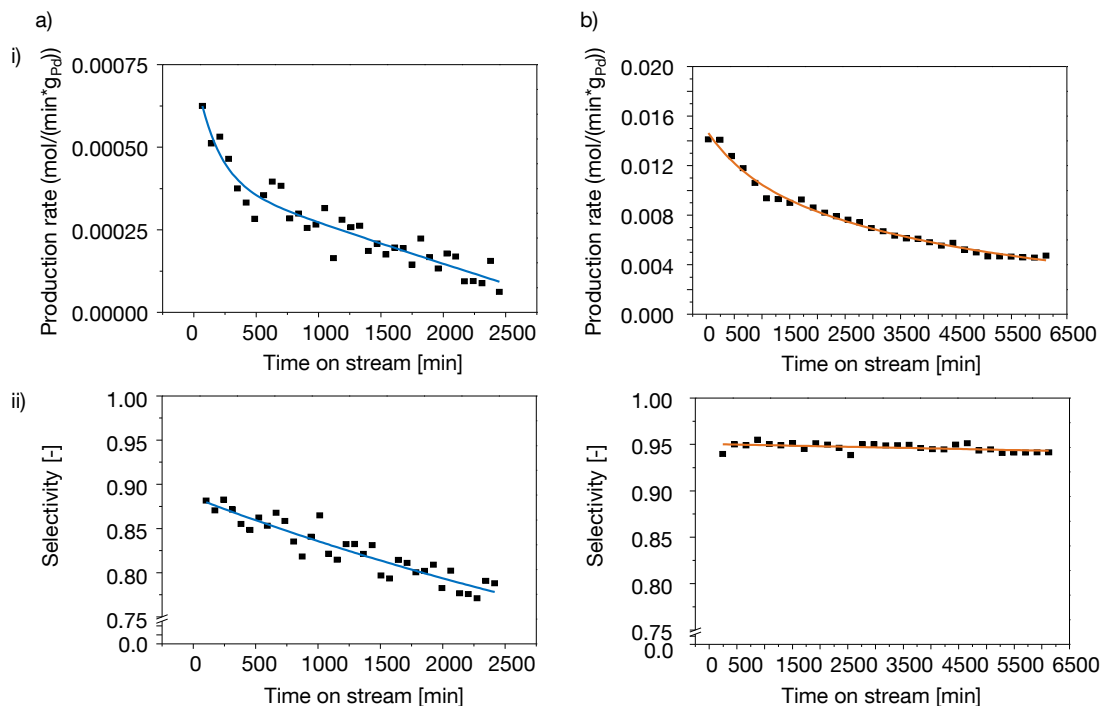
Figure 4-5: Vinyl acetate formation (top row) and selectivity (bottom row) as function of time-on-stream for Pd(OAc)$_2$ – SiO$_2$ with 1.5 wt.-% Pd a) without potassium promoter and b) with KOAc (5 wt.-% K). Temperature 150 °C, total pressure 8.8 bar. Gas composition: 60 vol.-% C$_2$H$_4$, 13 vol.-% AcOH, 4.5 vol.-% O$_2$, N$_2$ balance; 8.8 bar total pressure.

Comparing the time-on-stream behavior of the impregnated palladium acetate promoted with KOAc and bimetallic PdAu catalysts (Figure 4-5 and 4-6), it becomes evident that on the palladium acetate based catalyst the deactivation started initially and an initiation period was not observed. The rate (normalized to the Pd concentration) of palladium acetate on SiO$_2$ promoted with KOAc is close to that of Pd-rich bimetallic catalysts (compare blue curves in Figure 4-1 with 4-5b-i). Furthermore, the the Pd(OAc)$_2$ based sample showed a lower selectivity towards VAM (< 96 vs. < 97) compared with the bimetallic supported catalysts, but in contrast to the Pd(OAc)$_2$ based catalyst, bimetallic samples exhibited an increase in selectivity with time-on-stream.
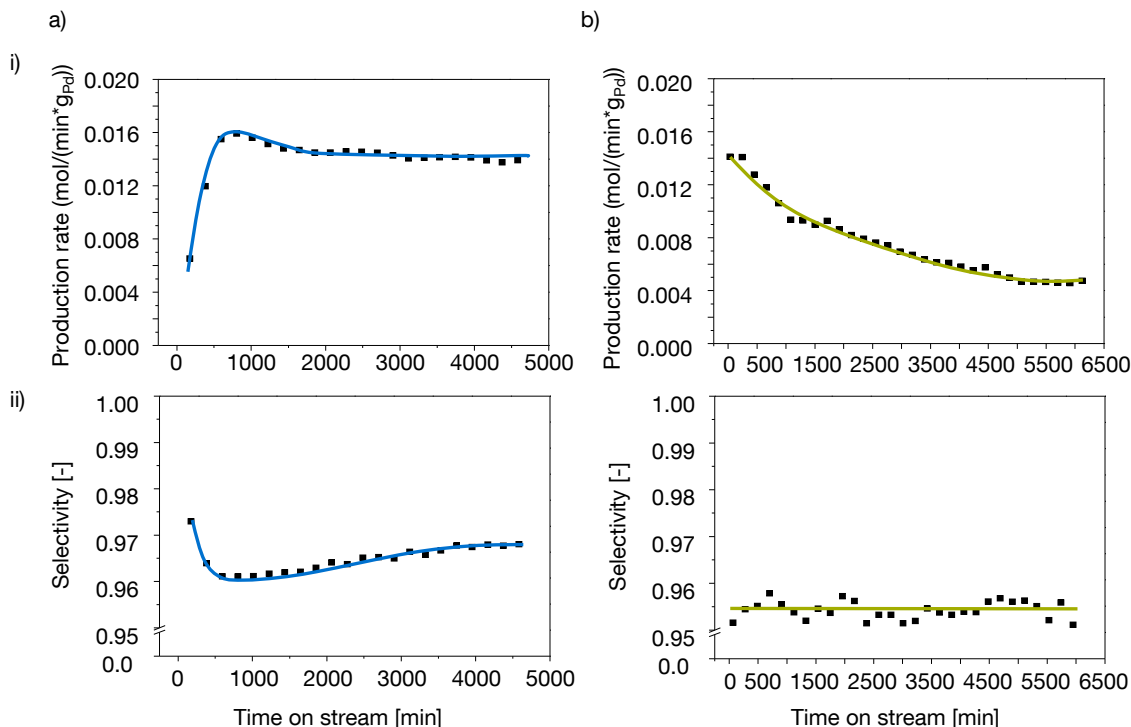
Figure 4-6: i) Vinyl acetate formation and ii) Selectivity with time-on-stream for a) the bimetallic Pd/Au 2.0 with 5 wt.-% K and b) Pd(OAc)$_2$ – SiO$_2$ with 1.5 wt.-% Pd and 5 wt.-% K (in form of KOAc). Temperature 150 °C, total pressure 8.8 bar. Gas composition: 60 vol.-% C$_2$H$_4$, 13 vol.-% AcOH, 4.5 vol.-% O$_2$, N$_2$ balance; 8.8 bar total pressure.

The TOF of the bimetallic catalysts (based on the total amount of accessible Pd) as function of the palladium concentration are compared in Figure 4-7 (orange squares). Due to the strong deactivation found for Au-rich catalysts, the Pd/Au 0.8 sample is not included. In addition, the TOF for Pd within the Pd$_1$Au$_1$ phase (blue triangles), calculated according to Equation 4-1 and the TOF for Pd within the dispersed Pd acetate phase, calculated from the steady state activity shown in Figure 4-5 b-i is shown in Figure 4-7. The TOF within the Pd$_1$Au$_1$ phase for all bimetallic catalysts is similar. For catalysts with high concentrations of dispersed palladium, a large fraction of the overall activity originates from the dispersed monometallic palladium species, whereas for catalysts with higher Au concentrations, the activity mainly originates from the bimetallic equimolar Pd$_1$Au$_1$ phase. The activity per accessible Pd in the bimetallic equimolar phase (blue curve in Figure 4-7) is approximately 5 times higher than the activity per accessible Pd in the dispersed palladium phase.
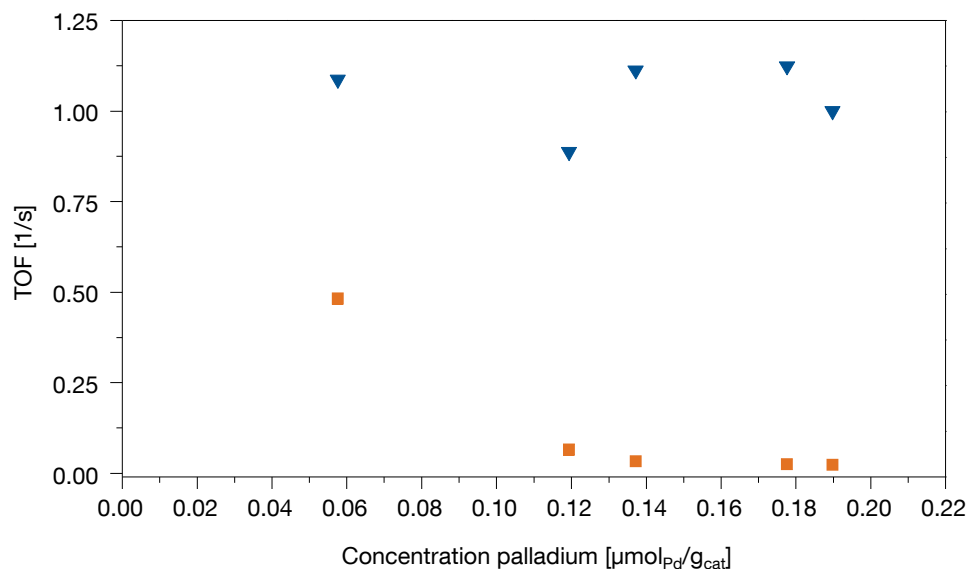
Figure 4-7: Vinyl acetate production normalized to accessible palladium plotted against the total palladium concentration per catalyst. ■ **TOF normalized to total amount of accessible palladium.** ▼ **TOF normalized to accessible palladium within a Pd₁Au₁ particle.**

4.3.3. Stability tests – Pd/Au 0.8 additionally impregnated with Pd(OAc)$_2$

As the time-on-stream behavior of bimetallic samples indicates a stabilizing effect of high concentrations of the dispersed Pd phase, Pd/Au 0.8 was additionally impregnated with Pd(OAc)$_2$ (1.5 wt.-% Pd). The sample was tested under industrial conditions for 160 hours time-on-stream. Figure 4-8 shows the selectivity and activity levels.

Compared to the non-modified Pd/Au 0.8 sample, which exhibited a pronounced deactivation with time on stream, the additional impregnation led to an improved stability (compare Figure 4-8 with Figure 4-1 and 4-2). Despite a large fraction of Pd being present in form of Pd(OAc)$_2$, the time on stream behavior of the modified Pd/Au 0.8 differs significantly from the one observed for Pd(OAc)$_2$ solely impregnated onto SiO$_2$ (compare Figure 4-8 to Figure 4-5b). Whereas Pd(OAc)$_2$ - SiO$_2$ showed a pronounced deactivation, the Pd/Au 0.8 sample additionally impregnated with Pd(OAc)$_2$ exhibited an initiation period, typical for bimetallic samples. The restructuring period observed for the modified Pd/Au 0.8 sample is the shortest observed over bimetallic samples.

a)

b)
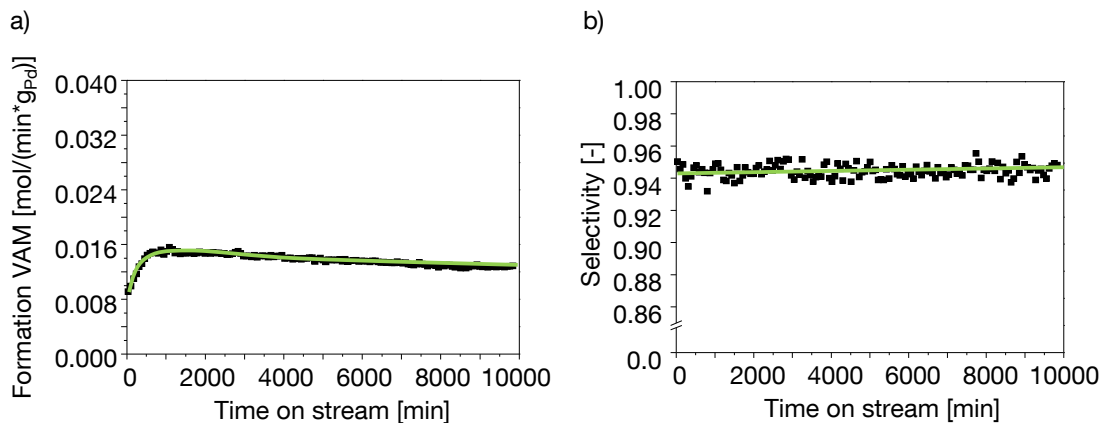
Figure 4-8: a) Vinyl acetate formation and b) selectivity with time-on-stream for Pd/Au 0.8 with additional 1.5 wt.-% Pd in form of Pd(OAc)$_2$ and 5 wt.-% K (in form of KOAc). Temperature 150 °C, total pressure 8.8 bar. Gas composition: 60 vol.-% C$_2$H$_4$, 13 vol.-% AcOH, 4.5 vol.-% O$_2$, N$_2$ balance; 8.8 bar total pressure.

4.3.4. Temperature dependency of the vinyl acetate formation

Activation energies were determined over the series of Pd/Au catalysts with constant total metal loading of 3 wt.-%. The Arrhenius type plots of the Pd/Au 1.1 sample for the main product vinyl acetate monomer and the by-product CO$_2$ are shown in Figure 4-9a i) and ii). The data sets were recorded in a conversion range of less than 10 % regarding O$_2$ conversion as limiting reactant and the activity was determined after the initiation period (approximately 30 hours time-on-stream for bimetallic samples, more than 100 hours for the Pd(OAc)$_2$/SiO$_2$ sample). Two regimes were observed in the Arrhenius type plots over the temperature range of 140 °C – 190 °C, separated by a distinct change in the slope at a temperature of 160 °C indicating a decrease of E$_a$ for vinyl acetate and an increase of E$_a$ for CO$_2$ (Figure 4-9a-i) and ii)) formation. Since this effect was observed for both products with an opposite trend, it cannot originate from a loss in overall activity or from diffusion limitations, but indicates a change in the selectivity from VAM to the byproduct CO$_2$ at higher temperatures. Figure 4-9 b) and c) show the Arrhenius type plots regarding i) VAM and ii) CO$_2$ over Pd/Au 2.0 and 6.0. The change in the slope is visible for catalysts with Pd/Au ratios up to 2.0, while for catalysts with higher Pd/Au ratios it was not observed.

The activation energies with respect to vinyl acetate monomer and for the formation of CO_2 are summarized in Table 4-3 and 4-4, respectively. The activation energies for vinyl acetate formation increased with the addition of Au in comparison to the monometallic sample. The samples with molar Pd/Au ratios of 2.0, 1.1 and 0.8 showed two selectivity regimes. Within the high temperature regime (170 – 190 °C) activation energies with respect to vinyl acetate formation decreased with increasing gold concentration, while in the low temperature regime the activation energies were similar for all catalysts. The opposite trend in the activation energies was observed for the main byproduct CO_2. Samples with high concentrations of palladium showed constant activation energies over the whole temperature range.
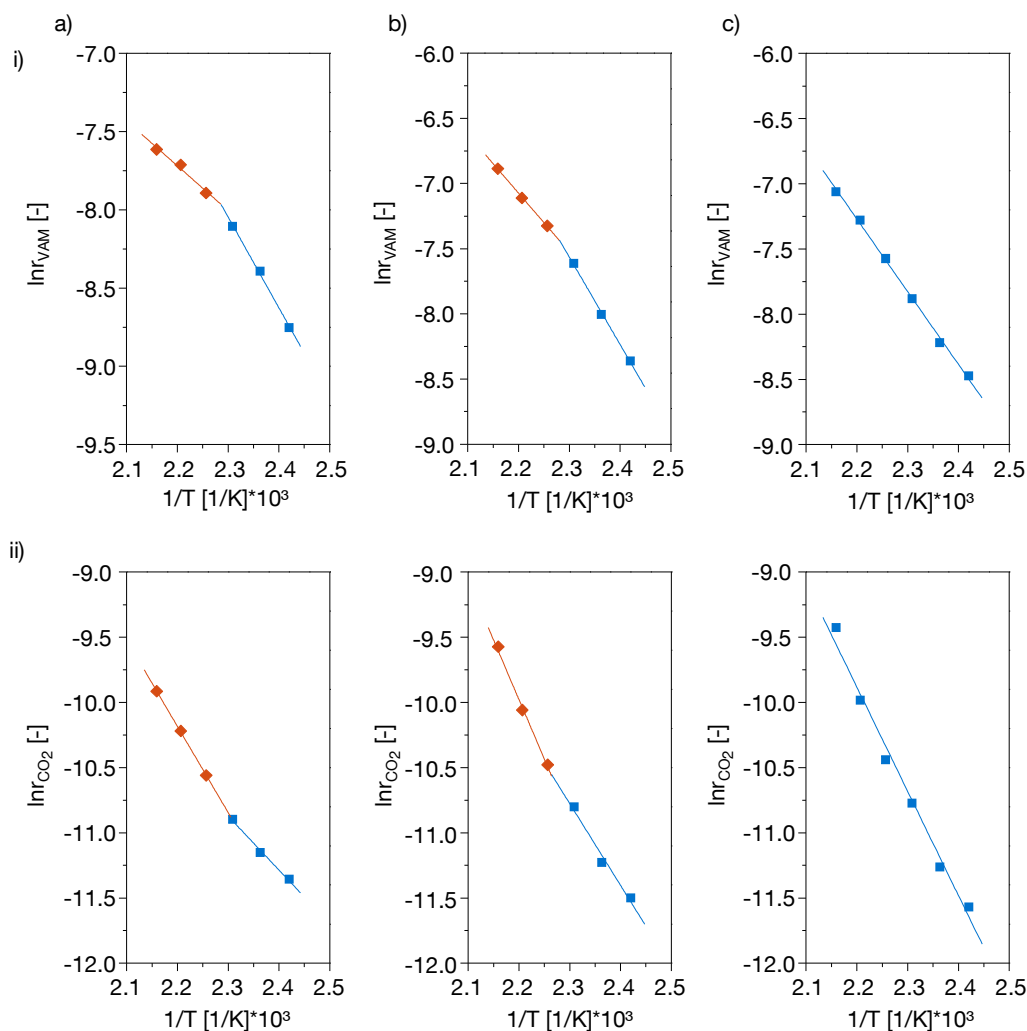
Figure 9: Arrhenius type plots with i) regard to vinyl acetate and ii) CO_2 for a bimetallic PdAu sample with a Pd/Au molar ratio of a) 1.1, b) 2.0 c) 6.0. Temperature range: 140 °C – 190 °C. Gas composition: 60 vol.-% C_2H_4, 13 vol.-% AcOH, 4.5 vol.-% O_2, N_2 balance; 8.8 bar total pressure.

Neither the monometallic palladium samples with loadings of 1.5 and 3.0 wt.-% palladium, nor the $Pd(OAc)_2$ on SiO_2 sample showed a change in selectivity at elevated temperatures (see Figure 4-10). The activation energies with respect to vinyl acetate formation observed for the monometallic Pd samples are similar to the values previously reported by Goodman et al.[18] and showed higher values for smaller metal particles as already reported in [18] (compare Table 4-3).
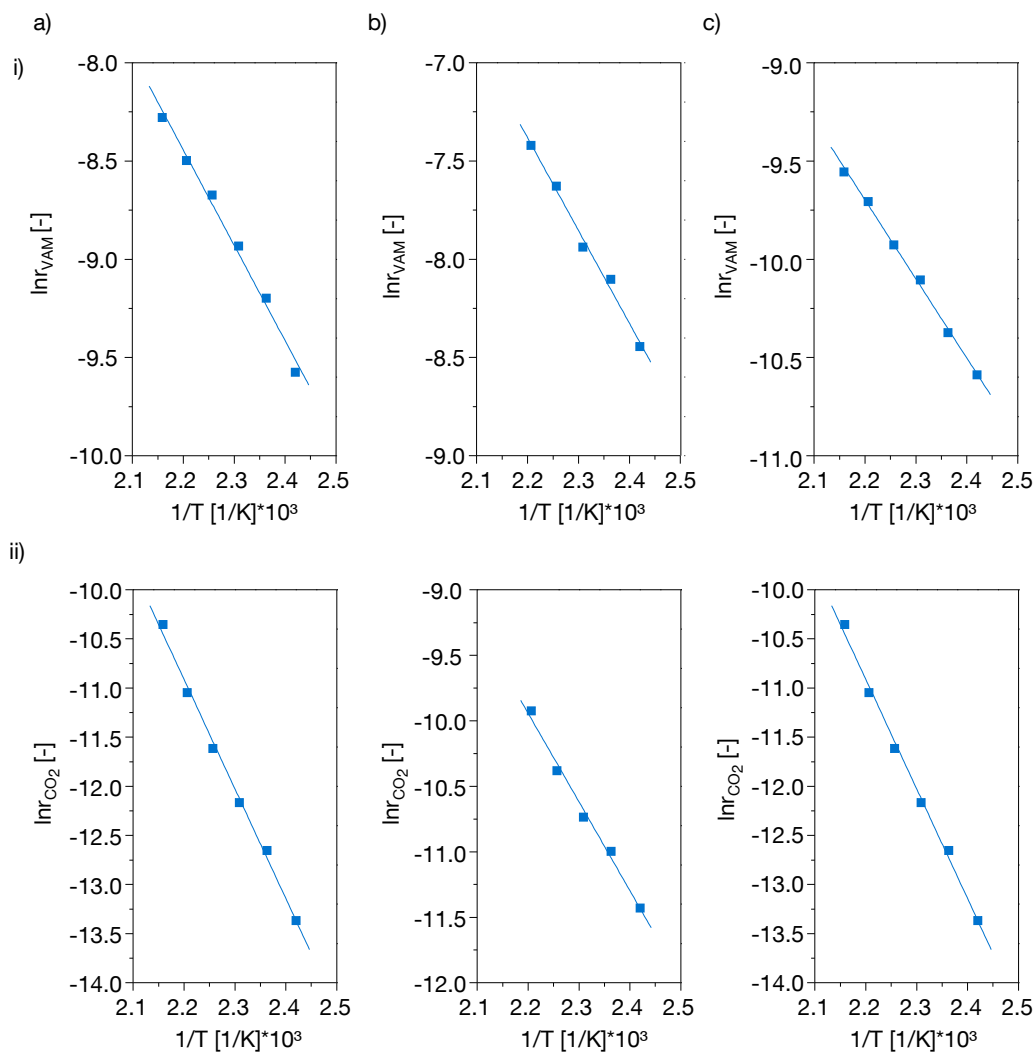
Table 4-3: Activation energies with respect to vinyl acetate monomer over Pd/Au catalysts with constant total metal loading of 3 wt.-%.

Pd/Au molar ratio	Total E_A	E_A in low temperature regime	E_A in high temperate regime	Transition temperature [°C]
Pd/Au 7.0	51.1 kJ/mol	-	-	-
Pd/Au 6.0	46.8 kJ/mol	-	-	-
Pd/Au 5.0	55.7 kJ/mol	-	-	-
Pd/Au 2.0	-	55.8 kJ/mol	50.6 kJ/mol	170
Pd/Au 1.1	-	57.6 kJ/mol	37.5 kJ/mol	160
Pd/Au 0.8	-	60.3 kJ/mol	31.1 kJ/mol*	160
Pd only (3.0 wt.-%)	39.2 kJ/mol	-	-	-
Pd only (1.5 wt.-%)	40.4 kJ/mol	-	-	-
$Pd(OAc)_2$ on SiO_2	33.6 kJ/mol	-	-	-

*For Au rich samples deactivation regarding VAM production rate at higher temperatures was observed within the respective temperature step. Thus activation energy values at the high temperature regime are influenced by deactivation and exhibit lower values.

On Pd-rich bimetallic catalysts the activation energies with respect to CO_2 formation were higher than the activation energies regarding VAM over the whole temperature range, resulting in a selectivity decrease with increasing temperatures. Bimetallic catalysts with higher concentrations of gold showed the opposite trend in the low temperature regime (< 170 °C), where the activation energy for VAM was higher than the one for the byproduct CO_2. Thus on these catalysts the selectivity increases with increasing temperature within the low temperature regime. However, within the high

temperature regime the pronounced decrease in activation energies for VAM formation and the significant increase in activation energies for CO_2 led to a strong decrease in selectivity with increasing temperature. Figure 4-12 shows the selectivity as function of the temperature for bimetallic samples.

Figure 4-10: Arrhenius type plots with i) regard to vinyl acetate and ii) CO₂ for a bimetallic PdAu sample with a Pd/Au molar ratio of a) Pd/SiO₂ 1.5 wt.-%, b) Pd/SiO₂ 3.0 wt.-% c) Pd(OAc)₂-SiO₂ 1.5 wt.-% Pd. Temperature range: 140 °C - 190 °C. Gas composition: 60 vol.-% C₂H₄, 13 vol.-% AcOH, 4.5 vol.-% O₂, N₂ balance; 8.8 bar total pressure.

Table 4-4: Activation energies with respect to CO$_2$ over Pd/Au catalysts with constant total metal loading of 3 wt.-%.

Pd/Au molar ratio	Total E$_A$	E$_A$ in low temperature regime	E$_A$ in high temperate regime	Transition temperature [°C]
Pd/Au 7.0	80.6 kJ/mol	-	-	-
Pd/Au 6.0	71.2 kJ/mol	-	-	-
Pd/Au 5.0	68.2 kJ/mol	-	-	-
Pd/Au 2.0	-	53.1 kJ/mol	77.2 kJ/mol	170
Pd/Au 1.1	-	34.1 kJ/mol	55.2 kJ/mol	160
Pd/Au 0.8	-	22.7 kJ/mol	51.2 kJ/mol	160
Pd only (3.0 wt.-%)	56.3 kJ/mol	-	-	-
Pd only (1.5 wt.-%)	50.6 kJ/mol	-	-	-
Pd(OAc)$_2$-SiO$_2$	60.1 kJ/mol	-	-	-
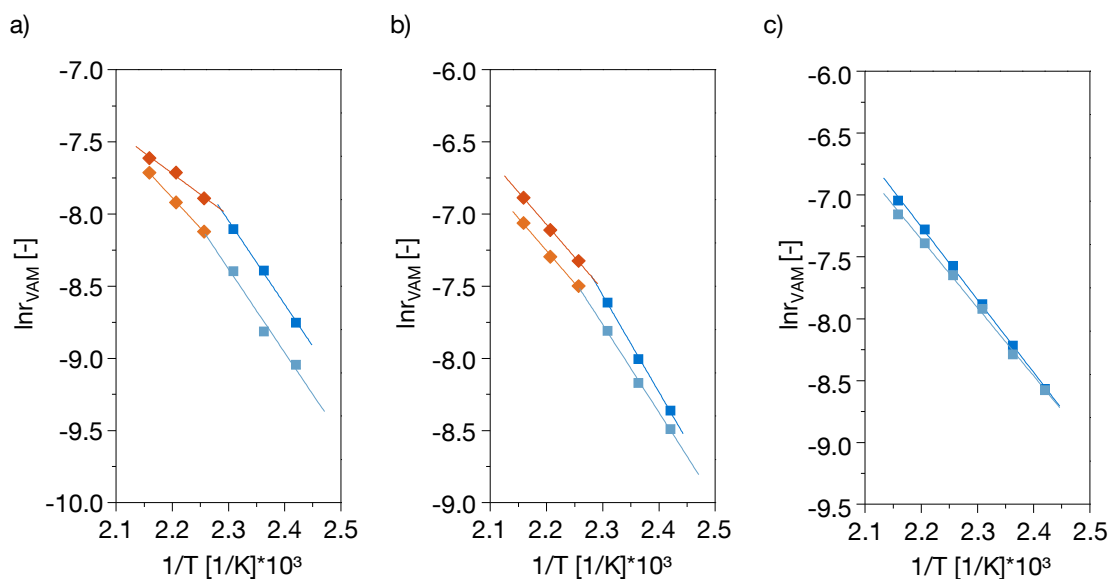
Figure 4-11: Activation energies regarding vinyl acetate for two consecutive series of temperature dependent studies over bimetallic samples with a Pd/Au molar ratio of a) 1.1, b) 2.0 c) 6.0. Temperature range: 140 °C - 190 °C. Gas composition: 60 vol.-% C$_2$H$_4$, 13 vol.-% AcOH, 4.5 vol.-% O$_2$, N$_2$ balance; 8.8 bar total pressure. Light colors represent the second run.

In order to evaluate the role of structural changes induced by reactions carried out at temperatures up to 190 °C the selectivity was studied in two succeeding temperature dependent experiments. In both series of experiments constant activation energies over the temperature range of 140 to 190 °C were observed over Pd/Au 6.0 (see Table 4-5 and 4-6 and Figure 4-11c), however, the activation energy with regard to vinyl acetate decreased for the second run. Samples containing a higher concentration of Au (Pd/Au 2.0 and 1.1) show a pronounced change in activation energies with increasing temperature for the first run, while in the second run this effect appears to a lesser degree as the activation energy regarding VAM formation in the high temperature regime is only slightly lower than the one observed in the low temperature regime. (Values are given in Table 4-5 and 4-6.) Samples with high Au concentrations show a pronounced decrease in VAM formation rate for the second run, which was not observed for Pd-rich samples (compare dark and bright colored graphs in Figure 4-11). Thus for catalysts with low Pd/Au ratios, the reconstruction at elevated temperatures led to a pronounced loss in selectivity towards VAM (compare Figure 4-11a and 4-12a). For the highly Pd rich catalysts a similar selectivity was observed for both runs.

Table 4-5: Activation energies with respect to vinyl acetate over Pd/Au 1.1, 2.0 and 6.0 catalysts with constant total metal loading of 3 wt.-%. Temperature program was performed a second time after an equilibration period at 140 °C.

Pd/Au molar ratio	Temperature regime	First run	Second run
7.0	low temperature regime	52.4 kJ/mol	46.1 kJ/mol
7.0	high temperate regime	52.4 kJ/mol	46.1 kJ/mol
6.0	low temperature regime	49.0 kJ/mol	45.9 kJ/mol
6.0	high temperate regime	49.0 kJ/mol	45.9 kJ/mol
2.0	low temperature regime	55.8 kJ/mol	50.6 kJ/mol
2.0	high temperate regime	37.6 kJ/mol	37.2 kJ/mol
1.1	low temperature regime	48.2 kJ/mol	47.4 kJ/mol
1.1	high temperate regime	23.6 kJ/mol*	34.9 kJ/mol*

*For Au rich samples strong deactivation regarding VAM production rate at higher temperatures was observed for the first temperature dependent run. Thus activation energy values at the high temperature regime are influenced by deactivation and exhibit lower values. Deactivation at high temperatures was less severe for the second run.

Table 4-6: Activation energies with respect to CO₂ over Pd/Au 1.1, 2.0 and 6.0 catalysts with constant total metal loading of 3 wt.-%. Temperature program was performed a second time after an equilibration period at 140 °C.

| Pd/Au molar ratio	Temperature regime	First run	Second run
7.0	low temperature regime	80.6 kJ/mol	82.3 kJ/mol
7.0	high temperate regime	80.6 kJ/mol	82.3 kJ/mol
6.0	low temperature regime	71.2 kJ/mol	72.5 kJ/mol
6.0	high temperate regime	71.2 kJ/mol	72.5 kJ/mol
2.0	low temperature regime	53.1 kJ/mol	39.9 kJ/mol
2.0	high temperate regime	77.2 kJ/mol	79.5 kJ/mol
1.1	low temperature regime	34.1 kJ/mol	42.4 kJ/mol
1.1	high temperate regime	55.2 kJ/mol	56.5 kJ/mol
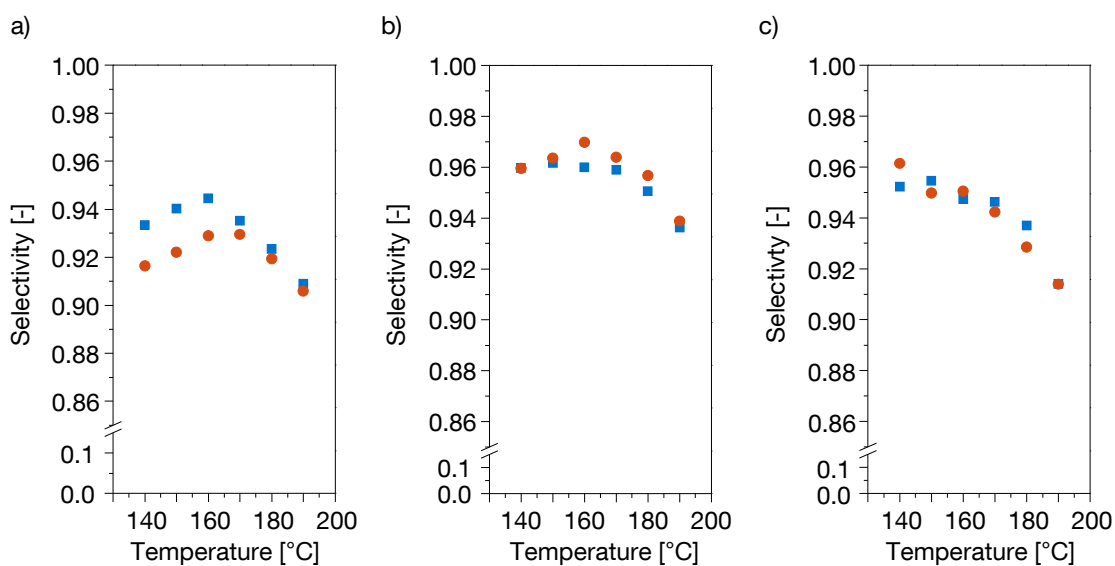
Figure 4-12: Selectivity to VAM as function of the temperature for bimetallic samples a) Pd/Au 1.1, b) 2.0 and c) 6.0. (■) Temperature dependent study over fully restructured samples. (●) Second temperature dependent study after reconditioning at 140 °C. Temperature range: 140 °C - 190 °C. Gas composition: 60 vol.-% C₂H₄, 13 vol.-% AcOH, 4.5 vol.-% O₂, N₂ balance; 8.8 bar total pressure.

4.4. Discussion

4.4.1. Activity and selectivity behavior with time-on-stream

After the synthesis bimetallic particles of various compositions were present[16], which underwent severe restructuring during the first hours time-on-stream, resulting in higher activity and selectivity levels.

The proposed restructuring mechanism is schematically described in Figure 4-13. Pd is leached from the core of the bimetallic particle via the formation of palladium acetate species. As soon as the surface is highly intermixed, the electronic influence of neighboring Au on Pd leads to a change in the oxidizability of Pd, since electrons are transferred from Au to Pd.[19] Thus the formation of Pd–acetate species is limited and the leaching process is slowed down. Besides this electronic alteration of Pd by neighbored Au atoms, high concentrations of Pd-acetate in the liquid surface layer limit Pd-leaching from the metallic particles into the liquid surface layer.
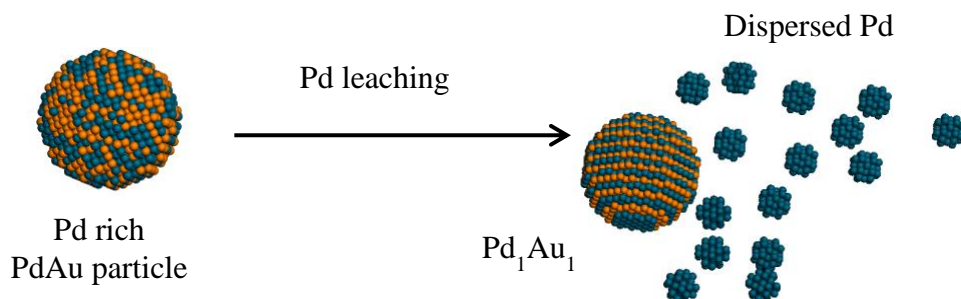
Figure 4-13: Proposed restructuring mechanism of bimetallic PdAu particles during vinyl acetate monomer synthesis.

The formation of Pd_1Au_1 via Pd leaching in form of palladium acetate species creates more active and more selective bimetallic particles, resulting in initiation periods. The process of surface intermixing via Pd leaching is extended with increasing concentration of Pd in the bimetallic particles after synthesis and thus maximum selectivity and activity are reached at a later stage.

The pronounced selectivity loss with time-on-stream for catalysts with a Pd/Au ratio below 1 also results from Pd leaching in form of Pd acetate species, as the already

Au-rich bimetallic particles become depleted in Pd with progressive restructuring. The concentration of the palladium acetate phase in the liquid surface layer is low for Au-rich catalysts and thus leaching of Pd from the bimetallic particles is not retained by the saturation of the liquid surface layer with palladium acetate. The Au-rich bimetallic particles formed exhibit low concentrations of active ensembles for vinyl acetate formation, i.e. neighbored Pd monomers.[10] In addition to a low concentration of active palladium ensembles, the high surface concentration of Au favors the total combustion of ethylene.[20] Both effects combine to a significant selectivity decrease with time-on-stream.

The stabilizing effect of the Pd acetate phase by retaining the Pd leaching from the bimetallic particles was confirmed via the modification of the Au-rich Pd/Au 0.8 catalyst with $Pd(OAc)_2$, which led to a pronounced increase in stability. Although the main fraction of Pd present in the Pd/Au 0.8 – $Pd(OAc)_2$ sample is located within the palladium acetate phase, the catalyst behavior with time on stream corresponds to bimetallic catalysts (e.g. with respect to the intiation period). The unmodified Pd/Au 0.8 sample shows severe deactivation and a pronounced selectivity loss with time-on-stream, originating from the leaching of Pd and the formation of Au-rich particles. With the addition of $Pd(OAc)_2$, the liquid surface layer was saturated with palladium acetate and thus the Pd leaching process was slowed down, leading to a significant stabilization of the equimolar bimetallic phase, which exhibits high concentrations of highly active Pd monomer pairs. This was further confirmed via XRD measurements of Pd/Au 0.8 and Pd/Au 0.8-$Pd(OAc)_2$ after 160 hours time-on-stream, which revealed Au-rich bimetallic particles for the unmodified sample, while on the $Pd(OAc)_2$ impregnated samples bimetallic particles consisting of the Pd_1Au_1 phase were present. Data sets of the XRD measurements can be found in the supporting information.

The model catalyst $Pd(OAc)_2$-SiO_2, which represents the Pd acetate species created during the restructuring process of the bimetallic catalysts, showed a different behavior with time-on-stream. In order to simulate reaction conditions, $Pd(OAc)_2$-SiO_2 was additionally impregnated with KOAc. This model catalyst did not show a change in selectivity level and no intiation period towards higher activity levels was found. In contrast to the bimetallic catalysts, $Pd(OAc)_2$-SiO_2/KOAc showed a pronounced deactivation during the first hours of the reaction. This deactivation was attributed to the

formation of metallic palladium particles due to the reducing environment present during reaction. The formation of metallic particles, which were found via XRD and TEM analysis after 150 hours time-on-stream, decreased the concentration of accessible palladium and thus the activity per gram palladium (XRD profiles and TEM images of $Pd(OAc)_2$-SiO_2/KOAc can be found in the supporting information). The steady state activity level for the model catalyst is similar to the activity observed for bimetallic samples with high Pd/Au molar ratios, which additionally supports the presence of the monometallic dispersed phase in form of a Pd-ac species. A large fraction of Pd is present as Pd acetate species for samples with high Pd/Au molar ratios and thus the overall activity mainly originates from Pd within this dispersed species.

The TOF's calculated for Pd present in Pd_1Au_1 and Pd present in the dispersed monometallic phase showed that Pd in the Pd_1Au_1 phase is approximately 5 times more active than Pd in the monometallic phase.

4.4.2. Temperature dependent vinyl acetate formation

Arrhenius type plots for vinyl acetate and CO_2 over samples with low Pd/Au ratios (2.0, 1.1 and 0.8) show a distinct change in selectivity regime at elevated temperatures. For temperatures above 160 °C a selectivity transition from vinyl acetate towards CO_2 is observed. A similar selectivity drop was reported previously[21,22], however an explanation for the change in selectivity was not provided so far. Taking Part I of this contribution into account, the changes of selectivity with elevated temperatures can be assigned to a temperature dependent phase separation within the bimetallic particles towards a Pd-rich and a Au-rich phase. For temperatures below 160 °C, an equimolar Pd_1Au_1 phase is present, which exhibits high degrees of surface intermixing. On highly intermixed surfaces, plenty active ensembles for VAM synthesis (i.e. neighbored Pd monomers) are present. In contrast, Pd-rich and Au-rich surfaces, which are present at elevated temperatures, promote the total combustion of ethylene. For high palladium loadings this selectivity change was not observed since a large fraction of the total palladium content is located in the monometallic dispersed palladium phase, which is not influenced in terms of phase separation and consequently the selectivity drop is less distinct. As mentioned

above, the electronic influence of Au on Pd slows down the restructuring mechanism, however, at elevated temperatures the phase separation decreases the degree of intermixing and thus further removal of Pd from the formed Pd rich phase takes place.

For Pd rich samples and monometallic reference samples, activation energies with respect to CO_2 are higher than those found for vinyl acetate over the whole temperature range. This results in a decrease in selectivity to VAM with increasing temperature. However bimetallic samples with higher Au concentrations show a different behavior with temperature. For lower temperatures, the activation energies with respect to VAM are higher than those for CO_2, leading to an increase in selectivity to VAM with increasing temperature. The increase in the activation energies results from structural as well as from electronic alterations of Pd. The spatial separation of Pd monomers by Au atoms leads to a distance between Pd atoms favorable for the formation of vinyl acetate, since distances between Pd monomers match well with interatomic distances in the product (4.99 Å for PdAu(111) and 4.08 Å for PdAu (100)). The additional electronic alteration of Pd by Au causes additional differences in adsorption properties, e.g. lower the adsorption strength of both AcOH and ethylene.[23]

Above 160 °C, the selectivity also decreases for samples with high Au-concentrations, which is even more pronounced than that observed over Pd-rich samples. This behavior results from the phase separation towards a Pd-rich and a Au-rich phase, which favors the combustion of C_2H_4 to CO_2.

Repeating the reaction cycles at temperature up to 190 °C supports the phase separation and the additional leaching of palladium at elevated temperatures. For samples with low Pd/Au ratios, the bending in the Arrhenius type plot for elevated temperatures is less distinct in the second run. The formation of a Pd-rich phase at temperatures higher than 160 °C during the first run led to further removal of palladium from the bimetallic particle, since in Pd-rich phases the formation of Pd acetate species is facilitated compared to highly intermixed phases. The re-formation of the Pd_1Au_1 phase during the subsequent cooling period is limited, since the bimetallic particles are already depleted of Pd at this point. Thus after a treatment at elevated temperatures lower concentrations of particles consisting of the Pd_1Au_1 phase (respectively more Au-rich particles) and high concentrations of the particles consisting of the dispersed monometallic phase are

present. For samples with high Pd/Au ratios, the influence of the increase in the concentration of the monometallic palladium phase after VAM synthesis at elevated temperatures was not as significant and thus the subsequent temperature dependent VAM formation is more similar to the original run. However the activation energies for the second run were smaller than for the first run. The similarity of the activation energies found for the monometallic reference samples Pd/SiO$_2$ and Pd(OAc)$_2$ on SiO$_2$ reveals that the decrease in activation energies for the second run for Pd-rich samples arises from the increased formation of dispersed palladium. Note that the leaching process to some extent compensates particle agglomeration, which is in accordance to findings by Brückner et. al who found smaller particle sizes and less agglomeration for samples aged at higher temperatures.[24]

The activation energies for VAM found for samples with high Pd/Au ratios were close to the values found over the monometallic Pd samples. The increase in activation energies with increasing Au concentration can be related to electronic and geometric modification of palladium[25,26,27] and is in good accordance to literature[2,21,26]. The addition of Au acts as a spacer between Pd monomers and thus increases the concentration of ensembles active for VAM synthesis. Moreover an electron transfer from Au to Pd occurs, which was shown by CO adsorption at low temperatures and white line analysis of XAS data sets presented in part I of this work. Both effects influence the adsorption properties of the reactants. On highly intermixed bimetallic surfaces π-bonded ethylene adsorption is highly favored over σ-bonded adsorption[10,20,23], whereas on monometallic palladium surfaces σ-bonded ethylene is preferred. The bonding energy of C$_2$H$_4$ on Pd within PdAu in comparison to monometallic Pd is significantly decreased (30 %).[20,23] Neurock and Mei[29] studied the adsorption of C$_2$H$_4$ on Pd and PdAu via *ab initio*-based dynamic Monte Carlo simulations and found a lower adsorption enthalpy of 14 kJ/mol on the bimetallic surface. Moreover the formation of ethylidyne has a 10 kJ/mol higher barrier over bimetallic Pd/Au compared to monometallic Pd. Both effects favor ethylene desorption over bimetallic surfaces.

Additionally the electronic and structural effects caused by the addition of Au to the monometallic Pd system, lead to decreased decomposition tendencies of the adsorbed species.[30,31] For high Au coverages (> 0.5) acetic acid adsorbs and desorbes

molecularly.[30] Moreover vinyl acetate desorbs from the highly intermixed metal surfaces without decomposition, whereas for Pd-rich surfaces a pronounced formation of CO_2 was observed.[32]

4.5. Conclusions

The formation rate of vinyl acetate over bimetallic PdAu catalysts normalized to the Pd content was found to increase with increasing Au concentration. Paired Pd monomers in the Pd_1Au_1 particles formed at reaction temperatures $\leq 160\ °C$ are approximately 5 times more active than the monometallic Pd phase. The reassembling of the PdAu particles is reactant induced and based on Pd leaching form the bimetallic particles in form of Pd-acetate species.

A pronounced deactivation with time-on-stream was observed for catalysts with Pd/Au ratios below 1, which originates from the depletion of Pd within the bimetallic particles and the simultaneous decrease in the concentration of highly active and selective paired Pd monomers. The deactivation is also visible in the selectivity behavior with time-on-stream. The depletion of Pd through Pd leaching promotes the combustion of C_2H_4 over the formation of VAM. Deactivation over Pd-rich samples is less severe, since the concentration of Pd acetate in the liquid surface layer is high and thus leaching from the bimetallic particles is suppressed, leading to improved long time stability of the catalyst.

Temperature dependent studies showed a change in the selectivity at elevated temperatures, which originates from a phase separation towards a Pd-rich and a Au-rich phase for temperatures above $160\ °C$. Both phases favor the combustion of C_2H_4 over the formation of VAM, which results in a pronounced decrease in the selectivity. The selectivity as function of the temperature differs for Pd-rich and Au-rich samples. The higher the Pd/Au ratio, the higher is the fraction of Pd present in the monometallic dispersed palladium phase. Pd-rich samples show a continuous decrease in selectivity with increasing temperature originating from a higher activation energy for CO_2 than for VAM. However samples with higher concentrations of Au exhibit an increase in selectivity till the phase separation from an equimolar phase towards a Au-rich and a Pd-rich phase takes place, leading to a severe drop in selectivity.

We expect that the observed differences for Pd-rich and Au-rich samples with respect to restructuring and temperature dependence are essential to optimize long-time stability with respect to activity and selectivity.

4.6. References

1.   http://www.sriconsulting.com/WP/Public/Reports/vam/.

2.   D. Kumar, M. S. Chen, D. W. Goodman, *Catalysis Today* **2007**, *123*, 77.

3.   I. I. Moiseev, M. N. Vargaftic, Y. K. Syrkin, *Doklady Akademii Nauk SSSR* **1960**, *133*, 377.

4.   J. Smidt, W. Hafner, R. Jira, R. Sieber, J. Sedlmeier, A. Sabel, *Angewandte Chemie International Edition in English* **1962**, *1*, 80-88.

5.   in *World Pet. Congr. Proc. , Vol. 5*, **1968**, p. 41.

6.   in *Eur. Chem. News Vol. 11*, **1967**, p. 40.

7.   D. D. Kragten, R. A. van Santen, M. K. Crawford, W. D. Provine, J. J. Lerou, *Inorganic Chemistry* **1999**, *38*, 331-339.

8.   T. C. Bissot (E. I. Du Pont de Nemours and Company), *US 4048096*, **1977**.

9.   A. M. Venezia, V. L. Parola, B. Pawelec, J. L. G. Fierro, *Applied Catalysis A: General* **2004**, *264*, 43.

10.   M. Chen, D. Kumar, C.-W. Yi, D. W. Goodman, *Science* **2005**, *310*, 291-293.

11.   S. Nakamura, T. Yasui, *Journal of Catalysis* **1970**, *17*, 366.

12.   S. M. Augustine, J. P. Blitz, *Journal of Catalysis* **1993**, *142*, 312-324.

13.   C. R. Reilly, J. J. Lerou, *Catalysis Today* **1998**, *41*, 433-441.

14.   E. A. Crathorne, D. Macgowan, S. R. Morris, A. P. Rawlinson, *Journal of Catalysis* **1994**, *149*, 254-267.

15.   W. M. Haynes, *Handbook of Chemistry and Physics Vol. 91*, CRC Pr Inc, Cleveland, **2010-2011**.

16.   S. Simson, A. Jentys, J. A. Lercher, *The Journal of Physical Chemistry C* **2013**, *117*, 8161-8169

17.   H.-J. Eberle, R. Heidenreich, J. Weis (Wacker-Chemie GmbH), *DE 10200605800 A1* Germany, **2008**.

18.   D. Kumar, M. S. Chen, D. W. Goodman, *Catalysis Today* **2007**, *123*, 77-85.

19.   A. Christensen, A. V. Ruban, P. Stoltze, K. W. Jacobsen, H. L. Skriver, J. K. Nørskov, F. Besenbacher, *Physical Review B* **1997**, *56*, 5822-5834.

20.   F. Calaza, F. Gao, Z. Li, W. T. Tysoe, *Surface Science* **2007**, *601*, 714-722.

21.   Y. F. Han, J. H. Wang, D. Kumar, Z. Yan, D. W. Goodman, *Journal of Catalysis* **2005**, *232*, 467.

22.   K. Motahari, H. Atashi, F. Fazlollahi, F. F. Tabrizi, M. Sarkari, *Journal of Industrial and Engineering Chemistry* **2012**, *18*, 266-271.

23.   I. Rivalta, G. Mazzone, N. Russo, E. Sicilia, *Journal of Chemical Theory and Computation* **2009**, *5*, 1350-1360.

24.   Q. Smejkal, D. Linke, U. Bentrup, M. M. Pohl, H. Berndt, M. Baerns, A. Brückner, *Applied Catalysis A: General* **2004**, *268*, 67-76.

25.   A. M. Venezia, V. La Parola, G. Deganello, B. Pawelec, J. L. G. Fierro, *Journal of Catalysis* **2003**, *215*, 317-325.

26.   L. Hilaire, P. Légaré, Y. Holl, G. Maire, *Surface Science* **1981**, *103*, 125-140.

27.   M. Neurock, *Journal of Catalysis* **2003**, *216*, 73.

28.   B. K. Min, A. K. Santra, D. W. Goodman, *Catalysis Today* **2003**, *85*, 113-124.

29.   M. Neurock, D. Mei, *Topics in Catalysis* **2002**, *20*, 5-23.

30.   Z. Li, F. Calaza, F. Gao, W. T. Tysoe, *Surface Science* **2007**, *601*, 1351-1357.

31.   M. Bowker, C. Morgan, J. Couves, *Surface Science* **2004**, *555*, 145-156.

32.   Z. Li, F. Calaza, W. T. Tysoe, *Surface Science* **2012**, *606*, 1113-1119.

4.7. Supporting information

Activity and selectivity behavior with time on stream for Pd/Au catalysts with a constant Pd loading of 0.5 wt.-%

Table 4-S1 summarizes the total metal loading of the respective samples with a constant total metal loading of 0.5 wt.-%. Figure 4-S1 and 4-S2 show the VAM formation rates normalized to the palladium content and the selectivity behavior with time on stream for Pd/Au catalysts with a constant Pd loading of 0.5 wt.-%

Table 4-S1: Total metal loading in wt.-% for the catalyst series with a constant Pd loading of 0.5 wt.-%.

Pd/Au molar ratio	Total metal loading in wt.-%
7.0	0.6
5.0	0.7
2.0	0.9
1.1	2.0
0.8	2.5

In general the same behavior was found as already described for samples with constant total metal loading. Note that for samples with constant palladium and varying gold content, there is a difference in total metal loading and thus possible deviations in particle sizes have to be taken into account. Normalized to the total palladium concentration, the samples with a constant palladium content of 0.5 wt.-% show the same ranking in activity as it was found for the samples with constant total metal loading; the Au rich sample with a Pd/Au molar ratio of 0.8 shows the lowest activity at steady state level, whereas for all remaining samples the activity per gram Pd increases with increasing Au content. Moreover samples with constant Pd loading exhibit similar deactivation behavior as observed over samples with constant total metal loading; the higher the Pd concentration, the more stable is the respective catalyst.
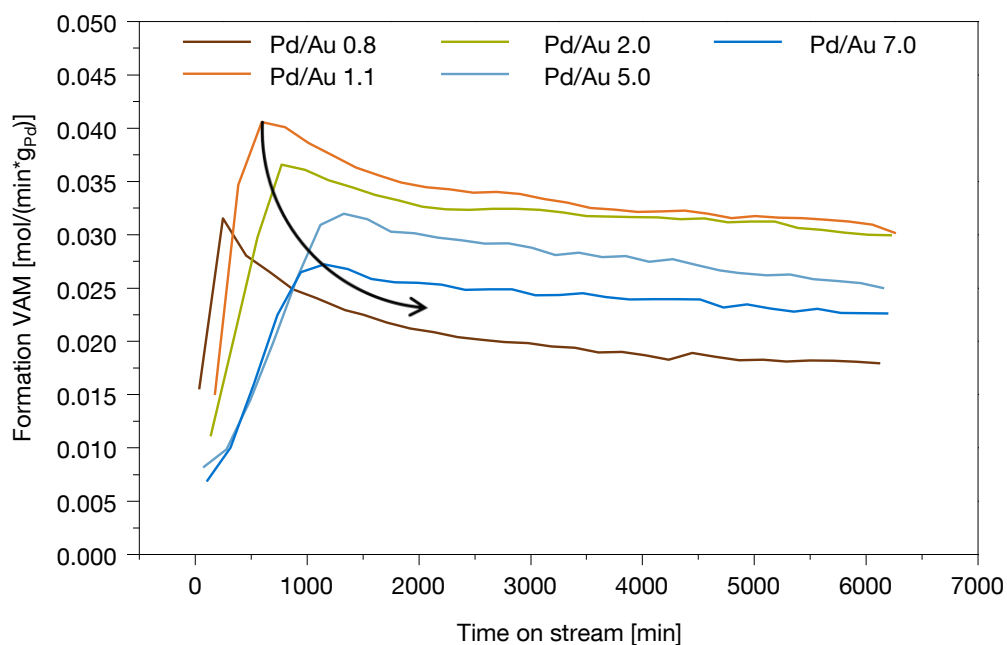
Figure 4-S1: Time on stream behavior of bimetallic samples with constant palladium loading of 0.5 wt.-% and additional 5 wt.-% KOAc. Reaction conditions: 60 vol.-% C_2H_4, 13 vol.-% AcOH, 4.5 vol.-% O_2, N_2 balance; 8.8 bar total pressure; temperature: 150 °C.
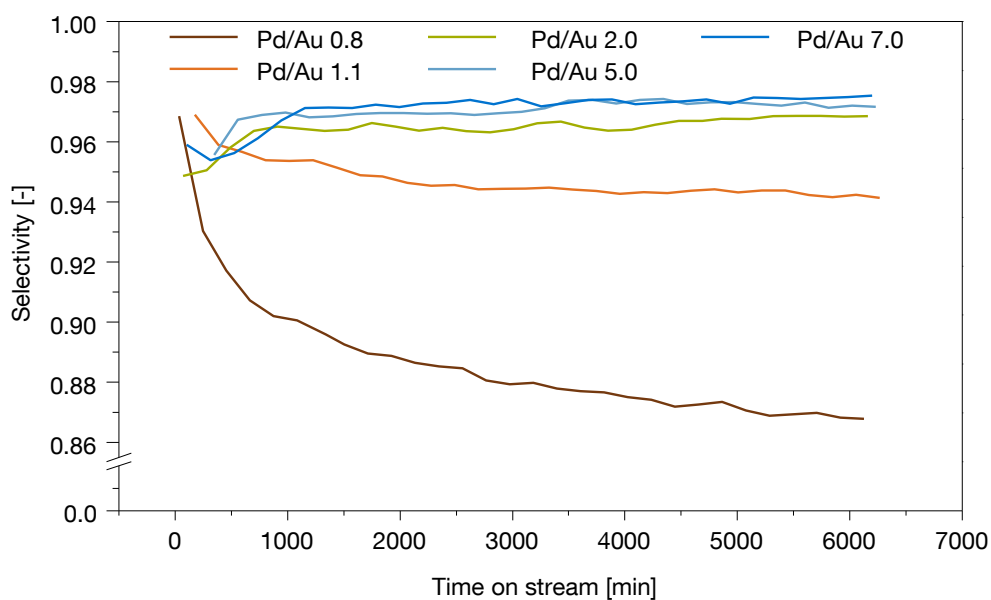
Figure 4-S2: Selectivity with time on steam of bimetallic samples with constant palladium loading of 0.5 wt. % and additional 5 wt.-% KOAc. Reaction conditions: 60 vol.-% C_2H_4, 13 vol.-% AcOH, 4.5 vol.-% O_2, N_2 balance; 8.8 bar total pressure; temperature: 150 °C.

Selectivity behavior with temperature for monometallic reference samples

The selectivity as function of the temperature for the monometallic reference samples Pd/SiO_2 containing 1.5 wt.-% palladium, Pd/SiO_2 with 3.0 wt.-% palladium and $Pd(OAc)_2$ impregnated onto SiO_2 with 1.5 wt.-% Pd loading is shown in Figure 4-S3.
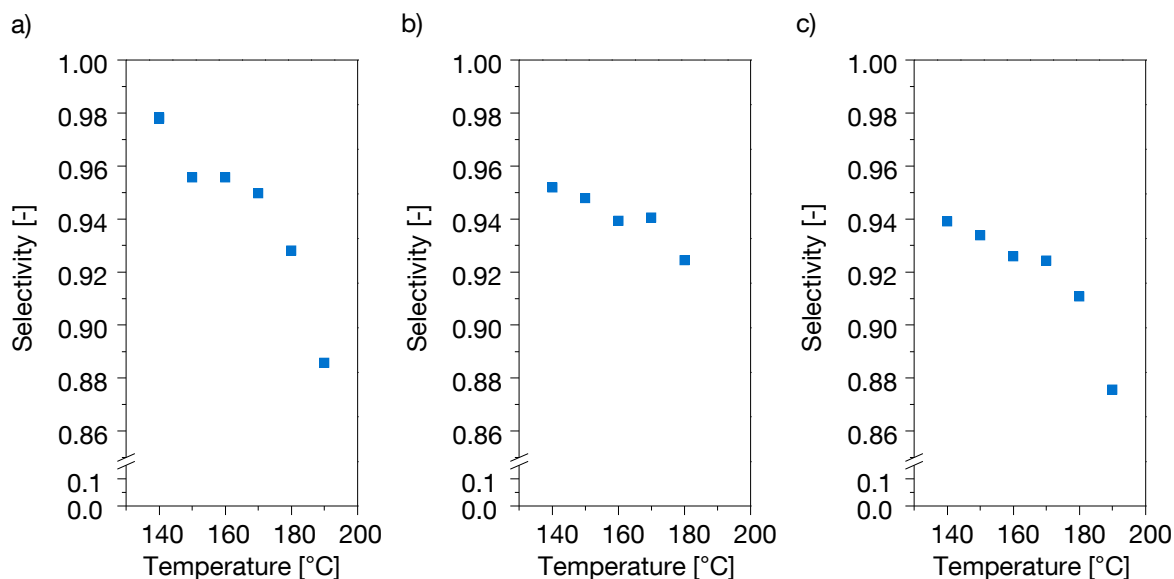

Figure 4-S3: Selectivity to VAM as function of the temperature for monometallic samples a) Pd/SiO_2 1.5 wt.-%, b) Pd/SiO_2 3.0 wt.-% and c) $Pd(OAc)_2$ – SiO_2 1.5 wt.-% Pd. Temperature range: 140 °C – 190 °C. Gas composition: 60 vol.-% C_2H_4, 13 vol.-% AcOH, 4.5 vol.-% O_2, N_2 balance; 8.8 bar total pressure.

None of the monometallic samples shows an increase in selectivity with increasing temperature as it was observed over low Pd/Au ratios in a temperature range from 140 °C – 160 °C. The continuous decrease in selectivity with increasing temperature for monometallic samples is based on higher activation energies towards CO_2 than towards vinyl acetate. Similar trends were found for highly Pd-rich samples. Thus the deviating selectivity behavior with temperature observed for low Pd/Au ratios originates from the bimetallic phase.

Pd(OAc)$_2$-SiO$_2$ KOAc – before and after reaction

The deactivation observed over Pd(OAc)$_2$/SiO$_2$-KOAc was attributed to the formation of metallic Pd particles out of Pd(OAc)$_2$ and the accompanied decrease in accessible Pd. The reaction mixture consisting of 60 vol.-% C$_2$H$_4$ is a reducing atmosphere and induces the reduction of Pd(OAc)$_2$ to Pd^0. Figure 4-S4 shows characterization data before and after 120 hours time on stream. Whereas before the application to vinyl acetate formation, metallic particles were neither observed via XRD nor TEM, after the reaction distinct reflections representing metallic Pd were detected via XRD and particles were found in TEM images.
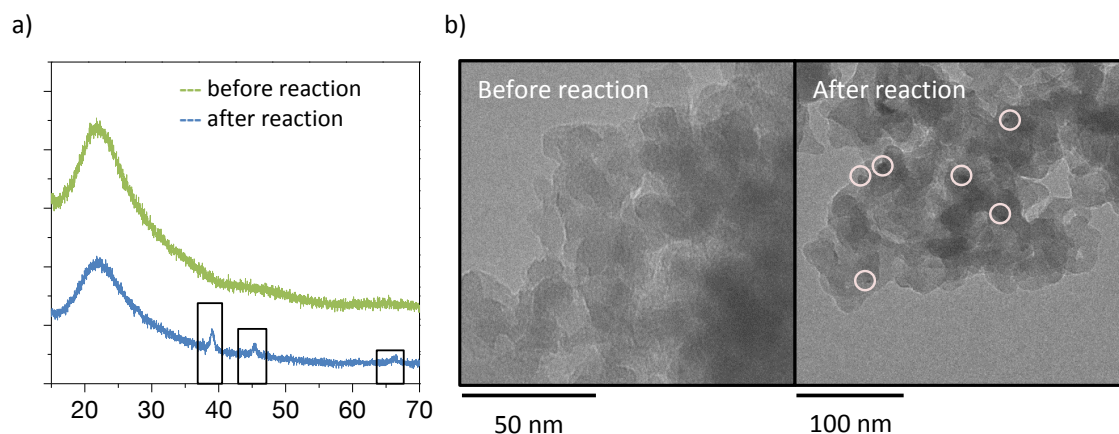
Figure 4-S4: a) XRD profiles of Pd(OAc)$_2$-SiO$_2$ KOAc (1.5 wt.-% Pd, 5 wt.-% K) before and after reaction. b) TEM images of Pd(OAc)$_2$-SiO$_2$ KOAc (1.5 wt.-% Pd, 5 wt.-% K) before and after reaction.

Pd(OAc)$_2$ modification of Au-rich catalysts – stabilization of bimetallic phase

The addition of Pd(OAc)$_2$ to the Au-rich Pd/Au 0.8 sample led to a significant increase in stability. The additional Pd(OAc)$_2$ in the liquid surface layer slows down the Pd leaching process, leading to a stabilization of the equimolar bimetallic phase. This was confirmed via XRD measurements of Pd/Au 0.8 and Pd/Au 0.8 with Pd(OAc)$_2$ after 160 hours time-on-stream, which revealed Au-rich bimetallic particles for the unmodified sample, however a Pd$_1$Au$_1$ phase for Pd/Au 0.8-Pd(OAc)$_2$. Table 4-S2 lists the 2Θ positions of the 111, 002 and 022 surface planes and the resulting alloy composition for the Pd/Au 0.8 and the Pd(OAc)$_2$ modified Pd/Au 0.8.

Table 4-S2: 2Θ positions of the the 111, 002 and 022 surface planes and the resulting alloy composition for the Pd/Au 0.8 and the Pd(OAc)$_2$ modified Pd/Au 0.8.

Sample	2Θ [°] 111	2Θ [°] 002	2Θ [°] 022	Alloy composition*
Pd/Au 0.8	38.84	45.15	65.79	Pd$_{0.3}$Au$_{0.7}$
Pd/Au 0.8 with Pd(OAc)$_2$	39.16	45.43	66.44	Pd$_{0.5}$Au$_{0.5}$

* Alloy compositions were calculated according to Vegard's law. 2Θ positions of monometallic Au and Pd were determined via reference measurements of monometallic samples prepared according to the same synthesis procedure as used for bimetallic samples.

Chapter 5

Summary

Vinyl acetate synthesis over SiO_2 supported bimetallic PdAu catalysts is a well-established industrial process. Catalyst structures are dynamically formed under working conditions and especially deactivation troubles long time usability. Within the bimetallic catalyst phases, two neighbored Pd atoms, separated by Au atoms, were identified as highly active and selective ensembles. Although high concentrations of these Pd pairs would be expected for catalysts with equal molar concentrations of Pd and Au, industry uses highly Pd-rich catalysts with Pd/Au molar ratios of up to 8.0. This discrepancy could be related to deactivation phenomena and was addressed in this study. Further goals were to 1) resolve the catalyst structure under working conditions, 2) to identify reasons for long time deactivation, 3) to evaluate the influence of reaction parameters on VAM formation and deactivation, and, 4) based on these results, to tailor catalysts according to the applied reaction conditions.

We were able to derive a restructuring mechanism for bimetallic catalysts under working conditions, by applying various surface and bulk sensitive characterization techniques on as synthesized and reacted samples, ranging from highly Pd-rich to Au-rich compositions. The reconstruction is attributed to the oxidation of Pd^0 (present in larger Pd ensembles), the formation of $Pd(OAc)_2$ by a reaction with the reactant and subsequent extraction from the bimetallic particle into the liquid phase consisting of AcOH and H_2O. The Pd leaching is slowed down as soon as the surface is highly intermixed, since the electronic influence of Au on Pd reduces the oxidizability of Pd. Moreover a saturation concentration of the Pd-ac species in the liquid surface layer limits further Pd extraction from the bimetallic particle into the liquid surface layer. The resulting phases were

identified as an ordered Pd_1Au_1 phase and a monometallic highly dispersed Pd-acetate species.

Palladium within the Pd_1Au_1 phase was found to be approximately five times more active than Pd within the monometallic Pd-acetate. Long time experiments with Au-rich catalysts showed severe deactivation combined with a pronounced decrease in selectivity. This was attributed to a depletion of Pd of the bimetallic particles which leads to a decrease in active and selective Pd monomer ensembles. For high Pd contents of the catalyst, high concentrations of the dispersed monometallic Pd phase are present besides the Pd_1Au_1 phase. Pd leaching is slowed down compared to more Au-rich samples, leading to a catalyst consisting of a quasi stable Pd_1Au_1 phase and high stability levels.

As two different Pd containing species were identified under working conditions, a different activity can be expected for catalysts with varying Pd/Au ratios. The formation of the bimetallic phase exhibits pronounced temperature dependence. For temperatures below 160 °C, a Pd_1Au_1 phase is present on the working catalyst. However at elevated temperatures a phase separation towards a Pd-rich and a Au-rich phase (i.e. Pd_3Au_1 and Pd_1Au_3) takes place. This leads to a severe decrease in VAM formation rate, since the concentration of highly active and selective Pd monomer ensembles is significantly decreased. Within Pd-rich phases large Pd ensembles are present, leading to an increased total combustion of C_2H_4. Also the Au-rich phase enhances the formation of CO_2, since C_2H_4 adsorption on Au takes place for high Au surface coverages, as it is the case for a Pd_1Au_3 phase. As the faction of Pd located within a Pd_1Au_1 phase is higher for low Pd/Au ratios, the influence of reaction temperature is more pronounced for these samples.

Due to the significant differences in the temperature dependence and restructuring properties over Pd-rich and more Au-rich catalysts, it is essential to tune reaction conditions according to the Pd/Au ratio of the applied bimetallic catalyst in order to reach high selectivity, activity and especially stability levels. Since the structure of the catalyst changes during reaction due to continuous Pd leaching from the bimetallic particles, reaction conditions have to be adjusted according to the current amount of dispersed Pd-acetate phase, in order to minimize long time deactivation.

Chapter 6

Zusammenfassung

Die Vinylacetate-Synthese über SiO_2 geträgerten, bimetallischen PdAu Katalysatoren ist ein fest etablierter großindustrieller Prozess. Die Katalysator-Strukturen werden unter Reaktionsbedingungen dynamisch ausgebildet und vor allem Selektivitätsverluste wirken sich negativ auf die Langzeitstabilität aus. Als hoch aktives und selektives Zentrum wurde eine Anordnung von zwei benachbarten Pd Monomeren identifiziert, die durch Au Atome räumlich getrennt sind. Obwohl hohe Konzentrationen an Pd Monomer Paaren in Katalysatoren mit einer Pd/Au (molaren) Zusammensetzung von 1/1 zu erwarten sind, werden industriell Katalysatoren mit hohem Pd Überschuss verwendet um primär das Deaktivierungsverhalten der bimetallischen Katalysatoren zu verbessern.

In diesem Umfeld waren die Ziele der vorliegenden Arbeit 1) die Katalysatorstruktur unter Reaktionsbedingungen aufzuklären, 2) die Gründe für die Langzeitdeaktivierung zu identifizieren, 3) den Einfluss der Prozessparameter auf die Vinylacetat-Synthese und die Deaktivierung zu bewerten und 4) basierend auf diesen Ergebnissen die Katalysatoren den verwendeten Reaktionsbedingungen anzupassen.

Der Mechanismus nach dem bimetallische Katalysatoren unter Reaktionsbedingungen restrukturieren wurde anhand der Charakterisierung der Proben vor und nach der Reaktion bestimmt, wobei sowohl Oberflächen- als auch Bulk-sensitive Methoden angewendet wurden. Die Restrukturierung wurde auf die Oxidation von Pd^0 (innerhalb größerer Pd Domänen) zu einer Pd-acetat Spezies zurückgeführt, die zu einem Herauslösen von Pd aus den bimetallischen Partikeln führt. Die gebildete Pd-acetat Spezies liegt in einem Flüssigfilm bestehend aus Essigsäure und H_2O vor, welcher unter Reaktionsbedingungen aus etwa 3-5 Monolayern besteht. Das Herauslösen von Palladium

wird verringert, sobald die Metalloberfläche stark vermischt ist, da der elektronische Einfluss von Au auf Pd die Oxidierbarkeit des Palladiums herabsetzt. Außerdem verlangsamt eine hohe Konzentration der gebildeten Pd-acetat Spezies innerhalb des Flüssigfilms den Extraktionsvorgang. Die ausgebildeten Strukturen wurden als geordnete Pd_1Au_1 Phase und als mono-metallische hochdisperse Pd-acetat Spezies identifiziert. Pd, welches innerhalb der Pd_1Au_1 Phase vorliegt ist ungefähr 5-mal so aktiv wie Pd innerhalb der dispersen Pd-acetat Spezies. Au-reiche Katalysatoren zeigten starke Deaktivierung bei gleichzeitigem ausgeprägtem Selektivitätsverlust. Dies wurde auf eine Pd-Verarmung der bimetallischen Partikel zurückgeführt, was eine Konzentrationsabnahme an aktiven und selektiven Pd Monomer Paaren zur Folge hat. Bei hohem Pd-Überschuss sind neben der Pd_1Au_1 Phase hohe Konzentrationen an der dispersen Pd-acetat Spezies vorhanden. Dies führt zu einer Verlangsamung der Pd-Extraktion aus dem Bimetall und damit zu einer quasi-stabilen Pd_1Au_1 Phase und somit zu hoher Langzeitstabilität.

Da unter Reaktionsbedingungen zwei verschiedene Pd Phasen vorhanden sind, wird abhängig von der jeweiligen Konzentration an Pd_1Au_1 Phase und disperser monometallischer Phase ein unterschiedliches Verhalten gegenüber variierenden Reaktionsparametern erwartet. Die Bildung der bimetallischen Phase unterliegt einer starken Temperaturabhängigkeit. Für Temperaturen unterhalb 160 °C liegt eine Pd_1Au_1 Phase vor. Bei höheren Temperaturen erfolgt eine Phasenseparierung innerhalb des Partikels zu einer Au-reichen und einer Pd-reichen Phase (i.e. Pd_3Au_1 and Pd_1Au_3). Dies führt zu einer Verringerung der VAM Bildungsrate, da die Konzentration an hoch aktiven und selektiven Pd Monomer Paaren abnimmt. Innerhalb der Pd-reichen Phase liegen große Pd Domänen vor, welche die vollständige Oxidation von C_2H_4 zu CO_2 fördern. Außerdem führen Au-reiche Oberflächen zu einer verstärkten Verbrennung, da C_2H_4 auf Oberflächen mit hoher Au Konzentration adsorbiert, wie es für die Pd_1Au_3 Phase der Fall ist. Da der Anteil an Pd, der innerhalb der Pd_1Au_1 Phase vorliegt, für niedrige Pd/Au Verhältnisse höher ist, ist die Temperaturabhängigkeit für diese Katalysatoren stärker ausgeprägt.

Durch die erheblichen Unterschiede in der Temperaturabhängigkeit und den Restrukturierungseigenschaften von Pd-reichen und Au-reichen Katalysatoren, ist es unerlässlich die Reaktionsbedingungen entsprechend des verwendeten Pd/Au

Verhältnisses zu optimieren, um hohe Aktivität, Selektivität und vor allem Stabilität zu gewährleisten. Da sich die Struktur des Katalysators mit der Reaktionszeit ändert, da stetig Pd aus dem Bimetall entfernt wird, müssen die Reaktionsbedingungen entsprechend der momentanen Struktur des Katalysators gewählt werden.

Curriculum vitae

Personal information

Name	Stefanie Simson (maiden name: Reiner)

Date of birth	6th of January, 1986
Place of birth	Bogen

Education

Since 07/2010	**Lehrstuhl für Technische Chemie II** **Technische Universität München** Doctoral candidate, Supervisor: Prof. Johannes A. Lercher, Topic: 'Stability of silica supported Pd/Au catalysts in gas phase vinyl acetate monomer synthesis'
10/2005 – 05/2010	**Technische Universität München** Studies in chemical engineering Diploma thesis: 'Hydroisomerization of n-Pentane over Lanthanum and Platinum exchanged Faujasite and Platinum promoted Sulfated Zirconium Oxide' Degree: Diplom-Ingenieur
10/2008 – 05/2009	**University of California, Berkeley (USA)**
09/1996 – 06/2005	**Dominicus-von-Linprun Gymnasium, Viechtach** Qualification: Abitur

Internships

10/2009 – 11/2009	**Südchemie AG, Moosburg**
03/2007 – 04/2007	**VTA GmbH Verfahrenstechnische Anlagen, Deggendorf**
06/2005 – 07/2005	**REHAU AG + Co United Polymers, Viechtach**

Awards and Scholarships

2010	Jürgen Manchot Award, **Jürgen Manchot Foundation**
2008	Ernest Solvay Research Scholarship, **Ernest Solvay Foundation**

List of publications

Publications in scientific journals

S. Simson, A. Jentys, J. A. Lercher, Dynamic Self-Organization of Supported Pd/Au Catalysts during Vinyl Acetate Synthesis. *The Journal of Physical Chemistry C* **2013**, *117* (16), 8161-8169.

S. Simson, A. Jentys, J. A. Lercher, Temperature dependent evaluation of two active species for vinyl acetate synthesis over Pd/Au-SiO$_2$ catalysts: Part I – physicochemical characterization, to be submitted.

S. Simson, A. Jentys, J. A. Lercher, Temperature dependent evaluation of two active species for vinyl acetate synthesis over Pd/Au-SiO$_2$ catalysts: Part II - structure activity correlation, to be submitted.

F. Schüßler, S. Simson, A. Holz, H. Shi, J. A. Lercher, Mechanistic studies on the hydroisomerization of n-pentane over lanthanum and platinum ion exchanged faujasites and platinum promoted sulfated zirconium oxide, in preparation.

G. Simson, E. Prasetyo, S. Reiner, O. Hinrichsen, Continuous precipitation of Cu/ZnO/Al$_2$O$_3$ catalysts for methanol synthesis in microstructured reactors with alternative precipitating agents. *Applied Catalysis A: General* **2013***, 450*, 1-12.

Selected conference presentations

S. Simson, A. Jentys, J. A. Lercher, 46. Jahrestreffen Deutscher Katalytiker, **2013**, Weimar, Germany, Reactive self-assembling of Pd/Au bimetallic particles for vinyl acetate synthesis, (Poster)

S. Reiner, Andreas Jentys, Johannes A. Lercher, 1st STCA Catalysis Conference, **2012**, Amsterdam, Netherlands, Characterization of reactively restructured Pd/Au bimetallic particles for vinyl acetate synthesis, (oral presentation)

S. Reiner, Andreas Jentys, Johannes A. Lercher, 45. Jahrestreffen Deutscher Katalytiker, **2012**, Weimar, Germany, Restructuring of Pd/Au bimetallic catalysts for gas phase vinyl acetate synthesis, (Poster)

S. Reiner, Andreas Jentys and Johannes A. Lercher , 15th International Congress on Catalysis, **2012**, Munich, Germany, Restructuring of Pd/Au bimetallic catalysts for gas phase vinyl acetate synthesis. (Poster)